2007

Immunoassay performance: recognition elements, equilibrium and mass transfer considerations

Karen Marie Kwarta
Iowa State University

Immunoassay performance: Recognition elements, equilibrium and mass transfer considerations

by

Karen Marie Kwarta

A dissertation submitted to the graduate faculty

in partial fulfillment of the requirements for the degree of

DOCTOR OF PHILOSOPHY

Major: Analytical Chemistry

Program of Study Committee:
Marc D. Porter, Major Professor
R.S. Houk
Patricia A. Thiel
Nancy Cornick
Andrew Hillier

Iowa State University

Ames, Iowa

2007

TABLE OF CONTENTS

ACKNOWLEDGEMENTS

This dissertation is a compilation of my completed projects at Iowa State University and could not have been accomplished without the support of many people in my life. First, I would like to thank my major professor, Marc Porter, for providing the guidance and academic freedom that allowed me to develop my analytical problem-solving skills. Thank you for teaching me how to enjoy the journey that is science, and that the most interesting insights sometimes come from unexpected places.

I would also like to thank past and present members of the Porter Group. I would like to specially thank Bob Lipert for his wise and insightful guidance, and for always encouraging me to ask the "stupid question". Also, thank you to Becky Staedtler for knowing everything and always being there to help solve any problem—personal or professional. I would also like to acknowledge members of the Raman subgroup (Jill Uhlenkamp, Betsy Yakes, and Radha Narayanan) for providing constructive criticism and helping generate exciting pursuits. I would like to specially thank Jeremy Driskell and Rachel Millen for all the wonderful (useful and otherwise) impromptu office meetings that helped me generate research ideas and kept me laughing during the rough times. Your support and encouragement will never be forgotten. A special thank you also, to Jill and Betsy for sharing the experience of moving to Arizona with me. The time we spent in the desert was unforgettable.

I would also like to thank my collaborators at the National Animal Disease Center, John Neill and Julia Ridpath. Thank you for providing an open and friendly collaboration that led to some of the most interesting work of my dissertation.

Also, thank you to Amie Yang, Mike Vasbinder, and Jeremy and Elizabeth Driskell for all the wonderful dinners, camping trips, and just plain fun. Additional thanks to Jeremy for being a wonderful friend for almost 10 years now, and thank you to Amie for being my most trusted confidant.

Many thanks to my family for providing support, guidance and love throughout my life. To my parents, Bob and Susan: you have always encouraged me to do whatever I wanted, and have supported every decision I have made. Thank you. Also, thank you for teaching me that if you work hard, you will reap many rewards. To my sisters: you are my best friends in the entire world, and I would not be the person I am today without you. Sara, you have always been "my rock" and the one I turn to in times of crisis. Ann, your spirit and sense of adventure has kept me from becoming a "total nerd". To my brother in law Jason—thank you for keeping my sister happy and for being the brother I never had. Also, thank you to my niece Abby for reminding me how precious life really is. A special thank you also to my uncle Tim for always making sure I was doing fine and keeping me updated on all the family gossip.

Additional thanks to my in-laws, Jim and Mary, for treating me as one of their family. Thank you for supporting Jared and I in all aspects of our lives. To my brother and sister-in laws (Nikki, Michelle, Kipp and Nathan), thank you for treating me as one of the Kwarta's.

Finally, and most importantly, thank you to my husband Jared. Thank you for being my best friend and for giving me your unconditional love and support. You always believed in me, even when I didn't, and have supported every decision regarding my graduate career. Thank you for moving to Arizona with me, and taking care of my every

need throughout my graduate career. Thank you for listening to boring chemistry talk and helping me keep my life in balance and in perspective, I could not have done this without you. Thank you.

I would like to dedicate this dissertation to the many loved ones whom have passed away throughout my graduate career. I miss and love you all.

Ames Laboratory is operated for the U.S. Department of Energy by Iowa State University under contract W-7405-eng-82.

ABSTRACT

This dissertation explores the importance of mass transfer, equilibrium, and recognition elements on performance of immunoassay platforms. Atomic Force Microscopy (AFM) and Surface-Enhanced Raman Scattering (SERS) are employed as readout methods. AFM was utilized to evaluate the effectiveness of monoclonal antibodies used in a heterogeneous immunoassay for porcine parvovirus (PPV) and feline calicivirus (FCV). These results were employed to develop immunoassay protocols for PPV and FCV, and to assess the effect of elevated temperatures on the rate of mass transfer, and therefore the accumulation of PPV and FCV. Theoretical accumulation rates were compared to experimental observations as monitored by AFM. The effect of sample volume and capture area on limits of detection was examined for PPV utilizing SERS as a readout method. A model of the equilibrium for heterogeneous immunoassays revealed that the use of small capture substrate areas and large sample volumes would prevent depletion of the analyte solution, and would provide the highest surface concentration of analyte. Experimental findings for the detection of PPV upheld this prediction. Finally, the use of aptamers as alternatives to antibodies in a SERS-based detection platform for thrombin was examined. The conditions for aptamer immobilization and thrombin extraction were evaluated, the limit of detection for the aptamer-based assay was compared to that for an antibody-based assay, and possible underpinnings for the differences in performance discussed.

GENERAL INTRODUCTION

Dissertation Organization

Heterogeneous immunoassays have been used for several years for detection of bioanalytes. Throughout this time improvements in sensitivity, selectivity, speed and specificity have continued to be critical focal points. This dissertation seeks to further advance these performance merits through investigation of two readout methodologies: atomic force microscopy (AFM) and surface enhanced Raman scattering (SERS).

This dissertation is organized into six sections. The first section gives a review of current methods for immunoassay detection highlighting the potential benefits of using AFM and SERS as readout methodologies. Approaches to improve the speed of these assays are briefly discussed along with a description of a new class of molecules known as aptamers. Aptamers are emerging as possible alternatives for antibodies as the selective recognition elements in a wide range of assays.

Four original research chapters follow the Introduction, each presented as a separate manuscript that will soon be submitted for publication. Chapter 1 discusses the optimization required for designing an immunoassay protocol utilizing AFM as a readout technique. This Chapter describes a method for detection of feline calicivirus (FCV) and porcine parvovirus (PPV) using AFM and this protocol is used for Chapters 2 and 3. Chapter 1 also demonstrates the importance of screening antibodies to identify those which give the best sensitivity. Chapter 2 extends the method developed in Chapter 1 by studying the effect of elevated temperature on the sensitivity and speed of the assay. Chapter 2 shows that elevated temperatures dramatically reduce incubation times with

only marginal loss in sensitivity. Chapters 3 and 4 employ SERS as a readout technique. Chapter 3 explores the benefits and drawbacks of decreasing the area of the capture substrate and increasing the sample volume as a means to achieve the highest possible surface concentration of analyte, allowing for improvements in detection limits. Chapter 4 investigates the use of aptamers as replacements for antibodies in a detection scheme for thrombin. The conditions for this assay were optimized and the results were compared to an assay employing antibodies. The dissertation concludes with a general summary and a discussion of the future directions building on this work.

Literature Review

Traditional Immunoassays

The term immunoassay refers to a measurement that employs antibodies as analytical reagents. The first immunoassays (radioimmunoassay) were developed in the 1960s for insulin and thyroxine.[1] At the time the importance of this type of analysis was underestimated by the scientific community. Since then, the specificity, stability and versatility of antibodies have been exploited to produce analytical methodologies for a wide range of targets. Today, immunoassays play a leading role in areas of human and veterinary medicine as a tool for early disease diagnosis and post-treatment monitoring.[2] Immunoassay technology has been applied to many other fields of research including food safety[3, 4] and environmental analysis.[5-7] Recent trends in the field of immunoassay research focus on development of multiplexed systems, real-time monitoring, automation,

and more specific reagents and labels (aptamers).[8, 9] In nearly all cases, approaches to further advances in speed, sensitivity, and specificity continue to be vital research areas.

Immunoassays rely upon the molecular recognition characteristics of antibodies. Antibodies are proteins in the immunoglobulin class that have binding sites specific for target antigens. The recognition between antibodies and antigens results from a combination of electrostatic, hydrophobic, hydrogen and Van der Waals interactions. Typical equilibrium constants between antibodies and antigens range from 10^7 to 10^{12} M^{-1}.[9] One advantage of using antibodies as analytical reagents is that many can be produced from hybridoma cell lines that can be continuously cultured to produce the antibody; therefore there are no limits to the amount of antibody that can be produced[10]. Other advantages are that the antigen used in identification of the antibody does not have to be in a purified form[10], and antibodies impart high selectivity and affinity to the methodology. Limitations of antibodies include the use of animals for production, which limits targets to those that are well tolerated in animals (i.e. toxins cannot be used). The identification and production of antibodies is labor intensive and expensive, and antibodies are prone to batch to batch variability. Finally, antibodies are sensitive to temperature, require physiological conditions, and undergo irreversible denaturation[10]. These limitations have inspired the study of aptamers as replacements for antibodies in biosensing applications, and aptamers are the topic of Chapter 4 of this dissertation.

Immunoassays can be categorized into two methods: competitive and non-competitive. Non-competitive assays (sandwich type) are the focus of this dissertation and will therefore be the subject of this review. Noncompetitive immunoassays require

the binding of two antibodies to the antigen, one being labeled to provide the analytical signal (Figure 1).

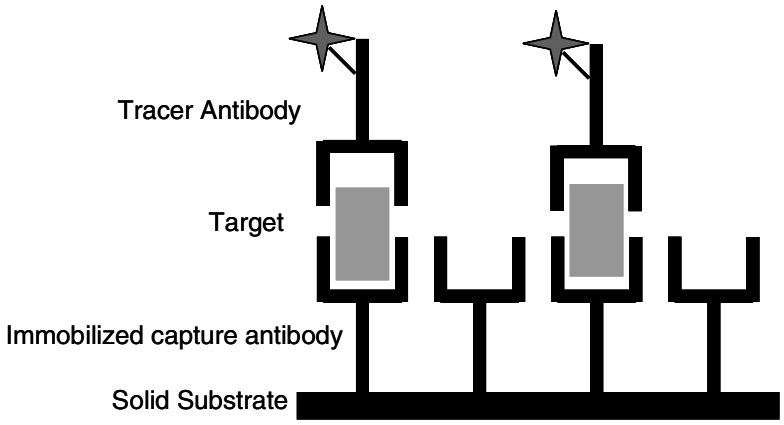

Figure 1. Solid-phase immunoassay in a non-competitive format.

In general, a solid phase is prepared with an excess of purified antibody specific to the target analyte. Many different solid phases have been explored for antibody immobilization, including plastic microtiter plates, polymer beads, and membranes.[9] Immobilization procedures for the antibody vary for each solid phase and include simple adsorption (through hydrophobic or hydrophilic interactions) and covalent tethering. When passively adsorbed, antibodies undergo conformational changes which decrease their activity up to 90%.[9] In the presence of other proteins, the antibodies may exchange with the excess proteins to the solid substrate reducing coverage by up to 15% in a 16 h period.[9] Nevertheless, passive adsorption continues to be used because of its ease of use and, even with the loss of antibody activity, assays performed in this manner still provide adequate limits of detections and dynamic ranges. Covalent immobilization requires the use of a liking agent such as glutaraldehyde[9] and provides a more rugged capture

substrate. However, these procedures can be complicated and add several steps to the overall procedure, sometimes without any tangible benefit.

The resulting solid phase, generally referred to as a capture substrate, is then blocked to reduce non-specific binding of the analyte and labeled antibody to the solid phase, and to coat non-specific epitopes of the immobilized antibody. The selection of a blocking agent must be optimized for each application. Blocking agents are typically proteins or nonionic detergents and include bovine serum albumin (BSA), casein, dilute skim milk, Tween, and Triton. Commercial blocking agents such as Superblock and Blotto are also available, which are unspecified mixtures of skim milk proteins, anti-foaming agents and nonionic detergents.[9] Small proteins are used for blocking since their small size has a greater probability to fill in the gaps left between the much larger antibodies which make up the capture substrate. Optimization of the blocking agent is crucial because some blockers may increase non-specific binding. Moreover, some assays may not require a blocking step. The mechanisms by which blocking agents reduce non-specific adsorption is not well understood, and blocking agents have been shown to interfere with specific as well as non-specific binding.[9]

Once the capture substrate is prepared, the target is exposed to the substrate and allowed to bind for a specific amount of time (incubation time). The time required for the solid phase immunoassay to reach equilibrium can be very long, and methods to improve diffusion of targets to the capture substrate are the focus of Chapter 2. Another key aspect of target extraction is the specificity of the interaction between the capture antibody and the analyte. The specificity of this interaction has a large impact on the sensitivity (i.e.

limit of detection) of the assay. This concept has been examined in Chapters 1 and 4 of this dissertation.

Finally, the captured analyte is labeled with excess of tracer antibody, and washed to remove extra tracer antibodies. This tracer antibody provides a signal that is directly proportional to the analyte concentration. The use of two different antibodies for the noncompetitive immunoassay often imparts greater specificity because cross-reacting species rarely bind both the capture and the tracer antibodies.

Detection limits for noncompetitive immunoassays are controlled by the affinity of the involved antibodies, experimental error, non-specific binding, and the strength of the signal from the tracer antibody. In this immunoassay format, the analytical signal is directly proportional to the amount of analyte present; thus low concentrations of analyte produce low signals. Therefore, to drive the limits of detection to lower levels, brighter labels are needed. Importantly, the analytical signal obtained from analyte binding must be distinguishable from that of non-specific binding.

The type of label used for the tracer antibody varies, and conventional immunoassay labels include radioactive isotopes, enzymes, and fluorophores. The next section will briefly examine each of these techniques, followed by the fundamental underpinnings of two alternative readout methodologies (AFM and SERS). The discussion will also detail their strengths and weaknesses.

Radioactive isotopes provided the analytical signal for the very first immunoassay, relying on the disintegration ("decay") of the radioactive isotope for quantification. With this approach, the unstable radioisotope is covalently attached to the tracer antibody, and the radiation can be of two types: β particles, or γ rays. The preferred

type is γ rays due to their greater emission and simpler instrumentation requirements. Radioactive isotopes have the distinct advantage of not being susceptible to environmental factors such as pH or ionic strength. Additionally, most biological matrices have very low radioactive backgrounds, contributing to their high sensitivity. Unfortunately, radioactive labels emit radiation over a broad energy range, providing a challenge for multiplexing due to overlapping spectra,[11] and the health hazards associated with radiation exposure have discouraged their use.[12]

Introduced in the 1970s,[13] enzymes are the most widely used label in immunoassays[9], the most typical format being an enzyme-linked immunosorbant assay (ELISA). For ELISA, an enzyme is conjugated to the tracer antibody, and as a final step in the assay, a substrate is added to the reaction vessel. The product of the enzyme-substrate reaction is monitored. Quantification of the reaction can be achieved with visual assessment, fluorescence, luminescence, and electrochemistry methods.[9] ELISA application offers high sensitivity due to the inherent amplification that results from the enzyme-substrate reaction. The challenges with enzyme labels are related to the diffusion limitation of immunoassays. Enzymes are large biomolecules with small diffusion coefficients, requiring long sample incubation times for the enzyme to reach the capture substrate. In addition, enzymes have similar properties as antibodies and therefore are prone to non-specific binding resulting in high background signals that limit sensitivity. Enzymes are also susceptible to environmental factors such as pH, temperature, and ionic strength, all which may alter the activity of the enzyme. Finally, multiplexing with enzyme labels is difficult because the products often have spectra that overlap.

Today, fluorescent labels are commonly used in immunoassays due to their improved sensitivity over absorbance measurements[9]. Unlike radioactive isotopic labels, fluorophores are sensitive to their local environment and produce high background signals from scattering and fluorescence of the sample or substrate. These limitations have been overcome by the use of time-resolved fluorescence measurements and labels with long-lived fluorescence[14]. The emission spectrum from many fluorophores is broad, presenting a challenge in multiplexing. However, spatial separation of multiple antibodies on the solid phase allows for the use of a single label in a multiplexed format (i.e. the location identifies the antigen, and the intensity determines concentration).

Alternative Readout Techniques

Atomic Force Microscopy (AFM)

In Chapters 1 and 2 of this dissertation, atomic force microscopy (AFM) has been explored as an alternative readout method for immunoassays due to its ability to distinguish nanometrically sized objects based upon morphology. Because of the ability of AFM to interrogate molecular level interactions at solid phase interfaces, it has been exploited as a tool to study many biological phenomena. AFM has also been used to image bacteria,[15] viruses,[16] and proteins.[17] AFM has also been applied as a detection method for viruses, offering a distinct advantage in that it can be carried out in a fluid environment that allows biological entities to be in their natural state.[16] AFM procedures also do not require sample preparation steps that can alter the structural properties of biological reagents.[17] The ability of AFM to probe into adsorption of proteins at the solid-

liquid interface provides information that is central to a range of bio-technologies including biosensors, biomaterials, and biomedical applications.[17]

First reports of AFM as a tool for analysis of immunosensing platforms were performed by our laboratory several years ago.[18] This study used compositionally patterned surfaces and determined that controlling orientation of antibodies to the solid phase increased epitope density.[18] Another application used substrates with micrometer-sized regions of rabbit IgG covalently bound and separated by a hydrophobic octadecanethiolate monolayer. AFM was used to monitor the height changes upon antigen binding, and real-time analysis revealed that the antigen was bound in ~5 min.[19] Other immunoassays utilizing AFM include detecting antigen-antibody binding through the use of colloidal gold-labeled antibodies to measure an increase in surface roughness.[20, 21] Researchers have also used AFM as a tool for immunosensing based upon height changes in a protein pattern. In a slightly different venue, AFM has been employed as a tool to fabricate protein patterns.[22, 23] These techniques have been extended to imaging of protein patterns, created with different protein immobilization procedures, to determine orientation of the proteins.[22, 23] AFM has also been used to study the viability of immobilized proteins on a microtiter plate, finding that only 5% of passively adsorbed antibodies were active.[24]

One application of AFM as a tool for biochemical analysis involves measurement of ligand-receptor binding forces. Molecular interactions between ligand binding pairs is of critical importance in determining biological function as it pertains to structural features.[17, 25] To interrogate these interactions, one of the binding pairs is typically immobilized on a tip and the other bound to a surface.[26-28] Adhesion (binding force) is

measured by conducting a pull-off experiment.[29] These experiments are sometimes difficult to interpret due to non-specific interactions from improper orientation of one of the ligands.[29, 30] The first reports on using AFM to probe ligand binding interactions involved the use of the well studied biotin-streptavidin system.[31-33] These experiments require immobilization strategies that allow spatial separation of ligands or receptors to ensure a response due to specific binding. In addition, these determinations require a statistically valid number of force curves to gain useful information about the interactions.

A more basic and direct use of AFM to study antibody-antigen binding is by topographical imaging. Advantages of AFM as a readout method in this manner are its ability to directly image/quantify the target. In many cases, a secondary labeling step is not required. Height changes of 3-4 nm have been observed for adsorption of anti-IgG to a surface and the same changes are observed when antigen is bound.[19]

AFM has also been used as a tool to image and detect viruses.[16, 34] High resolution images of viruses that have been immobilized on a variety of surfaces have been obtained with AFM, providing insight into the dimensions of virus particles and the architecture of their surfaces.[16] These images show the potential of AFM to differentiate viruses based upon their sizes and shapes, and viruses with diameters ranging from 17-150 nm have been examined.[16] At present, however, this technique lacks the sensitivity required for diagnosis in that the limit of detection for this platform in only 10^8 pfu/mL.[35]

The ability of AFM to measure individual biological events has allowed it to become a key instrument for biological analysis. Since AFM can image large areas and has the sensitivity to detect single antibody-antigen pairs, it can interrogate many

addresses in a single scan, providing a high throughput readout method.[19] However, the slow analysis speed limits this application. Advances in development of a high-speed AFM have allowed it to meet these needs,[36-40] including techniques to increase the scan speeds of contact and intermittent contact imaging[41], as well as a fast driving technique.[42] These developments, coupled with the imaging capabilities of AFM will continue to place AFM as an invaluable tool in analysis of biological interactions.

Surface-Enhanced Raman Scattering (SERS)

SERS has been employed as a readout technique for immunoassay because of several advantageous characteristics[43-53] and is the technique utilized in Chapters 3 and 4 of this dissertation. The first advantage is that, in contrast to normal Raman spectroscopy, SERS signals rival those of fluorescence. Raman bands, however, unlike those of fluorescence, are narrow, reducing spectral overlap and facilitating multiplexed detection with several Raman reporter molecules in one address. Another advantage of SERS is that optimum excitation wavelengths are dictated by the underlying enhancing substrate rather than the Raman reporter molecule, allowing only a single excitation wavelength to excite several labels. Finally, Raman scattering is unaffected by its environment, producing a stable and reproducible signal.

The earliest work in adapting SERS to immunoassay readout involved detection of thyroid stimulating hormone using antibodies bound to a roughened silver substrate.[53] The built in amplification of enzymes was adapted for SERS readout by choosing a product from the enzyme reaction that is Raman active.[46] The Raman active product was then adsorbed onto colloidal silver for SERS readout. Label free assays for SERS have

also been developed in which a biomarker for bacterial spores (calcium dipicolinate) that exhibits intrinsic Raman scattering was bound to a roughened silver substrate.[49]

Work in our laboratory has focused on the use of extrinsic Raman labels (ERLs) for SERS detection in a solid-phase sandwich immunoassay format.[43, 44] ERLs are designed to contain the immuno-recognition element as well as the Raman active molecule. The gold colloid then serves as the enhancing surface, and the ERLs are used as the tracer antibody in the sandwich format. The design has been implemented in the multiplexed detection of IgG protein[45] and has been shown to have femtomolar level sensitivity for prostate specific antigen, a biomarker for prostate cancer.[44] Finally, the use of ERLs has been applied to large bioanalytes through detection of feline calicivirus.[43]

Overcoming the Diffusion Limit

As mentioned above, a challenge in many immunoassay formats is the time required for analyte and label (tracer antibody) to diffuse to the solid substrate. The ideal kinetics for a bimolecular reaction occur in solution; constraining one analyte to a solid support imposes a strong effect of diffusion constraints.[54] Long incubation times are required for an equilibrium to be reached when one reactant is immobilized, as is the case in solid phase immunoassays.[9] Though only marginally investigated, ways to overcome the diffusion could offer significant improvements to the efficiency and possibly the sensitivity of immunoassays. Since antibody-antigen reactions are considered to be "instantaneous" (i.e., mass transfer limited), the rate limiting step of immunoassays is

diffusion to the substrate[55-59] as many biological molecules have small diffusion coefficients. The diffusion coefficient is described by:

$$D = kT/6\pi\eta r \qquad (1)$$

where k is Boltzmann's constant, T is temperature, r is the radius of the analyte and η is viscosity. Since r falls in the denominator, large values for r (i.e., large biomolecules) will decrease the diffusion coefficient, slowing diffusion rates.

Diffusion control of solid phase immunoassays has been supported by experimental evidence as well as theoretical models that describe solid phase immunoassay kinetics.[56, 57] Recent theoretical treatments argue that the time required for picomolar or better detection limits is unacceptably long when diffusion alone is used to transport large analytes to a solid phase.[60] This analysis suggests that limits of detection are restricted by the diffusional transport and not signal transduction. The opportunity, therefore, is found in increasing flux of analyte to the surface to take full advantage of the recent breakthroughs in readout methodology that allow quantification at ultra-low levels. It has been estimated that by applying stirring to protein microarrays, the speed of the reaction could be improved by 40-fold.[54]

Only a limited number of methods have been proposed for increasing mass transport of analytes and labels to the solid phase to exploit the instantaneous recognition rates of antibody-antigen interactions. One method involves electric-field driven assays in which analytes are driven to locations based upon their inherent charges. Two different strategies have been proposed. The first involves driving analytes electrophoretically through solution to spots on a microelectrode array.[61, 62] Another method manipulates analytes electroosmotically in microchannels.[63] These methods allow incubation times to

be reduced dramatically (1 min with electroosmotic transport) but suffer in that each analyte has a unique charge, and therefore different experimental conditions are required for each immunoassay.

A technique that can be more universally applied to overcoming mass transport has been developed in our laboratory and is based upon the electrochemical theory of rotated disk electrodes.[64] This concept was first applied in an immunoassay to increase flux of redox probes generated by an enzyme label for a sandwich immunoassay with amperometric detection. In our laboratory it was further exploited to drive the transport of analytes to the solid phase platform with a rotating disk. Porcine parvovirus was chosen as a model because of its small diffusion coefficients, and atomic force microscopy (AFM) was used as a readout method. The use of rotation reduced incubation times and resulted in an improved limit of detection over an assay preformed under diffusion controlled conditions. Rotation was also applied to a full sandwich immunoassay, providing increase in flux for both the analyte and the label, utilizing SERS as a readout method. This assay led to a reduction in incubation time from 24 h to 25 min with a tenfold improvement in the limit of detection.[64]

Elevated temperature has also been explored as a means to decrease incubation times and is the subject of Chapter 2 in this dissertation. An increase in temperature speeds up incubation times by 1) increasing the diffusion coefficient, 2) increasing the association constant between antibodies and antigens,[65] and 3) inducing convection through a thermal gradient. As shown in equation 1, an increase in temperature will increase the diffusion coefficient. Simultaneously, an increase in temperature decreases viscosity, which further improves the diffusion coefficient, offering a simple means for

decreasing incubation times. Finally, when assay samples are exposed to a heating element, the changes in temperature between the solid phase support and the solution may not occur at the same rate, causing a thermal gradient in the sample. The thermal gradient then induces convection, which delivers analyte to the substrate more quickly.

Aptamers

Aptamers are single stranded oligonucleotides (40-100 bases) thought to rival if not surpass antibodies as molecular recognition elements in selectivity, specificity and affinity.[10] Discovered in 1990 independently in the labs of Joyce,[66] Szostak,[67] and Gold,[68] through a process termed Systematic Evolution of Ligands by Exponential Enrichment (SELEX), aptamers can be developed for a variety of targets ranging in size from small organic molecules to proteins. Recent reviews summarize existing aptamers and their targets.[69-73] The development of aptamers has changed the way single stranded nucleotides are viewed. Traditionally looked upon as linear molecules that contain information (tapes), single stranded oligonucleotides are now described as globular molecules.[74] Since their invention, aptamers have been extensively studied and demonstrate great potential as a tool in molecular biology, diagnostics, molecular medicine, and drug discovery.[72] Aptamers have been isolated that bind tightly and specifically to targets for uses in sensor technology. Aptamers have also been found that inhibit proteins biological function, positioning them as potential therapeutic reagents.[75] The molecular discrimination that aptamers exhibit has been shown to be up to 10 times more efficient[76] than that of antibodies and can even discriminate between enantiomers.[77]

The SELEX process used to develop aptamers that bind selectively to targets involves the isolation of a nucleic acid sequence from a starting pool of ~10^{15} sequences. The molecular diversity contained in this large pool contributes to the success of finding a unique sequence that interacts specifically with the target, and the degree of this diversity supersedes that of other screening libraries.[10] Once isolated, these single stranded oligonucleotides exhibit complex molecular recognition properties based upon their three-dimensional conformation.

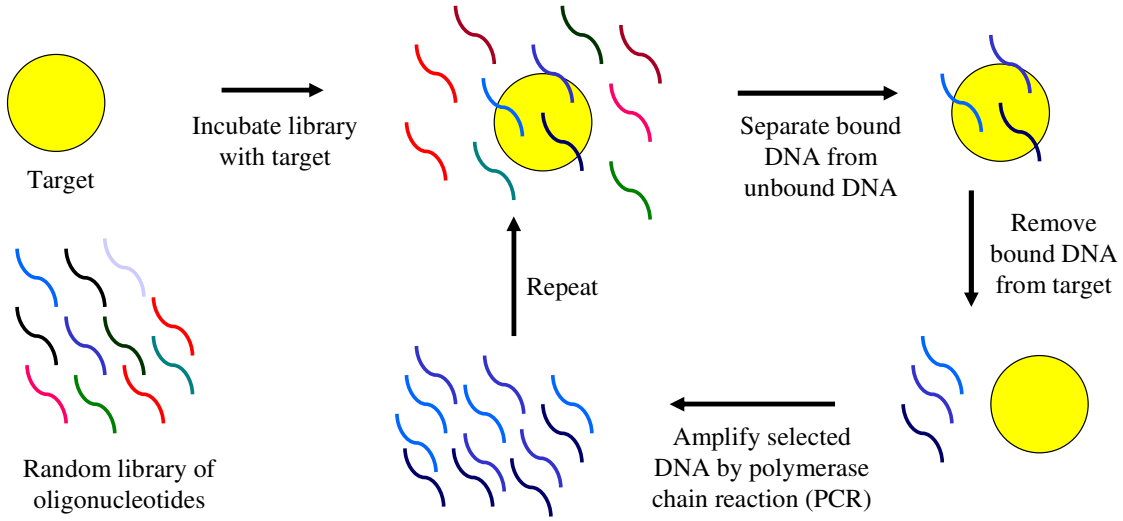

Figure 2. The SELEX process.

The SELEX process is shown in Figure 2. The isolation process of aptamers begins with a starting pool of single stranded oligonucleotides synthesized with random sequences flanked by primer sequences on either end for easy amplification during the selection process. The sequences are then exposed to a target molecule in the conditions of choice (i.e. buffer composition, temperature, etc)[10] and allowed to bind. Typically, the target is immobilized on a support to facilitate removal of sequences that do not bind the

target.[71] The weakly bound sequences are removed by washing or eluting them from the solid support. Sequences that strongly bind the target must then be eluted off the target, typically by using methods that denature the 3-D structure of the oligonucleotides (i.e. heat or basic pH). Once the sequences that bind strongly to the target have been eluted, they are amplified through the polymerase chain reaction (PCR). PCR is a technique that amplifies oligonucleotides through a series of heating and cooling steps with the use of an enzyme (typically Taq polymerase), primers (complimentary to the primer sequences flanking the random sequence of the initial pool), and deoxynucleotide triphosphates (dNTPs). This amplification procedure increases the concentration of the sequences that exhibit binding to the target. These sequences are then exposed to the target again and the process is repeated several times, allowing for competitive binding between the sequences until the oligonucleotides with the desired binding affinity have been selected. The number of rounds required for identification depends upon the stringency of each round and on the nature of the target. Typically enrichment is reached in 8-15 cycles.[10] Once the starting pool has been reduced to a few highly binding oligonucleotides, the sequences are determined.

Once an aptamer is selected and sequenced, its 3-D structure is determined by methods such as NMR, X-ray crystallography, and circular dichroism (CD). The highly selective binding of aptamers to their targets is attributed to specific interactions (i.e. hydrogen bonds, electrostatic interactions and stacking)[78] between the target and the phosphate groups of the oligonucleotides backbone and the bases.[73] The 3-D structure of the aptamer (sequence specific) provides the scaffold for binding of the target. Many 3-D structures of single stranded oligonucleotides have been characterized, including stem-

loop bulge, psuedoknot, hairpin, and G-quartet. In order to form these structures, the minimal sequence required is usually 15-50 bases; therefore, the random region of the starting pool for SELEX must be at least 15 bases.[69]

Limitations on the applicability of aptamers as analytical reagents include their susceptibility to nuclease attack. However, the concerns of stability are more important for aptamers used in vivo (therapeutics) than for aptamers used in sensor applications.[69] DNA can be stored for long periods of time without degradation in a laboratory setting, unlike antibodies which typically lose activity after long periods of storage.

Aptamers offer several advantages as alternatives for antibodies in biosensing applications. Once isolated, aptamers are more easily manufactured than antibodies, as they are produced synthetically by automated methods instead of involving animals and in vivo conditions. The synthetic production of aptamers allows them to be produced with extreme accuracy and reproducibility, unlike antibodies that are prone to batch to batch variations.[10] In addition, the synthetic production of aptamers allows them to be manipulated easily (i.e. attach enzymes or dyes) without changing the activity of the aptamer. The conformation stability and small nature of aptamers allows an increase in surface coverage and reduction of steric hindrance, possibly improving biosensor sensitivity. Also, the attachment of oligonucleotides to surfaces has been demonstrated to be very reproducible.[10] Aptamer conformation can be regenerated after denaturation through control of buffer and ion compositions, unlike antibodies whose activity cannot be restored after denaturation. Finally, aptamers can be generated for a greater number of targets than antibodies including toxic and non-immunogenic analytes,[10] and can be

selected in a wide range of conditions including non-physiological buffers and temperatures.[10]

Biosensors are only as good as the selectivity and affinity of the molecular recognition element they rely upon.[10, 71, 79] Since aptamers offer similar characteristics as antibodies but are more readily manufactured, they are well-poised to serve as replacements for biosensing applications, including therapeutics and diagnostics.[10] Many of the same traditional readout methods for immunoassays using antibodies have been explored using aptamers including radio isotopic,[80] fluorescence,[81-84] and enzyme[85-88] labeling. Other methods for detection include quartz crystal microbalance (QCM),[79, 89] and molecular beacons.[90, 91] Electrochemical detection has become a popular method for assays with aptamers because of the high sensitivity, fast response and low cost of electrochemical methods.[92-96] Typical electrochemical detection systems require labeling of the recognition moiety with an electrochemically active species. Aptamers can be more readily labeled with such species than antibodies, without loss of activity. An aptamer-based electrochemical sensor for platelet-derived growth factor has recently been shown to have picomolar sensitivity in complex clinical samples.[97]

Two-site binding assays (sandwich immunoassays) have been developed using aptamers as both recognition moieties and combining antibodies and aptamers for recognition.[10] Fluorescence detection using aptamers has been studied extensively and found to be highly sensitive and selective.[81-83] Aptamers have been used in a variety of biosensing platforms and have recently been extended to sensor arrays for the detection of proteins, proving to be superior over protein arrays by their ability to be regenerated multiple times.[98, 99] Fluorescence detection in an array format using aptamers has been

shown to simultaneously detect three cancer-associated proteins.[100] Aptamers have the potential to dramatically change sensor development by providing detection systems with tailor designed characteristics that can be applied to unlimited analytes in a variety of matrixes.[101]

One consideration when applying aptamers to biosensing platforms is that the optimal conditions for using the aptamer must be delineated for every assay. Unlike antibodies, aptamers do not have a universal set of conditions (physiological) for optimal performance.[88] For instance, the binding buffer composition must be optimized to include the appropriate ionic strength[83] as well as temperature and immobilization procedures.[87] Ionic strength typically has a large effect on aptamer performance, and therefore additions of cations such as Mg^{2+} and K^{+} must be examined. Each aptamer possesses a unique set of condition requirements to provide the most sensitive assay performance.[87]

Dissertation Overview

Based on the themes discussed above, this dissertation explores ways to improve upon immunoassay methods using AFM and SERS as readout techniques. Each of the following chapters is presented as an individual manuscript that describes the research efforts in improving immunoassay protocols, including antibody screening, assay time reduction, sample concentration, and aptamers as alternative reagents. Chapter 1 begins with describing the optimization of a universal protocol for virus detection with AFM readout, and use of this protocol to screen for the most sensitive antibodies for the detection method. Chapter 2 extends this concept by exploring elevated temperatures as a

means to decrease incubation times. Small substrates and large sample volumes are employed in Chapter 3, along with SERS, to achieve attomolar detection limits of PPV. Aptamers are explored in Chapter 4 as replacements for antibodies using SERS as a readout method. The dissertation is concluded with a summary of the research presented and a discussion of the future directions of the work.

References

(1) Yalow, R. S.; Berson, S. A. *Nature* **1959**, *184*, 1648-9.

(2) Sokoll, L. J.; Chan, D. W. *Anal. Chem.* **1999**, *71*, 356-62.

(3) Clemente, A.; Chambers, S. J.; Lodi, F.; Nicoletti, C.; Brett, G. M. *Food Control* **2004**, *15*, 65-9.

(4) Samira Sarter, N. Z. *Luminescence* **2004**, *19*, 345-51.

(5) Yu, Y.-Y.; Wang, Q.-E.; Zhuang, H.-S. *Anal. Lett.* **2006**, *39*, 937 - 46.

(6) Mauriz, E.; Calle, A.; Lechuga, L. M.; Quintana, J.; Montoya, A.; Manclus, J. J. *Analytica Chemica Acta* **2006**, *561*, 40-7.

(7) Mauriz, E.; Calle, A.; Montoya, A.; Lechuga, L. M. *Talanta* **2006**, *69*, 359-64.

(8) Hage, D. S. *Anal. Chem.* **1999**, *71*, 294R-304R.

(9) Diamandis, E. P.; Christopoulos, T. K. *Immunoassay*; Academic Press: San Diego, 1996.

(10) Jayasena, S. D. *Clin. Chem.* **1999**, *45*, 1628-50.

(11) Wians, F. H.; Dev, J.; Powell, M. M.; Heald, J. I. *Clin. Chem.* **1986**, *32*, 887-90.

(12) White, S. R.; Chiu, N. H. L.; Christopoulos, T. K. *Methods* **2000**, *22*, 24-32.

(13) Van Weemen, B. K.; Schuurs, A. H. W. M. *FEBS Lett.* **1971**, *15*, 232-6.

(14) Diamandis, E. P.; Christopoulos, T. K. *Anal. Chem.* **1990**, *62*, 1149A-57A.

(15) Amro, N. A.; Kotra, L. P.; Wadu-Mesthrige, K.; Bulychev, A.; Mobashery, S.; Liu, G.-y. *Langmuir* **2000**, *16*, 2789-96.

(16) Kuznetsov, Y. G.; Malkin, A. J.; Lucas, R. W.; Plomp, M.; McPherson, A. *J. Gen. Virol.* **2001**, *82*, 2025-34.

(17) Silva, L. P. *Curr. Protein Peptide Sci.* **2005**, *6*, 387-95.

(18) O'Brien, J. C.; Jones, V. W.; Porter, M. D. *Anal. Chem.* **2000**, *72*, 703-10.

(19) Jones, V. W.; Kenseth, J. R.; Porter, M. D.; Mosher, C. L.; Henderson, E. *Anal. Chem.* **1998**, *70*, 1233-41.

(20) Perrin, A.; Lanet, V.; Theretz, A. *Langmuir* **1997**, *13*, 2557-63.

(21) Perrin, A.; Theretz, A.; Mandrand, B. *Anal. Biochem.* **1998**, *256*, 200-6.

(22) Wadu-Mesthrige, K.; Xu, S.; Amro, N. A.; Liu, G.-y. *Langmuir* **1999**, *15*, 8580-3.

(23) Wadu-Mesthrige, K.; Amro, N. A.; Garno, J. C.; Xu, S.; Liu, G.-y. *Biophys. J.* **2001**, *80*, 1891-9.

(24) Davies, J.; Roberts, C. J.; Dawkes, A. C.; Sefton, J.; Edwards, J. C.; Glasbey, T. O.; Haymes, A. G.; Davies, M. C.; Jackson, D. E.; et al. *Langmuir* **1994**, *10*, 2654-61.

(25) Johnson, J. C.; Nettikadan, S. R.; Vengasandra, S. G.; Henderson, E. *J. Biochem. Biophys. Meth.* **2004**, *59*, 167-80.

(26) Dammer, U.; Hegner, M.; Anselmetti, D.; Wagner, P.; Dreier, M.; Huber, W.; Guntherot, H.-J. *Biophysical Journal* **1996**, *70*, 2437-41.

(27) Allen, S.; Chen, X.; Davies, J.; Davies, M. C.; Dawkes, A. C.; Edwards, J. C.; Roberts, C. J.; Sefton, J.; Tendler, S. J. B.; Williams, P. M. *Biochemistry* **1997**, *36*, 7457-63.

(28) Chen, X.; Davies, M. C.; Roberts, C. J.; Tendler, S. J. B.; Williams, P. M.; Davies, J.; Dawkes, A. C.; Edwards, J. C. *Langmuir* **1997**, *13*, 4106-11.

(29) Takano, H.; Kenseth, J. R.; Wong, S.-S.; O'Brien, J. C.; Porter, M. D. *Chem. Rev.* **1999**, *99*, 2845-90.

(30) Stuart, J. K.; Hlady, V. *Langmuir* **1995**, *11*, 1368-74.

(31) Allen, S.; Davies, J.; Dawkes, A. C.; Davies, M. C.; Edwards, J. C.; Parker, M. C.; Roberts, C. J.; Sefton, J.; Tendler, S. J. B.; Williams, P. M. *FEBS Lett.* **1996**, *390*, 161-4.

(32) Lee, G. U.; Kidwell, D. A.; Colton, R. J. *Langmuir* **1994**, *10*, 354-7.

(33) Moy, V. T.; Florin, E.-L.; Gaub, H. E. *Science* **1994**, *266*, 257-9.

(34) Kuznetsov, Y. G.; Low, A.; Fan, H.; McPherson, A. *Virology* **2004**, *323*, 189-96.

(35) Nettikadan, S. R.; Johnson, J. C.; Mosher, C.; Henderson, E. *Biochem. Biophys. Res. Commun.* **2003**, *311*, 540-5.

(36) van Noort, S. J. T.; van der Werf, K. O.; de Grooth, B. G.; Greve, J. *Biophys. J.* **1999**, *77*, 2295-303.

(37) Toshio Ando, N. K., Yasuyuki Naito, Tatsuya Kinoshita, Ken'ya Furuta, Yoko Y. Toyoshima, *Chem. Phys. Chem.* **2003**, *4*, 1196-202.

(38) Ried, R. P.; Mamin, H. J.; Terris, B. D.; Fan, L.-S.; Rugar, D. *J. Microelectromech. Sys.* **1997**, *6*, 294-302.

(39) Kodera, N.; Sakashita, M.; Ando, T. *Rev. Sci. Inst.* **2006**, *77*, 083704.

(40) Fantner, G. E.; Schitter, G.; Kindt, J. H.; Ivanov, T.; Ivanova, K.; Patel, R.; Holten-Andersen, N.; Adams, J.; Thurner, P. J.; Rangelow, I. W.; Hansma, P. K. *Ultramicrosc.* **2006**, *106*, 881-7.

(41) Sulchek, T.; Yaralioglu, G. G.; Quate, C. F. *Rev. Sci. Inst.* **2002**, *73*, 2928-36.

(42) Akiyama, T.; Staufer, U.; Rooij, N. F. d. *Rev. Sci. Inst.* **2002**, *73*, 2643-6.

(43) Driskell, J. D.; Kwarta, K. M.; Lipert, R. J.; Porter, M. D.; Neill, J. D.; Ridpath, J. F. *Anal. Chem.* **2005**, *77*, 6147-54.

(44) Grubisha, D. S.; Lipert, R. J.; Park, H.-Y.; Driskell, J.; Porter, M. D. *Anal. Chem.* **2003**, *75*, 5936-43.

(45) Ni, J.; Lipert, R. J.; Dawson, G. B.; Porter, M. D. *Anal. Chem.* **1999**, *71*, 4903-8.

(46) Dou, X.; Takama, T.; Yamaguchi, Y.; Yamamoto, H.; Ozaki, Y. *Anal. Chem.* **1997**, *69*, 1492-5.

(47) Xu, S.; Ji, X.; Xu, W.; Li, X.; Wang, L.; Bai, Y.; Zhao, B.; Ozaki, Y. *Analyst* **2004**, *129*, 63-8.

(48) Mulvaney, S. P.; Musick, M. D.; Keating, C. D.; Natan, M. J. *Langmuir* **2003**, *19*, 4784-90.

(49) Zhang, X.; Young, M. A.; Lyandres, O.; VanDuyne, R. P. *J. Am. Chem. Soc.* **2005**, *127*, 4484-9.

(50) Cao, Y. C.; Jin, R.; Mirkin, C. A. *Science* **2002**, *297*, 1536-40.

(51) Faulds, K.; Smith, W. E.; Graham, D. *Anal. Chem.* **2004**, *76*, 412-7.

(52) Cui, Y.; Ren, B.; Yao, J.-L.; Gu, R.-A.; Tian, Z.-Q. *J. Phys. Chem. B* **2006**, *110*, 4002-6.

(53) Rohr, T. E.; Cotton, T.; Fan, N.; Tarcha, P. J. *Anal. Biochem.* **1989**, *182*, 388-98.

(54) Kusnezow, W.; Syagailo, Y. V.; Goychuk, I.; Hoheisel, J. D.; Wild, D. G. *Expert Review of Molecular Diagnostics* **2006**, *6*, 111-24.

(55) Frackelton, A., Jr; Weltman, J. *J Immunol* **1980**, *124*, 2048-54.

(56) Stenberg, M.; Nygren, H. *J. Theor. Biol.* **1985**, *113*, 589-97.

(57) Stenberg, M.; Stiblert, L.; Nygren, H. k. *J. Theor. Biol.* **1986**, *120*, 129-40.

(58) Nygren, H.; Werthen, M.; Stenberg, M. *J. Immunol. Meth.* **1987**, *101*, 63-71.

(59) Myszka, D. G.; Morton, T. A.; Doyle, M. L.; Chaiken, I. M. *Biophys. Chem.* **1997**, *64*, 127-37.

(60) Sheehan, P. E.; Whitman, L. J. *Nano Lett.* **2005**, *5*, 803-7.

(61) Ewalt, K. L.; Haigis, R. W.; Rooney, R.; Ackley, D.; Krihak, M. *Anal. Biochem.* **2001**, *289*, 162-72.

(62) Yang, J. M.; Bell, J.; Huang, Y.; Tirado, M.; Thomas, D.; Forster, A. H.; Haigis, R. W.; Swanson, P. D.; Wallace, R. B.; Martinsons, B.; Krihak, M. *Biosens. Bioelectron.* **2002**, *17*, 605-18.

(63) Pribyl, M.; Snita, D.; Hasal, P.; Marek, M. *Chem. Eng. J.* **2004**, *101*, 303-14.

(64) Driskell, J. D.; Kwarta, K. M.; Lipert, R. J.; Vorwald, A.; Neill, J. D.; Ridpath, J. F.; Porter, M. D. *J. Virol. Meth.* **2006**, *138*, 160-9.

(65) Johnstone, R. W.; Andrew, S. M.; Hogarth, M. P.; Pietersz, G. A.; McKenzie, I. F. C. *Molec. Immunol.* **1990**, *27*, 327-33.

(66) Robertson, D. L.; Joyce, G. F. *Nature* **1990**, *344*, 467.

(67) Ellington, A. D.; Szostak, J. W. *Nature* **1990**, *346*, 818-22.

(68) Tuerk, C.; Gold, L. *Science* **1990**, *249*, 505-10.

(69) McGown, L. B.; Joseph, M. J.; Pitner, J. B.; Vonk, G. P.; Linn, C. P. *Anal. Chem.* **1995**, 633 A-68 A.

(70) Gold, L.; Polisky, B.; Uhlenbeck, O.; Yarus, M. *Annu. Rev. Biochem.* **1995**, *64*, 763-97.

(71) Clark, S. L.; Remcho, V. T. *Electrophoresis* **2002**, *23*, 1335-40.

(72) Famulok, M.; Mayer, G. **1998**, 123-36.

(73) Wilson, D. S.; Szostak, J. W. *Annu. Rev. Biochem.* **1999**, *68*, 611-47.

(74) Gold, L. *The Harvey Lectures* **1997**, *91*, 47-57.

(75) Famulok, M.; Mayer, G.; Blind, M. *Acc. Chem. Res.* **2000**, *33*, 591-9.

(76) Jenison, R. D.; Gill, S. C.; Pardi, A.; Polisky, B. *Science* **1994**, *263*, 1425-9.

(77) Geiger, A.; Burgstaller, P.; von der Eltz, H.; Roeder, A.; Famulok, M. *Nucl. Acids Res.* **1996**, *24*, 1029-36.

(78) Hermann, T.; Patel, D. J. *Science* **2000**, *287*, 820-5.

(79) Tombelli, S.; Minunni, M.; Luzi, E.; Mascini, M. *Bioelctrochem.* **2005**, *67*, 135-41.

(80) Conrad, R.; Ellington, A. D. *Anal. Biochem.* **1996**, *242*, 261-5.

(81) Potyrailo, R. A.; Conrad, R. C.; Ellington, A. D.; Hieftje, G. M. *Anal. Chem.* **1998**, *70*, 3419-25.

(82) German, I.; Buchanan, D. D.; Kennedy, R. T. *Anal. Chem.* **1998**, *70*, 4540-5.

(83) Fang, X.; Cao, Z.; Beck, T.; Tan, W. *Anal. Chem.* **2001**, *73*, 5752-7.

(84) Lee, M.; Walt, D. R. *Anal. Biochem.* **2000**, *282*, 142-6.

(85) Drolet, D. W.; Moon-McDermott, L.; Romig, T. S. **1996**, *14*, 1021-5.

(86) Yoshida, W.; Sode, K.; Ikebukuro, K. *Anal. Chem.* **2006**, *78*, 3296-303.

(87) Baldrich, E.; Restrepo, A.; O'Sullivan, C. K. *Anal. Chem.* **2004**, *76*, 7053-63.

(88) Baldrich, E.; Acero, J. L.; Reekmans, G.; Laureyn, W.; O'Sullivan, C. K. *Anal. Chem.* **2005**, *77*, 4774-84.

(89) Hianik, T.; Ostatna, V.; Zajacova, Z.; Stoikova, E.; Evtugyn, G. *Bioorgan. Med. Chem. Lett.* **2005**, *15*, 291-5.

(90) Li, J. J.; Fang, X.; Tan, W. *Biochem. Biophys. Res. Commun.* **2002**, *292*, 31-40.

(91) Hamaguchi, N.; Ellington, A.; Stanton, M. *Anal. Biochem.* **2001**, *294*, 126-31.

(92) Ikebukuro, K.; Kiyohara, C.; Sode, K. *Anal. Lett.* **2004**, *37*, 2901 - 9.

(93) Josep Lluis Acero Sánchez, E. B., Abd El-Gawad Radi, Srujan Dondapati, Pablo Lozano Sánchez, Ioanis Katakis, Ciara K. O'Sullivan, *Electroanalysis* **2006**, *18*, 1957-62.

(94) Radi, A.-E.; AceroSanchez, J. L.; Baldrich, E.; O'Sullivan, C. K. *J. Am. Chem. Soc.* **2006**, *128*, 117-24.

(95) Mir, M.; Vreeke, M.; Katakis, I. *Electrochem. Commun.* **2006**, *8*, 505-11.

(96) Radi, A.-E.; AceroSanchez, J. L.; Baldrich, E.; O'Sullivan, C. K. *Anal. Chem.* **2005**, *77*, 6320-3.

(97) Lai, R. Y.; Plaxco, K. W.; Heeger, A. J. *Anal. Chem.* **2007**, *79*, 229-33.

(98) Kirby, R.; Cho, E. J.; Gehrke, B.; Bayer, T.; Park, Y. S.; Neikirk, D. P.; McDevitt, J. T.; Ellington, A. D. *Anal. Chem.* **2004**, *76*, 4066-75.

(99) Li, Y.; Lee, H. J.; Corn, R. M. *Nucl. Acids Res.* **2006**, *34*, 6416-24.

(100) McCauley, T. G.; Hamaguchi, N.; Stanton, M. *Anal. Biochem.* **2003**, *319*, 244-50.

(101) O'Sullivan, C. K. *Anal. Bioanal. Chem.* **2002**, *372*, 44-8.

CHAPTER 1: HETEROGENEOUS IMMUNOASSAYS UTILIZING ATOMIC FORCE MICROSCOPY AS A READOUT METHOD: EVALUATION OF MONOCLONAL ANTIBODIES FOR FELINE CALICIVIRUS AND PORCINE PARVOVIRUS

A manuscript in preparation for submission to *Journal of Virological Methods*

Karen M. Kwarta, Jeremy D. Driskell, and Marc D. Porter*

Institute for Combinatorial Discovery, Departments of Chemistry and Chemical and Biological Engineering, Ames Laboratory-U.S. DOE, Iowa State University, Ames, Iowa 50011-3020

*Current address: Center for Combinatorial Sciences, Biodesign Institute, Department of Chemistry and Biochemistry, Arizona State University, Tempe, AZ 85287

John D. Neill and Julia F. Ridpath

Virus and Prion Diseases of Livestock Unit, National Animal Disease Center, United States Department of Agriculture, Ames, Iowa 50010

ABSTRACT

The ultrahigh resolution imaging capabilities of atomic force microscopy (AFM) is explored as a readout method for the detection of viruses and as a tool to screen the performance of monoclonal antibodies (mAbs) for solid-phase immunoassays. This paper

demonstrates that AFM is a potentially powerful readout method for viral pathogens, using feline calicivirus (FCV) and porcine parvovirus (PPV) as test systems. The viruses are captured directly via specific mAbs and quantified in a label free assay via AFM. The effectiveness of the platform was evaluated through assessment of cross-reactivity and non-specific binding. The results show that the capture substrate is specific for the virus of interest, and blocking of the solid-phase is not necessary for FCV detection. After specificity was established, mAbs for each virus were screened, and limits of detection were determined. Dose-response curves using the most effective antibodies are linear with a detection limit of 3.2×10^6 $TCID_{50}$/mL for FCV and 6.4×10^4 $TCID_{50}$/mL for PPV. Finally, insights into the effect of sample volume and solution depletion were made from preliminary data.

INTRODUCTION

Medical and veterinary hospitals demand rapid, sensitive, and specific diagnosis techniques to detect a wide range of bacterial and viral pathogens.[1] The methods available today for virus detection and quantification (e.g., immunosorbent electron microscopy,[2, 3] ELISA,[4, 5] PCR,[6-11] tissue culture infective dose ($TCID_{50}$),[12] fluorescent immunoassay,[13, 14] high frequency nanoelectromechanical devices[15] and serological testing[14]), however, tend to lack the speed and sensitivity necessary to mount a rapid response in the event of an outbreak. As a potential means to address this need, we have developed a label free, specific, and reproducible methodology for the detection of viral

pathogens utilizing the nanometric imaging capabilities of atomic force microscopy (AFM).

AFM, as an ultra high resolution imaging tool, not only can be used to enumerate biological objects[16] like viruses, but also can be used to distinguish differences based on size and shape. Immunoassays utilizing AFM for readout have been performed previously for the detection of immunoglobulin G molecules[17, 18] and for the detection of the capsid proteins of viruses.[19] Although previous reports have shown that AFM can be used to image whole viruses,[20, 21] there are few reports of immunoassays that make use of AFM to detect and quantitate whole viruses from complex solutions.[22] We therefore seek to exploit AFM as a readout method by drawing on its potential versatility for the label-free, size/shape-based detection of whole virues. We suggest that size-based discrimination may: (1) be beneficial by providing a means to minimize sample complications from non-specific adsorption and (2) simplify procedures by elimination of a labeling step.

The solid-phase assay platform herein employs an antibody-modified substrate to selectively capture viruses, which are then imaged and enumerated by AFM. Feline calicivirus (FCV) and porcine parvovirus (PPV) are employed to test the merits of AFM as a virus detection method. Both viruses are non-enveloped and have well defined spherical structures (diameter of 36 nm for FCV and 25 nm for PPV).[23] By establishing procedures for the detection of these model systems, we speculate that the protocol will be readily translatable to viruses with shared morphological similarities such as human caliciviruses, noroviruses, and saporviruses.[24]

The proposed method utilizes monoclonal antibodies (mAbs) that are covalently immobilized on a nanometrically smooth gold substrate via a thiolate adlayer, which is formed from a coupling agent, dithiobis(succinimidyl propionate) (DSP), as shown in Scheme 1. After mAb immobilization, the capture substrate is exposed to the virus solution. This step selectively extracts viruses from the sample solution. Finally, the substrates are rinsed, dried, and imaged with AFM. The simplicity of the assay platform allows for fast, accurate analysis of mAb specificity and sensitivity.

In order to further evaluate the capabilities of this strategy, AFM was used as a tool to study non-specific interactions as well as the effectiveness of antigen-antibody interactions in solid-phase immunoassays. To assess non-specific binding, bovine serum albumin (BSA) was employed as a blocking agent, a competitive assay was performed, and the cross-reactivity of the capture substrate was analyzed. Several antibodies for FCV and PPV were screened to evaluate the performance of the antibodies in a heterogeneous assay platform.

Methods for antibody screening include enzyme-linked immunoadsorbent assay (EIA),[25-27] kinetic exclusion fluorescence immunoassay (KinExA),[28] fluorescence photobleaching,[29] and immunoprecipitation of radiolabeled antigen.[30] Some of these methods chemically modify the mAb or antigen (e.g., radioimmunoassay and fluorescent immunoassays) which may affect the antibody-antigen interaction. Other methods require a secondary labeling step to measure the free antibody (e.g., EIA, and KinExA). AFM offers advantages over these methods by not requiring modification of either the antibody or antigen and providing a direct measure of the antibody-antigen complex. Affinity of the mAbs may be influenced by the assay conditions used,[27] and the straightforwardness

of the AFM detection platform allows assay conditions to be changed to reflect the antibody affinity under a variety of conditions.[31]

EXPERIMENTAL

Reagents. FCV (titer 5.0 x 10^8 $TCID_{50}$/mL) and PPV (titer 3.2 x 10^9 $TCID_{50}$/mL, 4.48 x 10^{12} PPV/mL[32]) were obtained from National Animal Disease Center (NADC). Monoclonal antibodies (mAbs) were supplied by NADC, purified with a protein G column (Bio-Rad) and were stored in 10 mM phosphate buffered saline (PBS). FCV mAbs are designated 2D10-1C4, 3B12-1C8, and 4G1-2F4, while mAbs for PPV have the identifiers #3, #8, and #9. DSP, PBS packs, BSA and octadecanethiol (ODT) were obtained from Sigma-Aldrich. Poly(dimethylsiloxane) (PDMS) Dow Corning Sulgard 184 was from Ellsworth Adhesives. Contrad 70, used for cleaning glass, was provided by Decon Labs, and two-part epoxy (EpoTek 377) used for making template stripped gold (TSG), was from Epoxy Technology. Borate buffer packs were from Pierce, and all buffers were passed through a 0.22-μm syringe filter (Costar) before use.

Preparation of TSG. Capture substrates were prepared using TSG. TSG has a roughness factor of 0.6 nm, which provides a sufficiently smooth "background" for the size/shape identification of FCV and PPV by AFM. The TSG was constructed by resistively evaporating 250 nm of gold (purity 99.9%) onto a clean p-type silicon wafer (University Wafer 4" (111)) using an Edwards 306A resistive metal evaporator at a deposition rate of 0.1 nm/s. Microscope slides were cut into 1 x 1 cm glass chips and then were sequentially cleaned ultrasonically in dilute surfactant solution (Contrad 70), deionized water, and ethanol for 30 min each. Epoxy was applied to the clean glass chips,

and the chip was placed epoxy-side down on the gold coated silicon wafer, and cured at 150 ˚C for 105 min. The glass chips were gently removed from the silicon wafer, leaving a flat layer of gold on top of the glass chips.

Capture Substrate Preparation. The 1 x 1 cm TSG pieces were immediately used to create an antibody-coated capture substrate. First, PDMS was cast over a fluorine-terminated p-type silicon wafer and cut into a 1 x 2 cm piece with a 3-mm circular well in the center. The PDMS stamp was soaked in a 1-mM ethanolic ODT solution for 1 min, dried with high-purity nitrogen, and then placed on the TSG pieces for ~ 30 s. This step creates a hydrophobic monolayer of ODT on the gold substrate with a bare gold spot[33-35] that confines small volumes of aqueous samples to a small area, minimizing material consumption. Substrates were rinsed with ethanol, dried with a stream of high purity nitrogen, and soaked in a 0.1 mM ethanolic solution of DSP for ~12 h. This procedure forms a 3-mm diameter adlayer of a succinimide ester terminated monolayer that can be used to covalently bind antibodies via an amide linkage.[17, 36-38] After adlayer preparation, the samples are rinsed with ethanol and dried under a stream of high purity nitrogen.

Anti-FCV and anti-PPV mAbs were covalently immobilized through coupling to the terminal succinimidyl ester of the DSP-derived monolayer[17, 37, 38] by applying 20 μL of the protein solution (100 μg/mL in 50 mM borate buffer (pH 8.5)) onto the substrate and reacting for ~8 h at room temperature in a humidity chamber. The surface concentration of each mAb is assumed to be the same because each antibody was purified to 99.9% with a protein G column before immobilization to the capture substrate. Afterwards, the substrates were rinsed three times with 2.5 mL 10 mM PBS (pH 7.4),

followed by addition of 20 μL of the virus solution and incubation for ~16 h in a humidity chamber. FCV was diluted in cell culture media, while PPV was diluted in 10 mM PBS. Finally, the substrates were rinsed three times with 2.5 mL of 10 mM PBS (pH 7.4), and once with a 3-s stream of deionized water to remove salt residue. Residue removal facilitated AFM enumeration. Finally, substrates were dried with a stream of high purity nitrogen.

For the blocking studies, the capture substrate was exposed to varying concentrations of BSA, diluted in 10 mM PBS, for ~16 h. BSA solutions were rinsed from the capture substrates three times with 2.5 mL of 10 mM PBS. Specificity studies were performed using anti-San Miguel sea-lion virus mAb (anti-SMSV) and anti-bovine viral diarrhea mAb (anti-BVD), mAbs that do not selectively bind to FCV or PPV.[4, 5, 23, 39] Competitive assays were performed using a 50-μL solution of FCV, inoculated with differing concentrations of anti-FCV mAb in 10 mM PBS for 8 h. The inoculated FCV solution was then exposed to the anti-FCV capture substrate for ~8 h.

Dose-response curves were constructed and repeated at least twice for each experiment. Error bars represent the standard deviation of the average number of viruses bound in 25 μm^2 from five different images on each sample.

Instrumentation. The substrates were characterized by collecting 5 x 5 μm AFM images with a MultiMode NanoScope IIIa SFM (Digital Instruments) equipped with a 150-μm scanner. Images were obtained under ambient conditions in TappingMode at a rate of 1.5 Hz, and the topography was recorded for further analysis. The setpoint oscillation amplitude was set to 80% of the free oscillation amplitude. Images were collected with n(+)-silicon TESP cantilever/tips (Nanosensors) with a length of 118 nm, a

width of 27-29 nm, thickness of 3.6-4.5 nm, a spring constant of 32-70 N/m, and a resonant frequency of 327-421 kHz. The number of viruses bound in each image was counted manually using a pen style colony counter (Sigma).

RESULTS AND DISCUSSION

FCV was used to establish the most favorable assay conditions and to determine the specificity of the immunoassay format with AFM readout. Three tests were performed to evaluate the specificity of the assay, and the optimized conditions were used to identify the most effective monoclonal antibodies for FCV and PPV detection. Detailed calibration curves were employed to delineate limits of detection and potential methods for improving performance were examined.

Tests for Specificity

Test I. Effect of BSA Blocking. Several studies were performed to determine if non-specific binding of the capsid proteins on the FCV to the un-reacted succinimidyl groups of the DSP-derived monolayer would prove problematic. These tests employed BSA, a small protein that is ~10 times smaller than FCV. BSA is often used as a blocking agent in immunoassays to "fill in" parts of the solid phase that are not covered by the immobilized antibody, thereby reducing non-specific binding.[36]

Figure 1 shows AFM images of capture substrates blocked with different percentages of BSA for ~16 h and then exposed for ~8 h to a 5.0 x 10^8 $TCID_{50}$/mL solution of FCV. The FCV appear as spherical objects with an average height of ~22 nm (Figure 1). The size of the viruses is somewhat smaller than expected (36 nm) because of

dehydration. Irregularly shaped objects are also evident in the images, and are attributed to cell debris and other components of the diluting media. We add that the viruses appear to have varying sizes in the x-y (surface) plane. This observation is attributed to tip convolution effects, which reflect the subtle differences in the size and shape of the tip asperity.[40, 41] These results, importantly, demonstrate the ability of AFM to distinguish objects based upon their height, regardless of tip convolution effects.

The images in Figure 1 illustrate that there is little difference in the number of captured FCV when different percentages of BSA are used for blocking. The results have been summarized in Figure 2. The amount of captured FCV was not affected by BSA blocking at each concentration of FCV (5.0×10^7, 2.5×10^8, and 5.0×10^8 $TCID_{50}$/mL) tested. The addition of BSA does not appear to have an impact on the assay, as samples prepared without BSA treatment have approximately the same surface concentration as those modified by exposure to BSA, as seen in Figure 2. These results lead us to believe that non-specific interactions between FCV and any un-reacted groups at the terminus of the DSP-derived monolayer are minimal.

We suspect that this finding is a result of the complex matrix of the freeze/thaw lysate used for FCV dilution. The lystate contains many small proteins and other additives that could be acting as blocking agents, much like BSA, when the FCV is exposed to the capture substrate. The exposures to FCV solutions without BSA blocking support this claim. We conclude from these results that blocking of the solid-phase is not required for FCV detection with AFM.

Test II. Competitive Assay. In order to further ensure that FCV binding to the capture substrate is due to specific mAb interactions, a competitive assay was performed

in which a standard solution of FCV was mixed with varying amounts of anti-FCV mAbs before exposure to the capture substrate. The ability of FCV to bind to the capture substrate should, therefore, progressively diminish as the number of epitopes on FCV available for binding decreases. The amount of anti-FCV mAb needed to fully coat all of the FCV epitopes was estimated as 4.5×10^{12} mAbs, given 50 μL of an FCV concentration of 5.0×10^{9} $TCID_{50}$/mL and 180 epitopes per FCV. Since the concentration of FCV is given in units of $TCID_{50}$/mL and not virus particles/mL, the number of molecules of anti-FCV mAb inoculated with FCV was varied from 1.0×10^{14} to 2.0×10^{10}.

The results of the competitive assay are presented in Figure 3. As anti-FCV mAb is added to the FCV solution, the number of captured FCV undergoes a dramatic reduction between 5×10^{11} and 1×10^{12} molecules of anti-FCV. At the highest concentration of anti-FCV mAb only an average of 11 viruses were bound in a 25-μm^2 area. At the lowest concentration of anti-FCV mAb, on average 375 viruses were bound in the same area. These results confirm that FCV is binding to the capture substrate through specific interactions between the epitopes on the FCV and the surface bound mAb.

These results also allow an estimation of the FCV concentration in number of virus particles/mL. Since the concentration of mAb required to fully coat all the FCV in the 50 μL sample can be determined from Figure 3, we can then calculate how many FCV particles are in the sample. At a concentration of 1.0×10^{12} mAbs, most of the FCV have been coated, giving rise to an FCV concentration of 1.1×10^{11} particles/mL. This

calculated concentration is 20 times larger than the $TCID_{50}$/mL value, meaning that every $TCID_{50}$ unit is the equivalent of ~20 virus particles.

Test III. Antibody Specificity. Lastly, the specificity (i.e., cross-reactivity) of the capture substrate was evaluated by constructing capture substrates with antibodies not produced for FCV. Figure 4 shows images of anti-SMSV mAb and anti-BVD capture substrates exposed to 5.0 x 10^8 $TCID_{50}$/mL of FCV. The anti-SMSV mAb is specific for a part of the capsid protein unique to SMSV but is not specific for an antigenic site common to the calicivirus family.[4, 5, 23] Anti-BVD mAb is specific for viruses that are unrelated to FCV.[36, 39] As seen in Figure 4, few FCV bind to either surface, showing that neither capture substrate takes up FCV, and confirming that the capture substrates are specific for FCV.

Dose-Response Curves and Limits of detection (LODs)

Dose-Response Curves. For each virus, several mAbs were screened for effectiveness. Three different mAbs for FCV and PPV, immobilized on capture substrates, were tested by developing separate dose-response curves. As found earlier, the viruses appear in Figure 5 as spherical objects with average heights of ~22 nm for FCV and ~17 nm for PPV. Figure 5A was collected using anti-FCV mAb 2D10-1C4 and a FCV concentration of 2.5 x 10^8 $TCID_{50}$/mL. Figure 5B utilized anti-PPV mAb #9 and a PPV concentration of 1.6 x 10^7 $TCID_{50}$/mL.

Dose-response curves, based on the AFM images, for each antibody are shown in Figure 6. The slopes of the dose-response curves are related to the binding affinities of the mAbs, and therefore can be used to identify the most effective antibody for this detection platform. Test solutions for FCV spanned from 2.5 x 10^8 to

5.0 x 10^6 $TCID_{50}$/mL and were diluted in freeze/thaw lysate media for FCV. PPV dilutions were carried out in 10 mM PBS and ranged from 1.6 x 10^7 to 3.2 x 10^5 $TCID_{50}$/mL. Figure 6 demonstrates that the most sensitive and effective anti-FCV mAb is 2D10-1C4, and the least sensitive is 4G1-2F4. While the differences in sensitivity are not nearly as pronounced for PPV as for FCV, the most sensitive mAb for PPV is anti-PPV mAb #9.

The differences in the dose-response curves for the different antibodies can be due to many factors, including a conformational change to the mAb when immobilized, which may cause a loss in activity.[30] Additionally, each mAb binds to different epitopes of the viruses, and these antigenic sites may be altered or blocked when immobilized, which would also result in a change of activity.[36] Some mAbs may undergo these changes more than others, and AFM offers a unique method to test the activity of individual immobilized Abs.

From the dose-response curves in Figure 6, limits of detection (LODs) for each mAb were determined. The LOD is defined as the concentration of virus that can be determined above the average blank signal plus three times the standard deviation of the blank samples. The blank signals are attributed to particles in solution that have a similar size and shape as the viruses, and also from contamination of the transfer pipettes. These data translate to a LOD of 3.2 x 10^6 $TCID_{50}$/mL for anti-FCV mAb 2D10-1C4, which is competitive with other methods of virus detection (e.g., 10^5 viruses/mL for fluorescence[13] and 10^8 viruses/mL for AFM detection[22]). For anti-FCV mAb 3B12-C8 the LOD is 6.9 x 10^6 $TCID_{50}$/mL and for anti-FCV mAb 4G1-2F4, the LOD is determined to be 3.2 x 10^7 $TCID_{50}$/mL, which follow intuitively from the dose-response curves. A LOD

for PPV is calculated for mAb #9 to be 6.4 x 10^4 $TCID_{50}$/mL and 6.5 x 10^4 $TCID_{50}$/mL for mAb #3. The mAbs #8 for PPV has a LOD of 8.6 x 10^4 $TCID_{50}$/mL. These results establish the performance of the mAbs and demonstrate the usefulness of AFM as a screening tool.

Given the calculated conversion of $TCID_{50}$/mL for FCV of 20, the LOD achieved for FCV is 6.4 x 10^7 virus particles/mL. The conversion factor for PPV from $TCID_{50}$/mL to virus particles is 1400 (derived by fitting experimental curves of PPV accumulation with respect to rotation rate),[32] yielding a LOD of 9.0 x 10^7 virus particles/mL. Readout by AFM is not the limiting factor in determining these LODs. In theory, AFM is able to detect a single binding event; the challenge arises from finding that single binding event on the relatively large capture area. Also, the capture of small numbers of viruses in large volumes is time consuming unless steps are taken to increase the rate of transport to the surface. Additionally, the use of small volumes may cause depletion of the virus concentration in solution, which further slows diffusion and limits the number of viruses that can be extracted. These issues are being investigated in depth by our research team.

Improvement of LODs. As a preliminary investigation into improving limits of detection, larger volumes of FCV were exposed to the same 3-mm diameter capture substrate. Figure 7 shows AFM images of four different volumes exposed to the 3 mm substrate for ~16 h. The results clearly show that the exposure volume has a large effect on the number of viruses that bind. Figure 8 summarizes the findings from Figure 7, and demonstrates that the number of viruses bound increases with sample volume and then levels off at about 40 μL. We speculate that increases in sample volume and/or decreases in substrate area may provide a simple means of improving LODs. These data suggest

that by using a 40-μL sample volume the LOD could be improved by at least a factor of 2 over a 20-μL sample volume. Further investigations into this observation are currently being studied.

CONCLUSIONS

AFM has been shown as a valid readout method for detection of viral pathogens based on the size and shape of the virus. The LOD for FCV was shown to be 3.2×10^6 $TCID_{50}$/mL with a dynamic range of 2.5×10^6 to 2.5×10^8 $TCID_{50}$/mL. The LOD for PPV was found to be 6.4×10^4 with a dynamic range of 6.4×10^4 to 1.6×10^7 $TCID_{50}$/mL. The technique was also shown to be a sensitive method for antibody screening for mAbs used in solid phase immunoassays. The specificity of the method was fully investigated, and it was shown that a blocking step is not required for AFM readout with FCV. The utility of AFM as a readout method to investigate the factors that affect immunoassay performance, including mAb effectiveness and blocking reagents, has been demonstrated. Additionally, we have shown a method for estimating virus concentration in virus particles/mL based upon known mAb concentrations virus epitopes.

ACKNOWLEDGEMENTS

This work was supported through a grant from USDA-NADC and by the Institute for Combinatorial Discovery at Iowa State University. Karen M. Kwarta gratefully acknowledges the support of a Dow Chemical Fellowship. The Ames Laboratory is

operated for the US Department of Energy through Iowa State University under contract W-7405-eng-82.

REFERENCES

(1) Sokoll, L. J.; Chan, D. W. *Anal. Chem.* **1999**, *71*, 356-62.

(2) Kjeldsberg, E. *J. Virol. Meth.* **1986**, *14*, 321-33.

(3) Zheng, Y. Z.; Hyatt, A.; Wang, L. F.; Eaton, B. T.; Greenfield, P. F.; Reid, S. *J. Virol. Meth.* **1999**, *80*, 1-9.

(4) Tajima, T.; Yoshizaki, S.; Nakata, E.; Tohya, Y.; Ishiguro, S.; Fujikawa, Y.; Sugii, S. *J. Vet. Med. Sci.* **1998**, *60*, 155-60.

(5) Tajima, T.; Takeda, Y.; Tohya, Y.; Sugii, S. *J. Vet. Med. Sci.* **1998**, *60*, 753-5.

(6) Sykes, J. E.; Studdert, V. P.; Browning, G. F. *Arch. Virol.* **1998**, *143*, 1321-34.

(7) Ogilivie, M. *Rev. Med. Virol.* **2001**, *11*, 351-4.

(8) Mackay, I. M.; EArden, K. E.; Nitsche, A. *Nucl. Acid Res.* **2002**, *30*, 1292-305.

(9) Helps, C.; Lait, P.; Tasker, S.; Harbour, D. *J. Virol. Meth.* **2002**, *106*, 241-4.

(10) Helps, C.; Harbour, D. *J. Virol. Meth.* **2003**, *109*, 261-3.

(11) Sykes, J. E.; Allen, J. L.; Studdert, V. P.; Browning *Vet. Microbiology* **2001**, *81*, 95-108.

(12) Payment, P.; Trudel, M. *Methods and Techniques in Virology*; Marcel Dekker: New York, 1993.

(13) Donaldson, K. A.; Kramer, M. F.; Lim, D. V. *Biosens. Bioelectron.* **2004**, *20*, 322-7.

(14) Yoon, K.-J.; Iowa State Univeristy College of Veterinary Medicine: Ames, IA, 2004.

(15) Ilic, B.; Yang, Y.; Craighead, H. G. *App. Phys. Lett.* **2004**, *85*, 2604-6.

(16) Santos, N. C.; Castanho, M. A. R. B. *Biophys. Chem.* **2004**, *107*, 133-49.

(17) Jones, V. W.; Kenseth, J. R.; Porter, M. D.; Mosher, C. L.; Henderson, E. *Anal. Chem.* **1998**, *70*, 1233-41.

(18) Quist, A. P.; Bergman, A. A.; Reimann, C. T.; Oscarsson, S. O.; Sundqvist, B. U. R. *Scanning Microscopy* **1995**, *9*, 395-400.

(19) Browning-Kelley, M. E.; Wadu-Mesthrige, K.; Hair, V.; Liu, G. Y. *Langmuir* **1997**, *13*, 343-50.

(20) Kuznetsov, Y. G.; Malkin, A. J.; Lucas, R. W.; Plomp, M.; McPherson, A. *J. Gen. Virol.* **2001**, *82*, 2025-34.

(21) Kuznetsov, Y. G.; Low, A.; Fan, H.; McPherson, A. *Virol.* **2004**, *323*, 189-96.

(22) Nettikadan, S. R.; Johnson, J. C.; Mosher, C.; Henderson, E. *Biochem. Biophys. Res. Comm.* **2003**, *311*, 540-5.

(23) Gillespie, J. H.; Scott, F. W. *Advan. Vet. Sci. Comp. Med.* **1973**, *17*, 163-200.

(24) Green, K. Y.; Ando, T.; Balayan, M. S.; Berke, T.; Clarke, I. N.; Estes, M. K.; Matson, D. O.; Nakata, S.; Neill, J. D.; Studdert, M. J.; Thiel, H. J. *J. Infect. Dis.* **2000**, *181*, S322-S30.

(25) Beatty, J. D.; Beatty, B. G.; Vlahos, W. G. *J. Immunol. Meth.* **1987**, *100*, 173-9.

(26) Friguet, B.; Chaffotte, A. F.; Djavadi-Ohaniance, L.; Goldberg, M. E. *J. Immunol. Meth.* **1984**, *77*, 305-19.

(27) Schots, A.; Van der Leede, B. J.; De Jongh, E.; Egberts, E. *J. Immunol. Meth.* **1988**, *109*, 225-33.

(28) Xie, L.; Jones, R. M.; Glass, T. R.; Navoa, R.; Wang, Y.; Grace, M. J. *J. Immunol. Meth.* **2005**, *304*, 1-14.

(29) Kaufman, E. N.; Jain, R. K. *J. Immunol. Meth.* **1992**, *155*, 1-17.

(30) Friguet, B.; Fedorov, A.; Serganov, A. A.; Navon, A.; Goldberg, M. E. *Anal. Biochem.* **1993**, *210*, 344-50.

(31) Johnson, J. C.; Nettikadan, S. R.; Vengasandra, S. G.; Henderson, E. *J. Biochem. Biophys. Meth.* **2004**, *59*, 167-80.

(32) Driskell, J. D.; Kwarta, K. M.; Lipert, R. J.; Vorwald, A.; Neill, J. D.; Ridpath, J. F.; Porter, M. D. *J. Virol. Meth.* **2006**, *138*, 160-9.

(33) Kumar, A.; Whitesides, G. M. *App. Phys. Lett.* **1993**, *63*, 2002-4.

(34) Chen, C. S.; Mrksich, M.; Huang, S.; Whitesides, G. M.; Ingber, D. E. *Biotechnol. Prog.* **1998**, *14*, 356-63.

(35) Libioulle, L.; Bietsch, A.; Schmid, H.; Michel, B.; Delamarche, E. *Langmuir* **1999**, *15*, 300-4.

(36) Diamandis, E. P.; Christopoulos, T. K. *Immunoassay*; Academic Press: London, 1996.

(37) Wagner, P.; Hegner, M.; Kernene, P.; Zaugg, F.; Semenza, G. *J. Biophys.* **1996**, *70*, 2052-66.

(38) Duhachek, S. D.; Kenseth, J. R.; Casale, G. P.; Small, G. J.; Porter, M. D.; Jankowiak, R. *Anal. Chem.* **2000**, *72*, 3709-16.

(39) Azimzadeh, A.; Weiss, E.; Van Regenmortel, M. H. V. *Molec. Immunol.* **1992**, *29*, 601-8.

(40) Tegenfeldt, J. O.; Montelius, L. *App. Phys. Lett.* **1995**, *66*, 1068-70.

(41) Montelius, L.; Tegenfeldt, J. O. *App. Phys. Lett.* **1993**, *62*, 2628-30.

Scheme 1

(A) Immobilize antibody on substrate via DSP

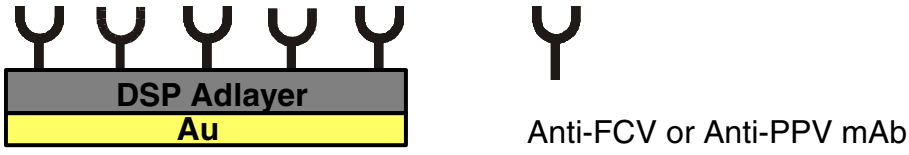

(B) Expose substrate to sample, capturing FCV or PPV

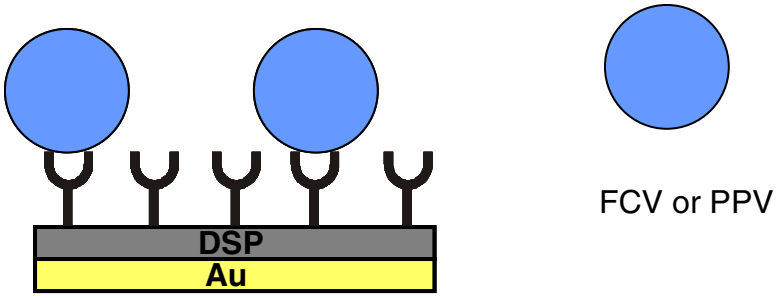

(C) Collect AFM images of FCV or PPV bound to capture substrate

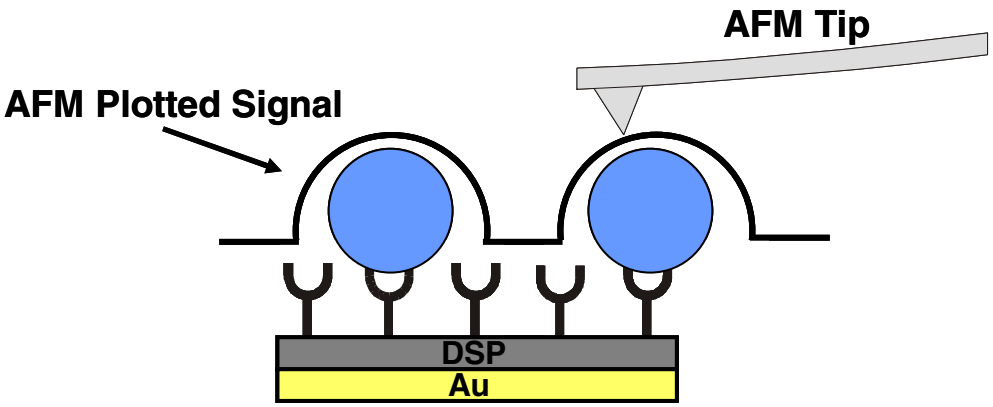

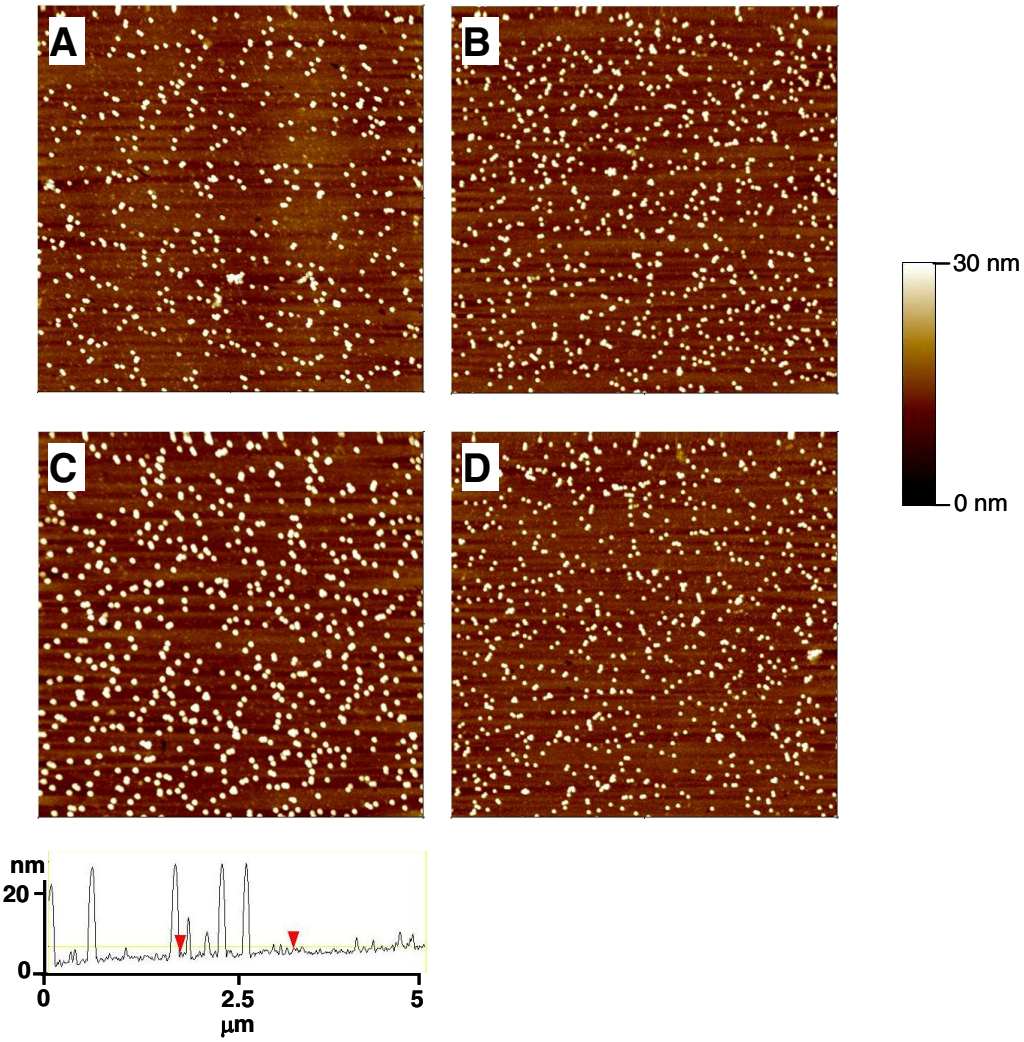

Figure 1. AFM micrographs (5 x 5 µm) of capture substrates blocked for ~16 h with different concentrations of BSA. The images represent the surface bound FCV after exposure to a 5.0 x 10^8 $TCID_{50}$/mL solution after blocking with 0% (A), 1% (B), 3% (C), 5% (D) BSA, and (E) topographic line scan of FCV showing an average height of ~22 nm.

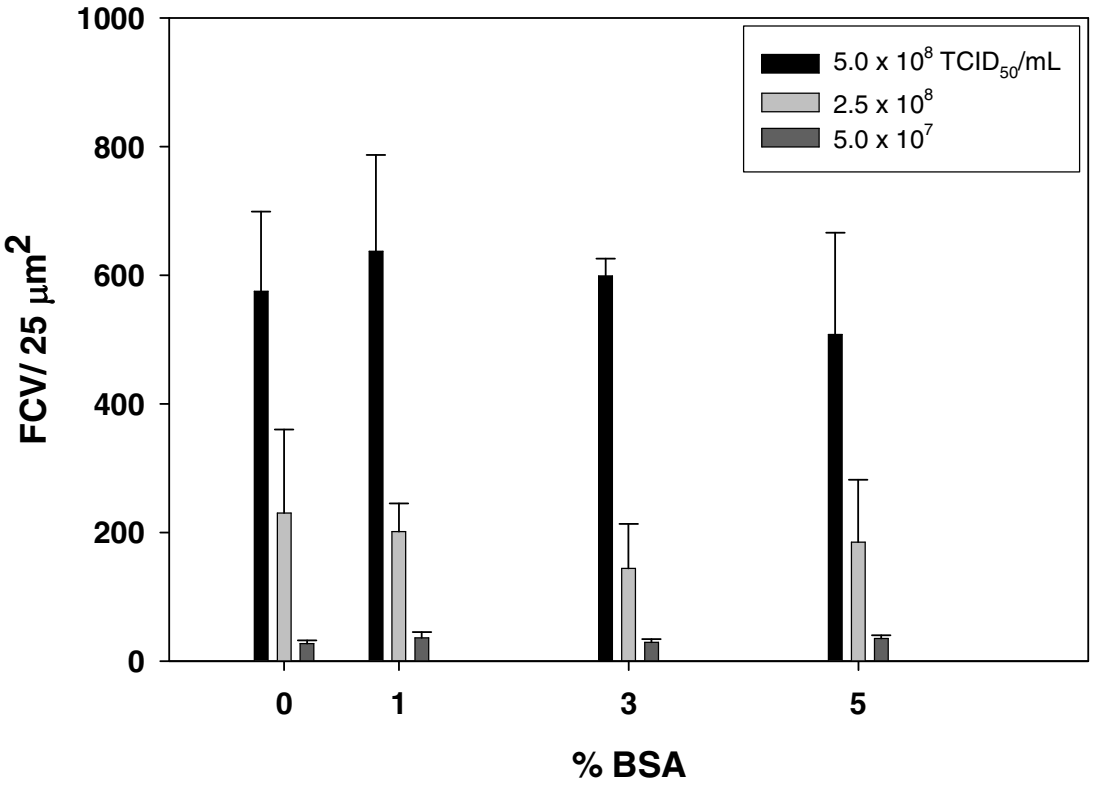

Figure 2. Bar graph showing the effect of different amounts of BSA used for blocking the capture substrate on three different concentrations of FCV.

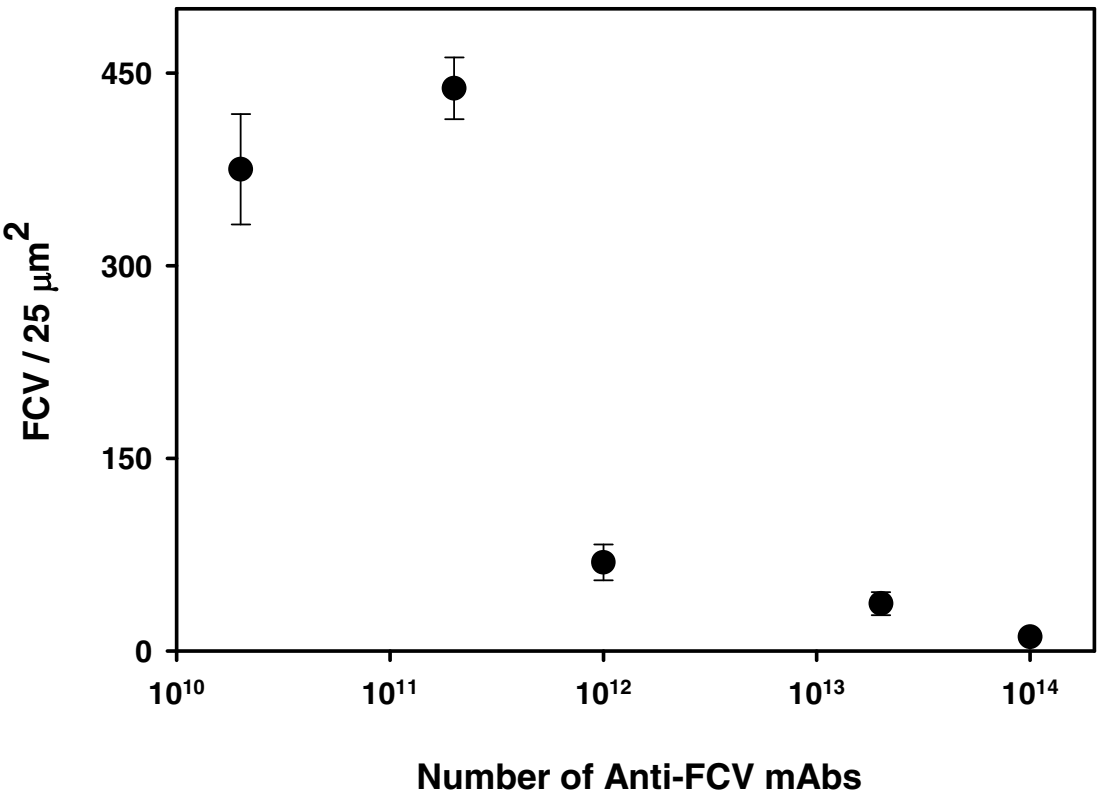

Figure 3. Competitive assay to test the specificity of the capture substrate. The data was obtained by collecting AFM micrographs (5 x 5 μm) of each sample exposed to varying amounts of anti-FCV mAb molecules prior to exposure to the capture substrate.

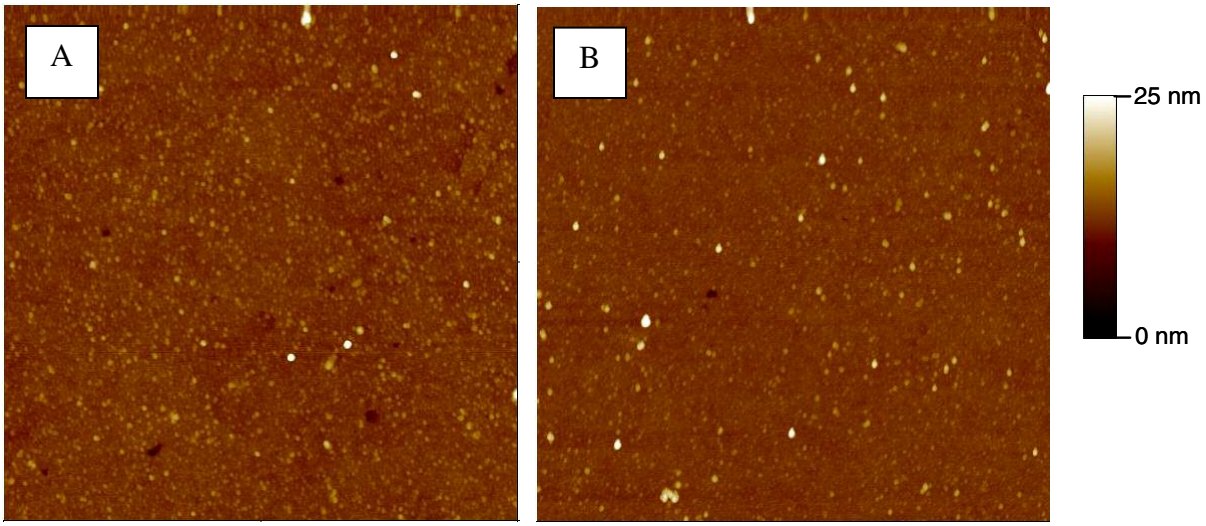

Figure 4. AFM images (5 x 5 μm) of anti-SMSV mAb (A) and anti-BVD mAb (B) capture substrates exposed to 5.0 x 10^8 $TCID_{50}$/mL of FCV.

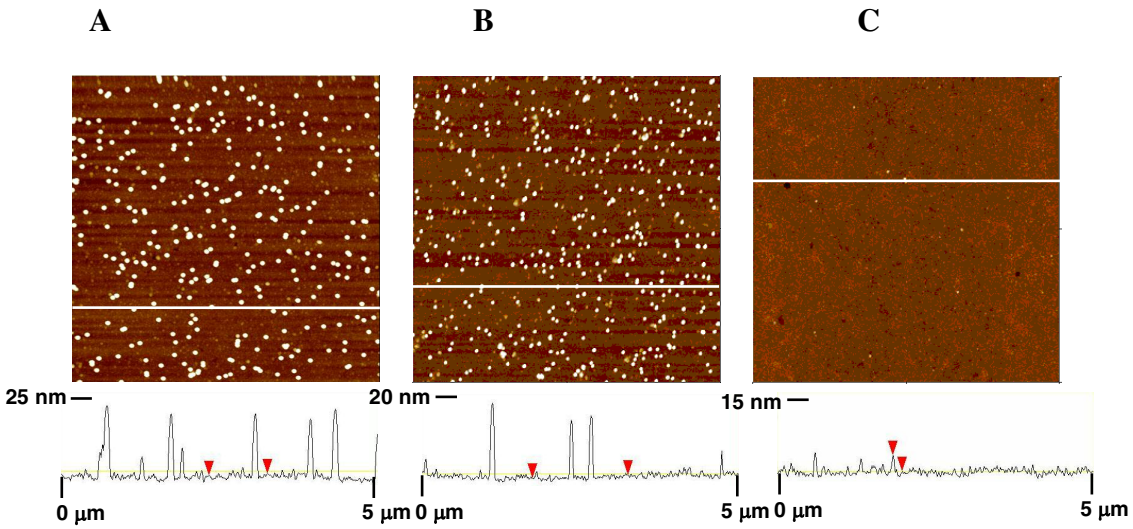

Figure 5. AFM micrographs (5 x 5 µm) and topographic line scans of (A) FCV (mAb 2D10-1C4, 2.5 x 10^8 $TCID_{50}$/mL), (B) PPV (mAb #9, 1.6 x 10^7 $TCID_{50}$/mL), and (C) blank samples.

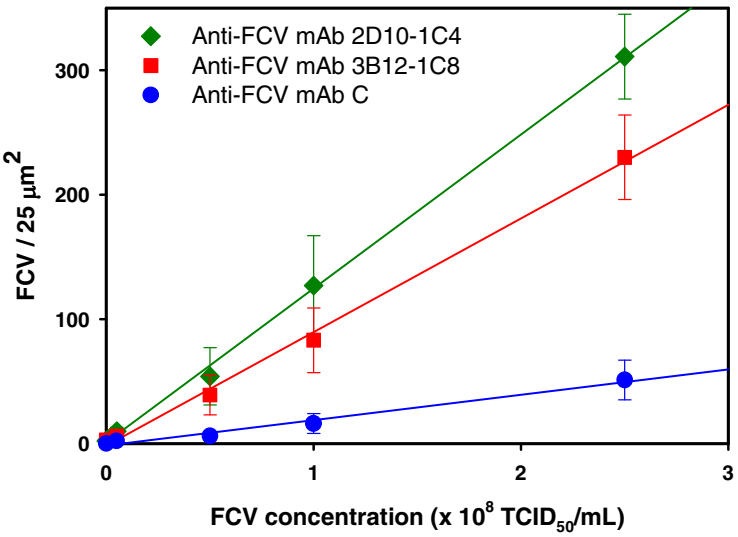

Figure 6A. Dose response curve responses for three different mAbs substrates exposed to FCV. Limits of detection are 3.2 x 10^6 $TCID_{50}$/mL for mAb 2D10-1C4, 6.9 x 10^6 $TCID_{50}$/mL for mAb 3B12-1C8, and 3.2 x 10^7 $TCID_{50}$/mL for mAb 4G1-2F4.

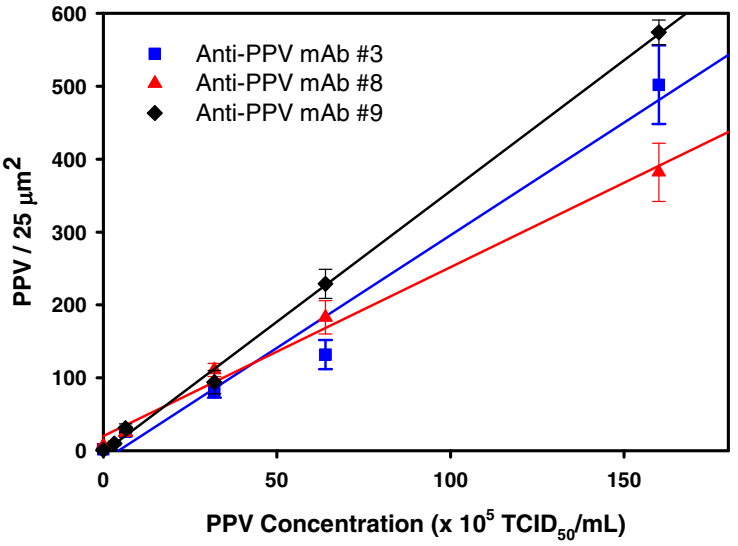

Figure 6B. Dose response curve responses for three different mAbs substrates exposed to PPV. Limits of detection are 6.4 x 10^4 $TCID_{50}$/mL for anti-PPV #9, 6.5 x 10^4 $TCID_{50}$/mL for anti-PPV mAb #3, and 8.6 x 10^4 $TCID_{50}$/mL for anti-PPV #8.

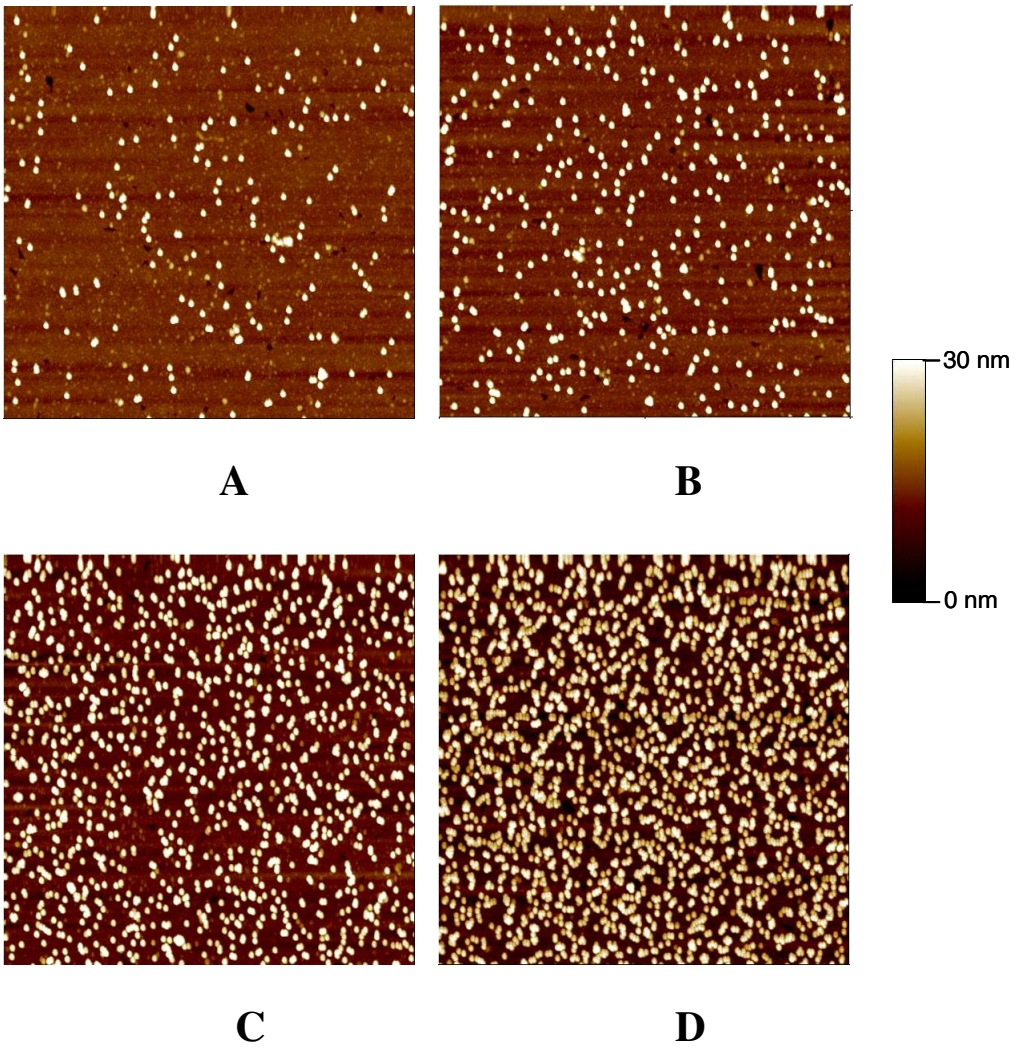

Figure 7. AFM images (5 x 5 μm) of FCV bound to capture substrates after exposure to (A) 5.0, (B) 10.0, (C) 20.0, and (D) 40.0 μL of a 5.0 x 10^8 $TCID_{50}$/mL solution.

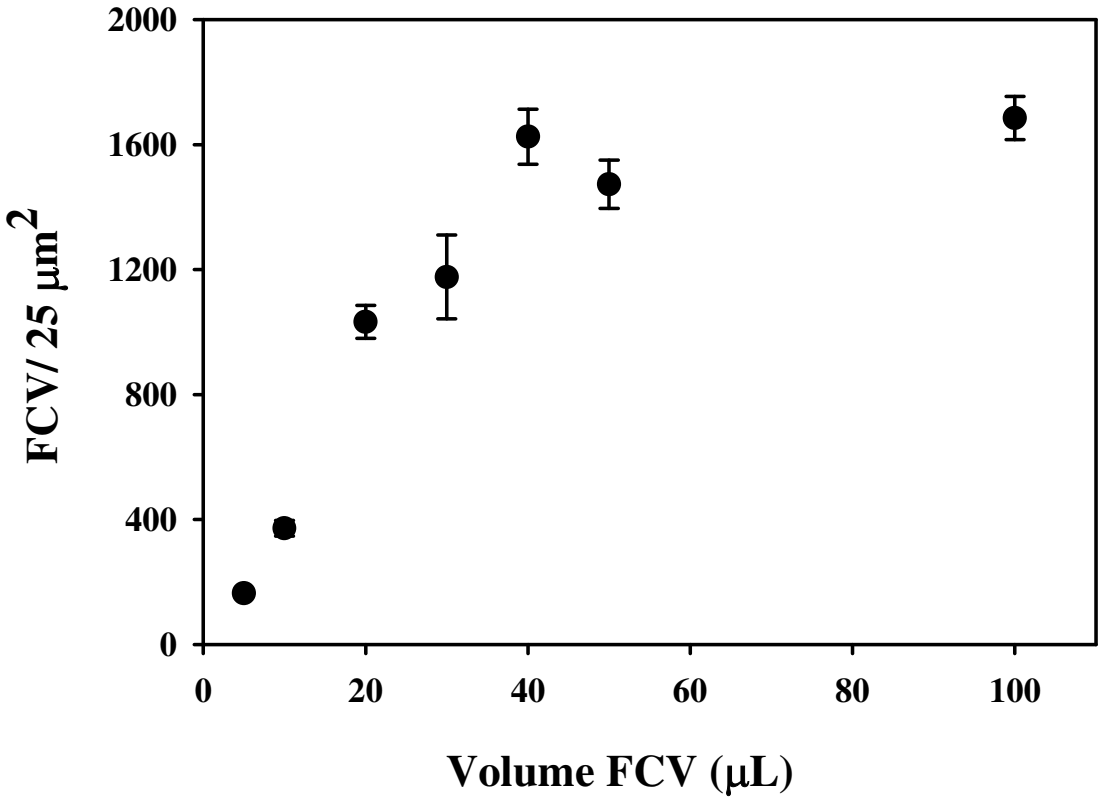

Figure 8. Dependence of captured FCV particle density as a function of FCV volume exposed to the capture substrate. The data were collected from AFM images (5 x 5 μm) after the capture substrate was exposed to different volumes of a 5.0 x 10^8 $TCID_{50}$/mL solution.

CHAPTER 2: EFFECT OF ELEVATED TEMPERATURE ON THE RATE OF THE SELECTIVE ACCUMULATION OF ANTIGENS AND PERFORMANCE OF IMMUNOASSAYS AS MONITORED BY ATOMIC FORCE MICROSCOPY

A manuscript in preparation for submission to *Analytical Chemistry*

Karen M. Kwarta[*], Jeremy D. Driskell, and Marc D. Porter*

Institute for Combinatorial Discovery, Departments of Chemistry and Chemical and Biological Engineering, Ames Laboratory-U.S. DOE, Iowa State University, Ames, Iowa 50011-3020

[*]Current address: Center for Combinatorial Sciences, Biodesign Institute, Department of Chemistry and Biochemistry, Arizona State University, Tempe, AZ 85287

John D. Neill and Julia F. Ridpath

Virus and Prion Diseases of Livestock Unit, National Animal Disease Center, United States Department of Agriculture, Ames, Iowa 50010

ABSTRACT

High throughput, sensitive, and rapid detection of viral pathogens is central to human and animal healthcare and diagnosis. The strategy relies on how elevated temperatures can be used to increase rates of mass transfer, potentially lowering the time

required for sample incubation. This paper describes the development of a virus detection method that extracts viruses at an elevated temperature to give a total sample workup time of less than 1 h. To evaluate the use of elevated temperatures, immunoassays for porcine parvovirus (PPV) and feline calicivirus (FCV) were studied using the direct readout method of atomic force microscopy (AFM). PPV represents a more ideal system in that the assays were carried out in buffered solutions. FCV, on the other hand, serves as a more realistic model for a complex matrix (i.e., spent cell culture medium). The accumulation rate of the viruses was examined at different temperatures. The accumulation rate for PPV qualitatively follows theoretical predictions based on diffusion considerations. The accumulation rate for FCV, however, exhibits a much more complex and less tractable dependence, which is attributed to competition from components in the sample matrix. It was determined that by increasing the temperature to 39 ˚C, an assay carried out with 1-h incubations gave limits of detection (LODs) comparable to those at 25 ˚C for 16 h. Moreover, LODs for 1-h incubations at 39 ˚C were 10-50 times lower than the 25 ˚C, 1 h analogs. The potential broad-based extension of this strategy is briefly discussed.

INTRODUCTION

Solid phase immunoassays are invaluable to clinical chemistry.[1] However the never-ending demand for more rapid and sensitive tests continues to push for enhancements in throughput, reductions in analysis time, and improvements in limits of detection (LOD).[1, 2] To these ends, recent breakthroughs, for example, in electrochemical,

optical, magnetic, and scanning probe microscopic detection methods[3-14] have driven the LODs to femtomolar levels and lower. However, the need for long incubation times remains problematic. This situation is due, in large part, to the small diffusion coefficients for large-sized biolytes (e.g., antibodies, viruses, and bacteria), which yield low rates of mass transfer to a capture substrate in quiet solutions.[15] Slow rates of mass transport can also have a negative impact on the apparent LOD because of the long times that may be required for the system to truly equilibrate.[15] In other words, the observed LOD may be an unrecognized artifact of slow mass transport limitations rather than signal transduction. The development of methods to increase the rate of delivery of analytes and labels to capture substrates, therefore presents opportunities to not only reduce incubation time, but also to improve LOD.

Examples of recent strategies that have focused on increasing mass transport include electric fields,[16-19] lateral flow assays,[20-24] rotation-induced convection,[25] and temperature.[26-31] Electric fields can drive analytes to specific addresses based upon the inherent charge of the target. While dramatically reducing incubation times, this approach must be finely tuned in order to optimally function for targets with different charges. Lateral flow assays, in contrast, typically use a porous solid phase that has a localized band of capture antibody positioned downstream of the sample inlet. The sample and label move through the solid phase, concentrating the antigen upon passage through the "capture zone."[20-24] Rotation of the capture substrate has been shown to decrease incubation times and to improve the LODs.[25]

As another possible pathway to overcome mass transport limitations, this paper investigates the use of elevated temperatures within the context of readout with atomic

force microscopy (AFM). Elevated temperatures have been exploited to improve mass transport for small molecules (i.e., antibodies in Enzyme-Linked ImmunoSorbent Assay (ELISA) applications).[27-31] There are few reports, however of utilizing elevated temperatures to increase the transport of large antigens such as viruses. We add that AFM provides a unique opportunity to explore the temperature dependence of assay performance due to its ability to readily image nanometer-sized objects such as viruses.[11, 32-34] Furthermore, AFM can function as a label-free readout method, eliminating complications from the secondary labeling required by many other techniques.

Our approach to investigate the use of elevated temperatures to decrease incubation times involves the capture of two different viruses, porcine parvovirus (PPV) and feline calicivirus (FCV) to an antibody-modified gold substrate. PPV and FCV are employed as model systems because their size (i.e., 25-nm diameter for PPV and 36-nm diameter for FCV)[35] facilitated AFM imaging and yielded small diffusion coefficients. The gold substrate was prepared with covalently immobilized monoclonal antibodies specific for each of the viruses. These substrates were then exposed to virus solutions for differing times (up to 16 h) and temperatures (25 ˚C and 39 ˚C) to experimentally monitor by AFM the rate of accumulation and potential effects on LODs. This paper, therefore, first examines the theoretical underpinnings of how the size of an antigen and temperature affect accumulation, and then roughly compares such predictions to our experimental observations. Finally, the effect of incubation time and temperature on analytical performance metrics (i.e., sensitivity and LOD) is discussed.

THEORETICAL CONSIDERATIONS

The impact of an elevation in temperature on analyte accumulation in a heterogeneous immunoassay is primarily an integration of three different factors. Two factors arise from the effect of temperature on mass transfer through increases in the diffusion coefficient,[36] and in convection.[37] The third results from enhancements in both the association, k_a, and dissociation, k_d, reaction rate constants for the complex, which directly translates to the equilibrium constant for the complex.[26] The contribution from the first factor, an increase in a diffusion coefficient with temperature, can be expressed by the following equation:

$$D = kT/6\pi\eta r \qquad (1)$$

where k is Boltzmann's constant, T is the absolute temperature, η is the solution viscosity, and r is the radius of the diffusing analyte.[36] As is evident, the magnitude of the diffusion coefficient is directly proportional to temperature, and inversely proportional to the size of the analyte. Note that the diffusion coefficient also exhibits an inverse dependence on solution viscosity, which undergoes an increase with elevations in temperature. Table 1 illustrates the temperature dependence of the diffusion coefficients for spherical objects that are comparable in size to a monoclonal antibody (mAb), PPV, and FCV at both 25 and 39 ˚C.

How these differences, albeit no more than a factor of 3.5, affect the number of particles that in quiet solution encounter the surface of the capture substrate as a function of time, t, can be estimated using:

$$\Gamma = n\,(Dt/2)^{1/2} \qquad (2)$$

where Γ is the surface concentration of accumulated antigens and n is the antigen particle concentration (antigens/mL).[36] The following criteria must be followed in order for Equation 2 to be predictive: 1) each antigen that collides with the surface is instantaneously captured; and 2) the level of accumulation is sufficiently low that the binding of an incoming antigen is not sterically occluded by previously captured antigens.

Based on Equation 2, Figure 1 plots Γ for the three different targets as a function of time and temperature (25 and 39 ˚C) at an initial concentration of 1.0×10^{10} antigens/mL (17 pM). This concentration was chosen to parallel the conditions of the experimental data. The accumulated antigen is well below the calculated jamming limit for each target (175000, 13500, 30000 particles/25 μm^2 for mAb, FCV, and PPV respectively). As is seen, all accumulations increase with time (all accumulations are greater at 39 ˚C), and the accumulation of mAbs is notably larger than either of the viruses.

These results yield two additional insights. The first reflects how reproducibility is intimately connected to the accurate control of incubation time. Temporal control is much more important at short times, and with smaller antigens. This situation becomes more readily apparent in Figure 2, which plots the derivative of the profiles in Figure 1 with respect to time. As expected, these plots show that the greatest change in accumulation occurs at small times. The need for careful temporal control is also more important at elevated temperatures because of the higher accumulation rates. The second observation relates to how the rate of accumulation evolves with time and its impact on LOD. In other words, the return in terms of improvements of LOD drops rapidly via a

$t^{-1/2}$ dependence. Thus, doubling the assay time will only improve the LOD by a factor of ~1.4.

A further perspective into this issue can be developed by examining the accumulation at different virus concentrations, as shown in Figure 3. Assays performed at short times and room temperature are clearly hampered because only small amounts of antigen can be captured. For example, after 600 min at 39 ˚C, a PPV concentration of 1×10^{10} viruses/mL has resulted in the capture of 175 viruses bound in a 25 μm^2 area, while a tenfold increase in concentration to 1×10^{11} viruses/mL yields 1750 viruses in the same area. When trying to detect ultra low levels of antigen, the amount of time required to accumulate a detectable amount will be considerably long. Lower concentrations of antigen require long times to diffuse to the surface, even when elevated temperatures are used to increase the amount of captured antigen. This situation, coupled with challenges in locating and detecting a low density of captured antigen, placing a premium on the development of approaches to enhance mass transport.

Elevated temperatures also have an effect on the equilibrium constant, K_{eq}, of antibody-antigen binding, which in turn, controls the total number of analytes that can potentially be captured. Since antibody-antigen binding is considered instantaneous,[38-41] changes in K_{eq} affect the equilibrated accumulation of antigen by changing the total number of antigen that can be bound. The association and dissociation reaction rate of an antibody-antigen system defines its K_{eq}:

$$K_{eq} = k_a/k_d \qquad (4)$$

where k_a is the association rate constant, and k_d is the dissociation rate constant. The rate constants are known to be dependent on temperature following a Boltzman equation:[37, 42]

$$k \propto \exp(-E_a/kT) \qquad (5)$$

If both k_a and k_d are equally affected by a temperature change, then the value of K_{eq} remains fixed, and there will be no change in accumulation. If, however, one rate constant is changed more than the other, the K_{eq} will be different, and the level of accumulation will be altered. In most of the studied cases, the dissociation rate of the antibody-antigen complex undergoes a much larger change than the association rate at increased temperatures.[26] The increase in k_d, and subsequent decrease in K_{eq}, may affect the sensitivity of the assay by limiting the total number of antigens that can be bound. Because antibody-antigen reactions are exothermic, an increase in temperature could also have a deleterious effect on assay performance by pushing the equilibrium to the un-conjugated state. The extent to which this dissociation happens impedes limits of detection by allowing fewer bound complexes at equilibrium. Therefore, the benefits of shorter incubation times must be evaluated with respect to decreases in sensitivity.

The final contribution of temperature to antigen accumulation is through a thermally induced convection, which increases mass transport. When capture substrates are heated, a temperature gradient can develop in the liquid sample, causing a convective mixing because of thermally generated density gradients. The resulting convection causes an increase in mass transport, which often accounts for the larger than expected accumulations that have been observed with respect to those based solely on diffusion.[37, 43] The challenge, however, is that temperature gradients can be difficult to control in multiphase systems, partially degrading reproducibility from assay-to-assay.[37] Nevertheless, convection has been shown to improve the rate of accumulation by as much as a factor of five, providing a useful method for reducing overall incubation times.[37]

Thus, the improvement in analyte accumulation due to convection and the increase in diffusion coefficients can yield reductions in incubation times without compromising limits of detection.

EXPERIMENTAL

Reagents. FCV (titer: 5.0 x 10^8 $TCID_{50}$/mL) and PPV (titer: 3.2 x 10^9 $TCID_{50}$/mL) were obtained from the National Animal Disease Center (NADC). We have recently shown that the conversion factors from $TCID_{50}$/mL to the number of virus particles/mL of PPV and FCV are ~1400 virus particles/$TCID_{50}$ for PPV[25] and ~20 virus particles/$TCID_{50}$ for FCV.[44] The conversion factor for PPV was ascertained from fitting experimental curves of PPV accumulation with respect to the rotation rate of the captured substrate.[25] The FCV conversion factor was determined by titrating the virus with known concentrations of antibody and then monitoring when the binding to the capture substrate was no longer detectable.[44] We note that the later analysis relies on knowing the number of epitopes on the virus and estimating the amount of antibody that can fully coat the outer surface of the virus.

Monoclonal antibodies (mAbs), also provided by NADC, were purified with a protein G column (Bio-Rad) to 99.9% and stored in 10 mM phosphate buffered saline (PBS). Dithiobis(succinimidyl propionate) (DSP) and PBS packs were purchased from Sigma. Octadecanethiol (ODT) was obtained from Aldrich. Poly(dimethylsiloxane) (PDMS) was acquired from Dow Corning, and utilized to fabricate microcontact printing stamps. Contrad 70, a mild detergent used for cleaning glass, was from Decon Labs, and

the two-part epoxy, employed for constructing template stripped gold, was from Epoxy Technology. Borate buffer packs were from Pierce. All buffers were passed through a 0.22-μm syringe filter (Costar) before use.

Preparation of Capture Substrate and Immunoassay Protocol. Template stripped gold (TSG) acted as the base for preparation of capture substrates. TSG has a low roughness factor (0.6) that facilitated the AFM-based enumeration of the two viruses, which have hydrated diameters of ~25 nm (PPV)[35] and ~36 nm (FCV).[35] TSG was constructed by evaporating 250 nm of gold (purity 99.9%) at a rate of 0.1 nm/s onto a 4-in, p-type silicon (111) wafer (University Wafer), using an Edwards 306A resistive metal evaporator. Microscope slides were cut into 1 x 1 cm glass chips and cleaned ultrasonically in dilute Contrad 70, deionized water, and ethanol for 30 min each. Epoxy cement was applied to one side of the clean glass chips, the chip was placed on the gold-coated silicon wafer, and the wafer was cured at 150 ˚C for ~100 min. The glass chips were then carefully detached from the silicon wafer in order to expose the underlying smooth gold surface.

TSG was used to create antibody-coated capture substrates. First, TSG was exposed for ~30 s to an ODT-soaked PDMS stamp with a 3.0-mm hole cut in its center. This step creates a ring-shaped hydrophobic coating that both confines small volumes of aqueous samples within the center of the substrate and minimizes sample and reagent consumption. The substrates were subsequently rinsed with ethanol, dried with nitrogen, and soaked in a 2-mM ethanolic solution of DSP for ~8 h.

The next step in the process pipetted 20 μL of either anti-FCV or anti-PPV mAbs (100 μg/mL in 50 mM borate buffer (pH 8.5)) onto the DSP-modified domain of the

substrate, with the covalent coupling reaction allowed to proceed for ~7 h at room temperature. After the substrates were rinsed three times with 10 mM PBS (pH 7.4), 20 μL of room temperature virus solutions were placed on room temperature substrates, which were then incubated either at 25 or 39 ˚C for different time intervals by placement in a temperature equilibrated Yamato IC 400 incubator. The PPV solution was prepared by dilution in 10 mM PBS, while FCV was diluted in spent cell culture media. Finally, the substrates were rinsed three times with 10 mM PBS (pH 7.4), and once with a 3-s stream of deionized water. The water rinse was necessary in order to remove salt residue, which interfered with the enumeration of captured viruses by AFM. The substrates were then dried with a stream of nitrogen. The steps for these immunoassay procedures reflect earlier optimizations, which also included specificity controls to validate the use of the two mAbs.[44]

Instrumentation. The substrates were characterized by collecting 25-μm^2 AFM images with a MultiMode NanoScope IIIa AFM (Digital Instruments) equipped with a 150-μm scanner. Topographic images were acquired under ambient conditions in TappingMode using n(+)-silicon TESP cantilever/tips (Nanosensors) with a length of 118 nm, a width of 27-29 nm, thickness of 3.6-4.5 nm, a spring constant of 32-70 N/m and a resonant frequency of 327-421 kHz. The set-point amplitude of the cantilever was set to 80% of the free oscillation amplitude, and images were collected with a scan rate of 1.5 Hz. The number of viruses bound in each image was counted manually using a pen style colony counter (Sigma).

RESULTS AND DISCUSSION

The goal of this work was to investigate the effect of elevated temperatures on incubation times and analytical performance (i.e., sensitivity and LOD) for virus assays. To achieve this goal, viruses bound to the capture substrates were enumerated with AFM, which enables assessment of the capture step in a label-free format. AFM images and topographical cross-sectional plots of a FCV, PPV, and blank sample (10 mM PBS) are shown in Figure 4. The sizes of these images (25 μm^2) represent interplay between image resolution, which is a function of virus size, and scan area. As is evident in Figure 4, the viruses appear as spherically shaped objects, while the blank sample shows no distinguishable objects. PPV has ~17-nm height, while FCV is ~25 nm tall spheres, while. We attribute the smaller than expected sizes to dehydration of both of the viruses. The viruses, however, retain their general shape because of the stability of the capsid protein coating. We add that the lateral (x-y plane) appearances of some of the viruses vary and are somewhat asymmetrical, because of tip convolution effects.[45] Importantly, all of the captured viruses have the same average height, which allows for accurate enumeration.

PPV Accumulation at 25 ˚C. These experiments exposed anti-PPV capture substrates to a PPV sample (6.4 x 10^6 $TCID_{50}$/mL, 8.9 x 10^9 virus particles/mL) over a range of times. Figure 5 plots both the experimentally determined and theoretically predicted (Equation 2) accumulation of PPV as a function of time. The curve exhibits slightly lower accumulation than expected because the virus accumulation does not follow the assumptions of Equation 2 (i.e., all viruses that reach the surface bind). The experimental conditions require that the viruses reach the surface and find an available

binding site (i.e., an antibody that is active and oriented correctly). In preparing capture substrates, the orientation of the capture antibodies is not controlled, leaving many inactive sites, limiting the number of binding sites available for virus capture. Additionally, the viruses are large in size and may block active antibody sites on the capture surface, limiting the number of virus binding sites even further (on average one virus blocks nine antibodies). These considerations predict that the experimental accumulation will follow Equation 3.

The curve in Figure 5 exhibits an apparent saturation at ~150 PPV bound/25 μm^2, while the predicted trend shows a continued slow increase in the accumulation. This observation can be attributed to two factors: 1) equilibrium has been established, and/or 2) the solution has been sufficiently depleted to where the bulk concentration is changing (i.e. the reaction has become volume dependent). If the system has reached equilibrium, then the total number of PPV accumulated will not change, regardless of time. In the case of depletion, the sample solution concentration is being reduced, which in turn decreases Γ according to Equation 2. By calculating the total number of PPV that have been extracted out of solution onto the capture substrate, and subtracting this number from the initial concentration, the bulk solution concentration has been reduced by ~30%. Additionally, after 16 h, an estimation of the diffusion layer thickness suggests that ~60% of solution has been perturbed. These observations lead us to believe that the system has not reached equilibrium.

PPV Accumulation at 39 ˚C. In an effort to reduce extraction times of viruses to the capture substrate, binding curves for PPV were determined at 39 ˚C, shown in Figure 6. As seen in Figure 6, the curve levels off in ~2 h, a dramatic decrease compared to ~8 h

at 25 ˚C. The curves for PPV at 39 ˚C follow the trend expected for accumulation according to Equation 2. However, unlike at 25 ˚C, the accumulation at 39 ˚C is faster than the predicted curve for 8.9 x 10^9 virus particles/mL, and thus does not follow Equation 3. The predictions based on Equations 2 and 3 account for faster accumulation due to increases in diffusion coefficients and decreases in solution viscosity, but do not account for increases due to convection. The faster accumulation at 39 ˚C for the experimental results as compared to the predictions is attributed to convection. Convection has a considerable effect on the accumulation of the viruses, and control of the convection, therefore, may provide an appealing method to reducing mass transfer limitations.

Since we believe our systems have not reached equilibrium, it is difficult to determine the impact of a change in K value on our systems. As with any immunoassay protocol, a balance must be found between incubation time and sensitivity, since the accumulation at short times (< 2 h) at 39 ˚C is less than the number of bound viruses at room temperature for long times (> 8 h). A direct comparison of limits of detection using different incubation times and temperatures is discussed below.

FCV Accumulation at 25 ˚C. Substrates for FCV were exposed to 5.0 x 10^8 $TCID_{50}$/mL (1.0 x 10^{10} virus particles/mL) and rinsed after different incubation times. FCV accumulation at 25 ˚C as a function of time is shown in Figure 7. In this case, a limiting surface concentration appears to be reached in ~8 h at ~200 viruses/ 25 μm^2. Moreover, the evolution of accumulation is much different from the predicted curve for accumulation according to Equation 3. The experimental accumulation is very slow at short times and then increases sharply between 5 and 10 h and finally levels off.

An important difference in the experimental conditions for FCV is the use of spent cell culture media in the dilutions that contain many proteins and molecules not found in PBS used for diluting PPV. These medium contain a large number of small proteins and molecules which can potentially cover the capture substrate at a rapid rate (see Table 1 and Figure 1). Such a coating potentially competes with antigens for surface sites, which can slow accumulation. However, while only speculative, it appears that once a few viruses bind, the rate of accumulation increases, suggesting that some type of cooperative mechanism may be of importance. Nonetheless, more experiments are necessary to realistically address this issue.

FCV Accumulation at 39 ˚C. Accumulation rates of FCV at 39 ˚C are shown in Figure 8. Equilibrium is reached after ~2 h and is a marked improvement over those at 25 ˚C. The shape of the binding curve is similar to that observed at 25 ˚C, in that virus accumulation is slow at first, rises quickly and then levels off.

Interestingly, the saturation points for FCV are lower at elevated temperatures (i.e. ~200 viruses/25 μm^2 at 25 ˚C and ~120 viruses/25 μm^2 at 39 ˚C). We believe that this difference, at least in part, is due to the effect of temperatures on K.

The results from these data show that in order to achieve satisfactory performance (i.e. low detection limits) at room temperature, the viruses must be extracted for at least 8 h. The slow mass transfer of the viruses to the capture substrate illustrates how the sensitivity of the assay is a mass transport limitation and not an artifact of the readout methodology, emphasizing the importance of overcoming mass transfer in order to achieve low limits of detection in short time frames. The use of elevated temperatures can decrease the amount of time needed to extract viruses, but may have a deleterious effect

on the achievable limit of detection. It is our speculation that the faster extraction times are due to convection and larger diffusion coefficients, and not a change in the association constant since it is well documented that the rate of antibody-antigen binding is limited by mass transport rather than recognition rate.[38-41]

FCV and PPV Dose-Response Curves. To understand the compromise between fast accumulation due to increased temperature and LOD, dose-response curves for FCV and PPV were constructed at 39 ˚C for 1 h, 25 ˚C for 1 h, and 25 ˚C for 16 h. FCV was diluted in spent cell culture media, while PPV was diluted in 10 mM PBS. Figure 9 plots the dose-response curves for PPV, while those for FCV are presented in Figure 10. Limits of detection were defined by the concentration yielding a signal equal to the blank signal plus three times the standard deviation of the blank signal. From these dose-response curves, the limit of detection for PPV is 2.1×10^5, 1.8×10^5, and 8.1×10^5 $TCID_{50}$/mL for 1 h at 39 ˚C, 16 h at 25 ˚C and 1 h at 25 ˚C, respectively. The limit of detection for FCV is 5.1×10^6, 8.1×10^5, and 4.2×10^7 $TCID_{50}$/mL for 1 h at 39 ˚C, 16 h at 25 ˚C and 1 h at 25 ˚C, respectively. Upon analysis of the dose response curves, it is clear that the best limits of detection can be achieved by long extraction times at room temperature. This result is expected based upon the theoretical predictions and experimental evidence shown above. Assays conducted at room temperature for only 1 h exhibit the worst limits of detection, emphasizing the impact of mass transport on assay sensitivity. Increasing the extraction temperature to 39 ˚C and decreasing incubation time to 1 h changes the LOD by less than a factor of 2, as compared to 25 ˚C for 16 h. These results show that the elevated temperatures speed up accumulation for both viruses while maintaining assay

performance, implying that this methodology for improving mass transport may easily be applied to solid phase immunoassays for large biological analytes.

CONCLUSIONS

Decreases in accumulation time of viruses from solution were observed when elevated temperatures were utilized. Surface accumulation of PPV and FCV at 25 ˚C and 39 ˚C as a function of time was used to evaluate the effect of temperature on equilibrium and assay sensitivity. These curves show that accumulation is increased at 39 ˚C, presumably due to increases in mass transport arising from convection and larger diffusion coefficients. Overall, it is shown that elevated temperatures are a simple method for speeding up immunoassay extraction times and do not significantly compromise assay performance. Total assay time can be reduced to less than 1 hour while retaining limits of detection that are competitive with other methods.

ACKNOWLEDGEMENTS

This work was supported through a grant from USDA-NADC and by the Institute for Combinatorial Discovery of Iowa State University. Karen M. Kwarta gratefully acknowledges the support of a Dow Chemical Fellowship. The Ames Laboratory is operated for the US Department of Energy through Iowa State University under contract W-7405-eng-82.

REFERENCES

(1) Sokoll, L. J.; Chan, K. W. *Anal. Chem.* **1999**, *71*, 356R-62R.

(2) Diamandis, E. P.; Christopoulos, T. K., Eds. *Immunoassay*; Academic Press: San Diego, CA, 1996.

(3) Cao, Y. C.; Jin, R.; Mirkin, C. A. *Science* **2002**, *297*, 1536-40.

(4) Cousino, M. A.; Jarbawi, T. B.; Halsall, H. B.; R., H. W. *Anal. Chem.* **1997**, *69*, 544A-9A.

(5) Donaldson, K. A.; Kramer, M. F.; Lim, D. V. *Biosen. Bioelectron.* **2004**, *20*, 322-7.

(6) Driskell, J. D.; Kwarta, K. M.; Lipert, R. J.; Porter, M. D.; Neill, J. D.; Ridpath, J. F. *Anal. Chem.* **2005**, *77*, 6147-54.

(7) Ferguson, J. A.; Steemers, F. J.; Walt, D. R. *Anal. Chem.* **200**, *72*, 5618-24.

(8) Grubisha, D. S.; Lipert, R. J.; Park, H.-Y.; Driskell, J. D.; Porter, M. D. *Anal. Chem.* **2003**, *75*, 5936-43.

(9) Kjeldsberg, E. *J. Virol. Meth.* **1986**, *14*, 321-33.

(10) Llic, B.; Yang, Y.; Craighead, H. G. *Appl. Phys. Lett.* **2004**, *85*, 2604-6.

(11) Nettikadan, S. R.; Johnson, J. C.; Mosher, C.; Henderson, E. *Biochem. Biophys. Res. Commun.* **2003**, *311*, 540-5.

(12) Richardson, J.; Hawkins, P.; Luxton, R. *Biosen. Bioelectron.* **2001**, *16*, 989-93.

(13) Wang, H.; Branton, D. *Nat. Biotechnol.* **2001**, *19*, 622-3.

(14) Zheng, Y. Z.; Hyatt, A.; Wang, L.-F.; Eaton, B. T.; Greenfield, P. F.; Reid, S. *J. Virol. Meth.* **1999**, *80*, 1-9.

(15) Sheehan, P. E.; Whitman, L. J. *Nano. Lett.* **2005**, *5*, 803-7.

(16) Ewalt, K. L.; Haigis, R. W.; Rooney, R.; Ackley, D.; Krihak, M. *Anal. Biochem.* **2001**, *289*, 162-72.

(17) Heller, M. J.; Forster, A. H.; Tu, E. *Electrophoresis* **200**, *21*, 157-64.

(18) Pribyl, M.; Snita, D.; Hasal, P.; Marek, M. *Chem. Eng. J.* **2004**, *101*, 303-14.

(19) Yang, J. M.; Bell, J.; Huang, Y.; Tirado, M.; Thomas, D.; Forster, A. H.; Haigis, R. W.; Swanson, P. D.; Wallace, R. B.; Martinsons, B.; Krihak, M. *Biosen. Bioelectron.* **2002**, *17*, 605-18.

(20) Qian, S.; Bau, H. H. *Anal. Biochem.* **2003**, *322*, 89-98.

(21) Oku, Y.; Kamiya, K.; Kamiya, H.; Shibahara, Y.; Ii, T.; Uesaka, Y. *J. Immunol. Meth.* **2001**, *258*, 73-84.

(22) Chan, C. P. Y.; Sum, K. W.; Cheung, K. Y.; Glatz, J. F. C.; Sanderson, J. E.; Hempel, A.; Lehmann, M.; Renneberg, I.; Renneberg, R. *J. Immunol. Meth.* **2003**, *279*, 91-100.

(23) O'Keeffe, M.; Crabbe, P.; Salden, M.; Wichers, J.; Van Peteghem, C.; Kohen, F.; Pieraccini, G.; Moneti, G. *J. Immunol. Meth.* **2003**, *278*, 117-26.

(24) Fernandez-Sanchez, C.; McNeil, C. J.; Rawson, K.; Nilsson, O. *Anal. Chem.* **2004**, *76*, 5649-56.

(25) Driskell, J. D.; Kwarta, K. M.; Lipert, R. J.; Vorwald, A.; Neill, J. D.; Ridpath, J. F.; Porter, M. D. *J. Virol. Meth.* **2006**, *138*, 160-9.

(26) Johnstone, R. W.; Andrew, S. M.; Hogarth, M. P.; Pietersz, G. A.; McKenzie, I. F. C. *Mol. Immunol.* **1990**, *27*, 327-33.

(27) Richardson, M. D.; Stubbins, J. M.; Warnock, D. W. *J. Clin. Pathol.* **1982**, *35*, 1134-7.

(28) Bora, U.; Chugh, L.; Nahar, P. *J. Immunol. Meth.* **2002**, *268*, 171-7.

(29) Bora, U.; Kannan, K.; Nahar, P. *J. Immunol. Meth.* **2004**, *293*, 43-50.

(30) Lew, A. M.; Thomas, L. M.; Huntignton, P. J. *Vet. Microbiol.* **1993**, *34*, 1-5.

(31) Yolken, R. H.; Leister, F. J. *J. Clin. Microbiol.* **1981**, *13*, 738-41.

(32) Kuznetsov, Y. G.; Malkin, A. J.; Lucas, R. W.; Plomp, M.; McPherson, A. *J. Gen. Virol.* **2001**, *82*, 2025-34.

(33) Kuznetsov, Y. G.; Low, A.; Fan, H.; McPherson, A. *Virol.* **2004**, *323*, 189-96.

(34) Kwarta, K. M.; Driskell, J. D.; Porter, M. D.; Neill, J. D.; Ridpath, J. F. *Manuscript in prep.* **2007**.

(35) Murphy, F. A.; Gibbs, E. P. J.; Horzinek, M. C.; Studdert, M. J. *Veterinary Virology*, Third ed.; Academic Press: San Diego, 1999.

(36) Park, K.; Simmons, S. R.; Albrecht, R. M. *Scan. Microsc.* **1987**, *1*, 339-50.

(37) Beumer, T.; Haarbosch, P.; Carpay, W. *Anal. Chem.* **1996**, *68*, 1375-80.

(38) Myszka, D. G.; Morton, T. A.; Doyle, M. L.; Chaiken, I. M. *Biophys. Chem.* **1997**, *64*, 127-37.

(39) Nygren, H.; Werthen, M.; Stenberg, M. *J. Immunol. Meth.* **1987**, *101*, 63-71.

(40) Stenberg, M.; Nygren, H. *J. Theor. Biol.* **1985**, *113*, 589-97.

(41) Stenberg, M.; Stiblert, L. *J. Theor. Biol.* **1986**, *120*, 129-40.

(42) Atkins, P. *Physical Chemistry*, Sixth ed.; W. H. Freeman and Company: New York, 1999.

(43) Beumer, T.; Timmerman, B. *Anal. Chem.* **1997**, *69*, 5182-5.

(44) Kwarta, K. M.; Driskell, J. D.; Porter, M. D.; Neill, J. D.; Ridpath, J. F. *Manuscript in prep.* **2007**.

(45) Montelius, L.; Tegenfeldt, J. O. *Appl. Phys. Lett.* **1993**, *62*, 2628-30.

Table 1. Effect of temperature on solution viscosity and the diffusion coefficients for mAb, PPV and FCV.

Temperature (˚C)	η (g/cm s)[a] x 10^{-2}	D (cm^2/s)[b] x 10^{-7}		
		mAb	PPV	FCV
25	0.89	5.0	2.0	1.4
39	0.65	7.0	2.8	2.0

(a) Values from reference 36.

(b) Calculated using radii of 5, 12, and 18 nm for mAb, PPV and FCV respectively (see text for further details).

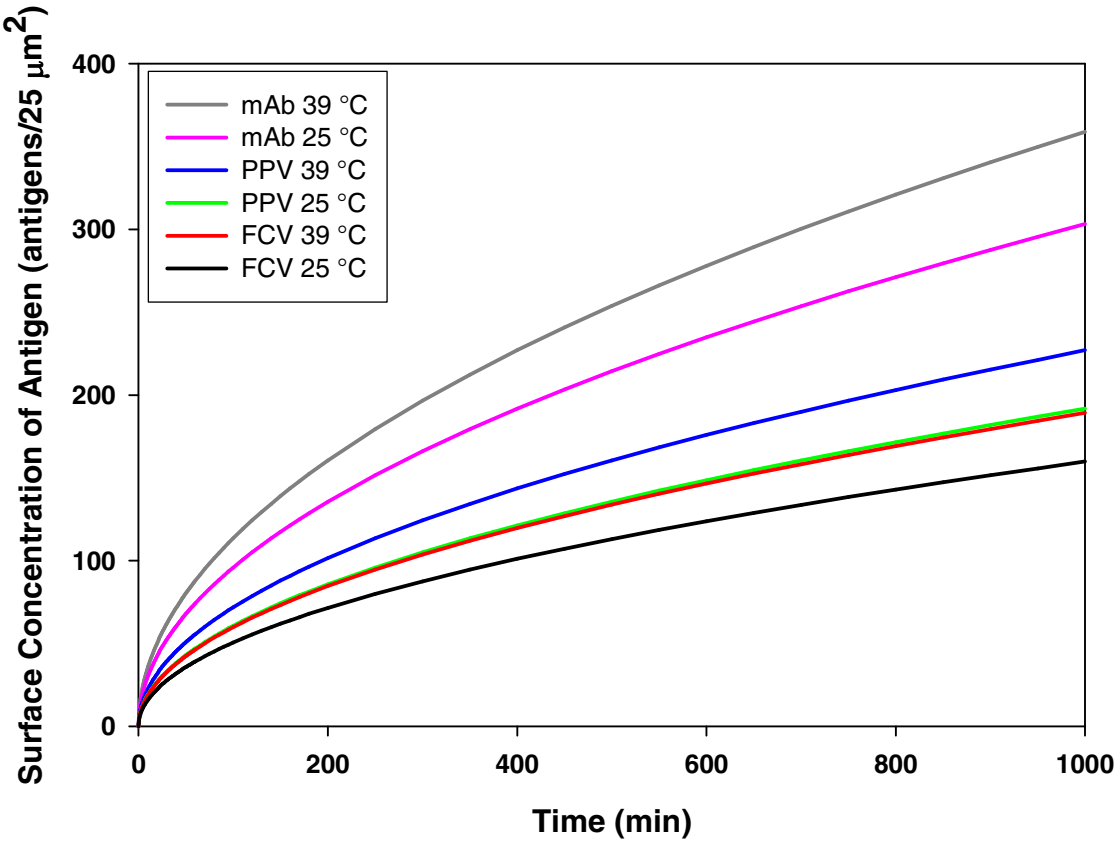

Figure 1. Theoretical accumulation of PPV, FCV, and mAb as a function of time at different temperatures and a concentration of 1.0 x 10^{10} antigens/mL (17 pM).

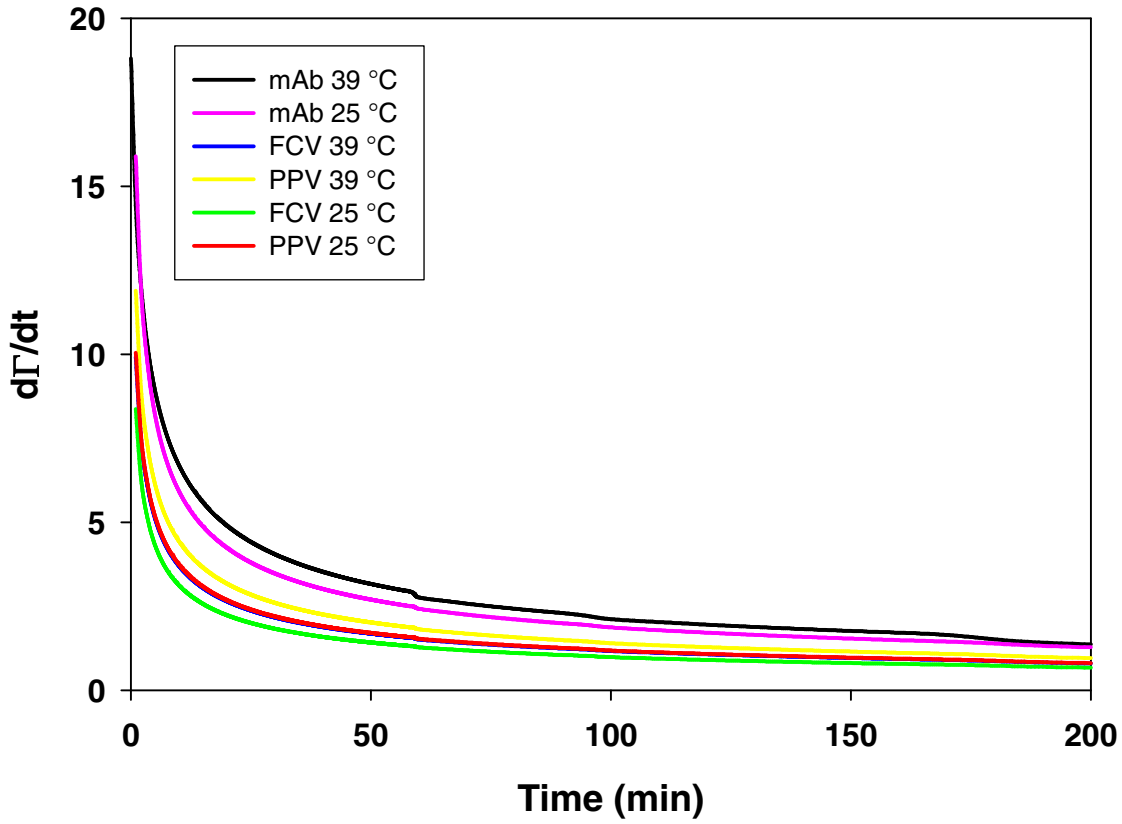

Figure 2. Plot of the derivative of Figure 1 with respect to time.

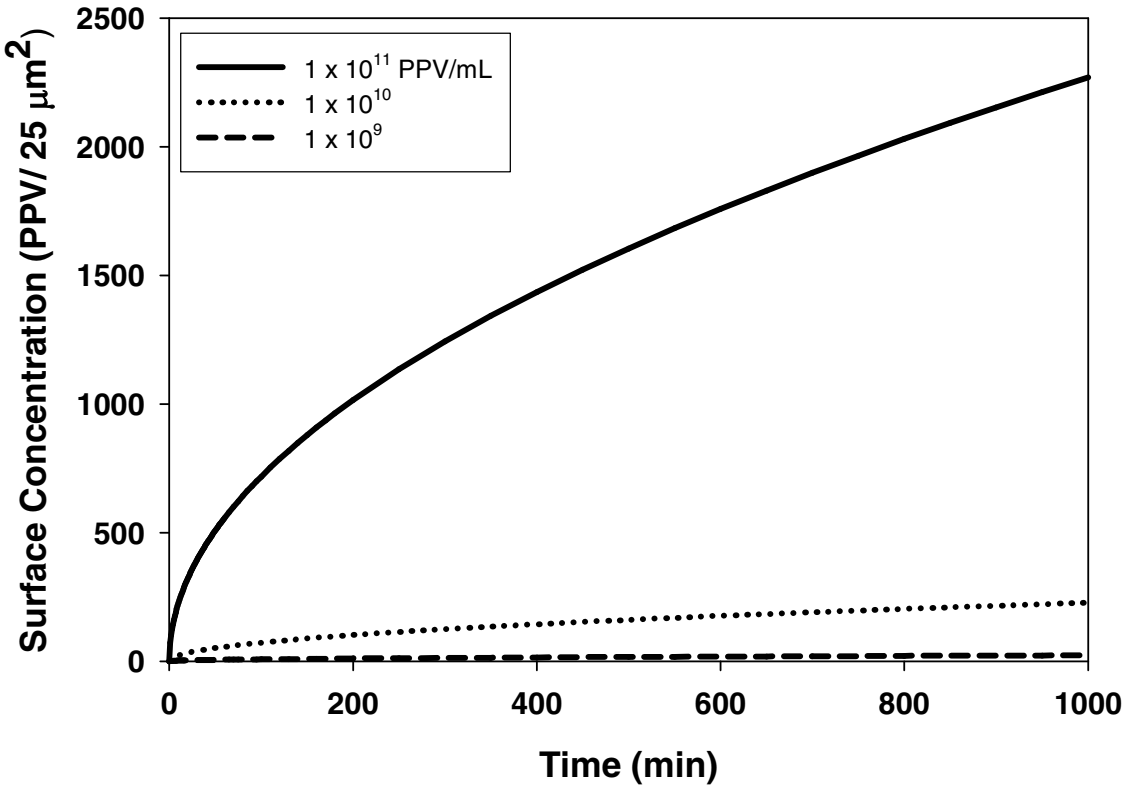

Figure 3. Surface accumulation of PPV at 39 ˚C at different PPV concentrations (viruses/mL).

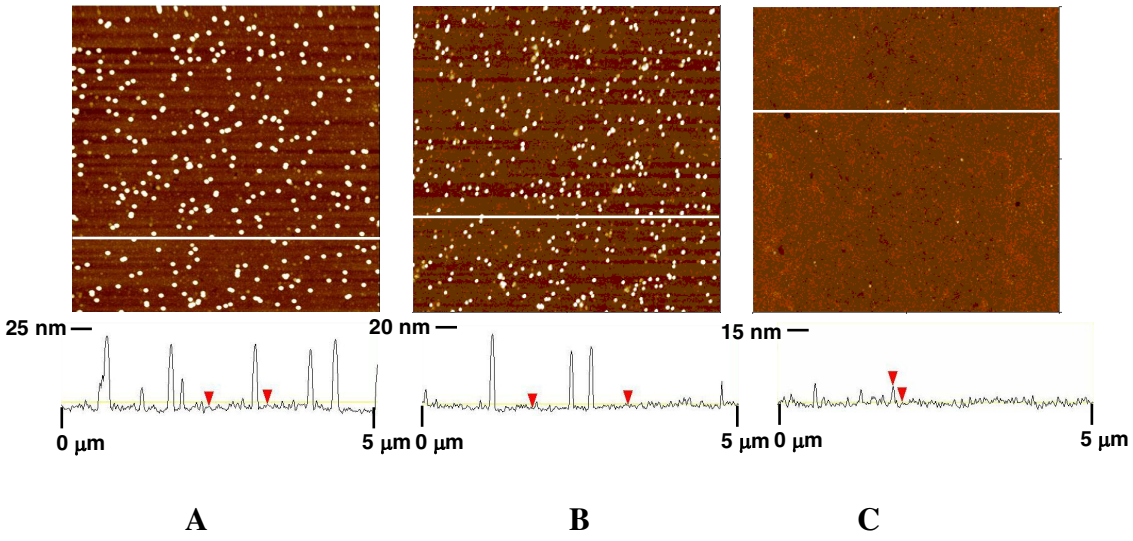

Figure 4. AFM micrographs (5 x 5 μm^2) and topographic cross-sectional plots of viruses bound to capture substrates at 25 ˚C for 16 h for A) FCV (5 x 10^8 $TCID_{50}$/mL), B) PPV (6 x 10^6 $TCID_{50}$/mL), and C) blank (10 mM PBS).

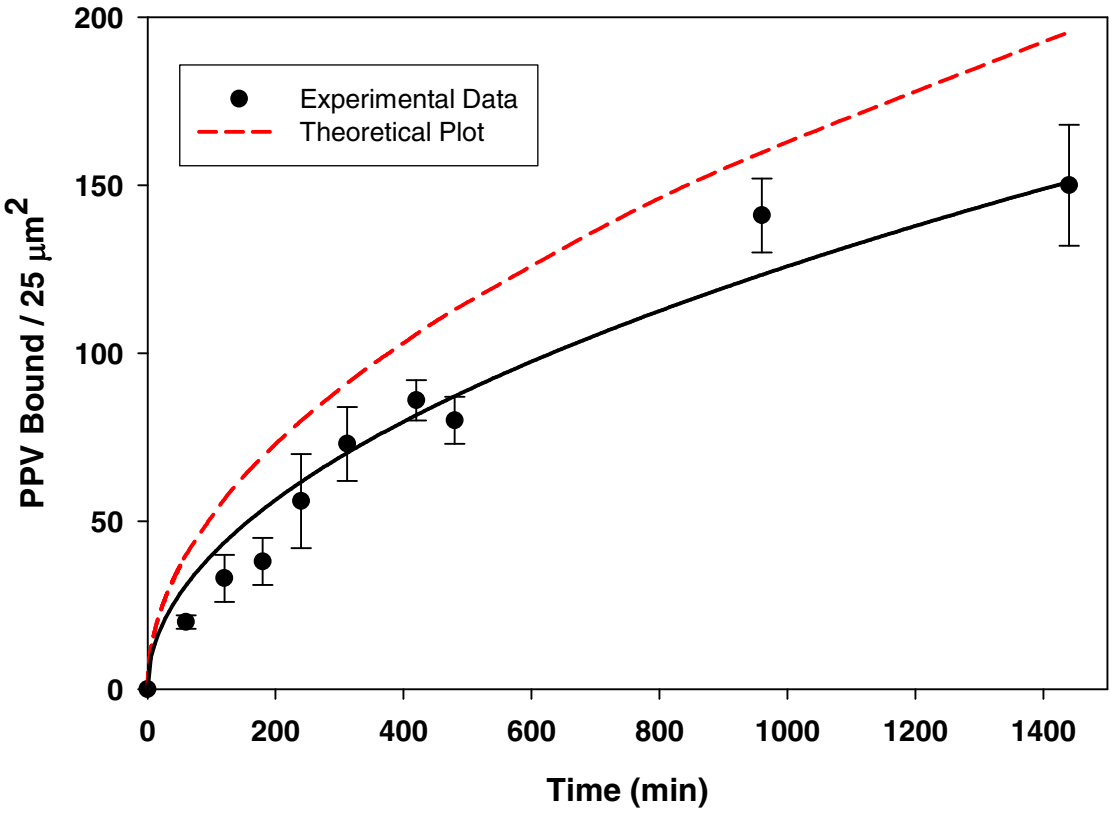

Figure 5. Accumulation as a function of incubation time at 25 ˚C for a PPV concentration of 8.9 x 10^9 virus particles/mL. The experimental data were obtained by collecting AFM micrographs (5 x 5 μm) and averaging the number of enumerated PPV in five separate locations. The experimental data were then fit to Equation 2, which yielded $\Gamma = 4.0t^{1/2}$ with an r^2 value of 0.96. The theoretical curve was determined according to Equation 2 by calculating Γ values at given times for a PPV concentration of 8.9 x 10^9 virus particles/mL, and a diffusion coefficient of 2.0 x 10^{-7} cm^2/s (see Table 1).

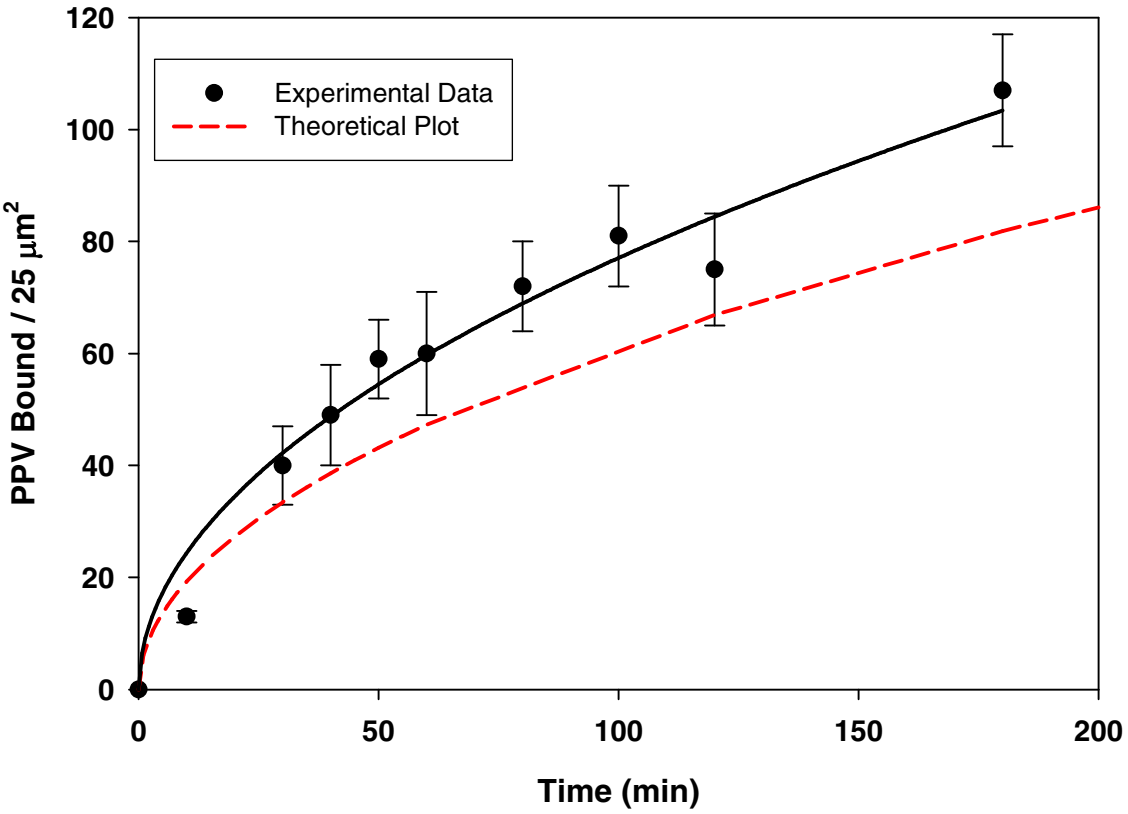

Figure 6. Accumulation as a function of incubation time at 39 ˚C for a PPV concentration of 8.9 x 10^9 virus particles/mL. The experimental data were obtained by collecting AFM micrographs (5 x 5 μm) and averaging the number of enumerated PPV in five separate locations. The experimental data were then fit to Equation 2, which yielded $\Gamma = 7.7t^{1/2}$ with an r^2 value of 0.97. The theoretical curve was determined according to Equation 2 by calculating Γ values at given times for a PPV concentration of 8.5 x 10^9 virus particles/mL, and a diffusion coefficient of 2.8 x 10^{-7} cm^2/s (see Table 1).

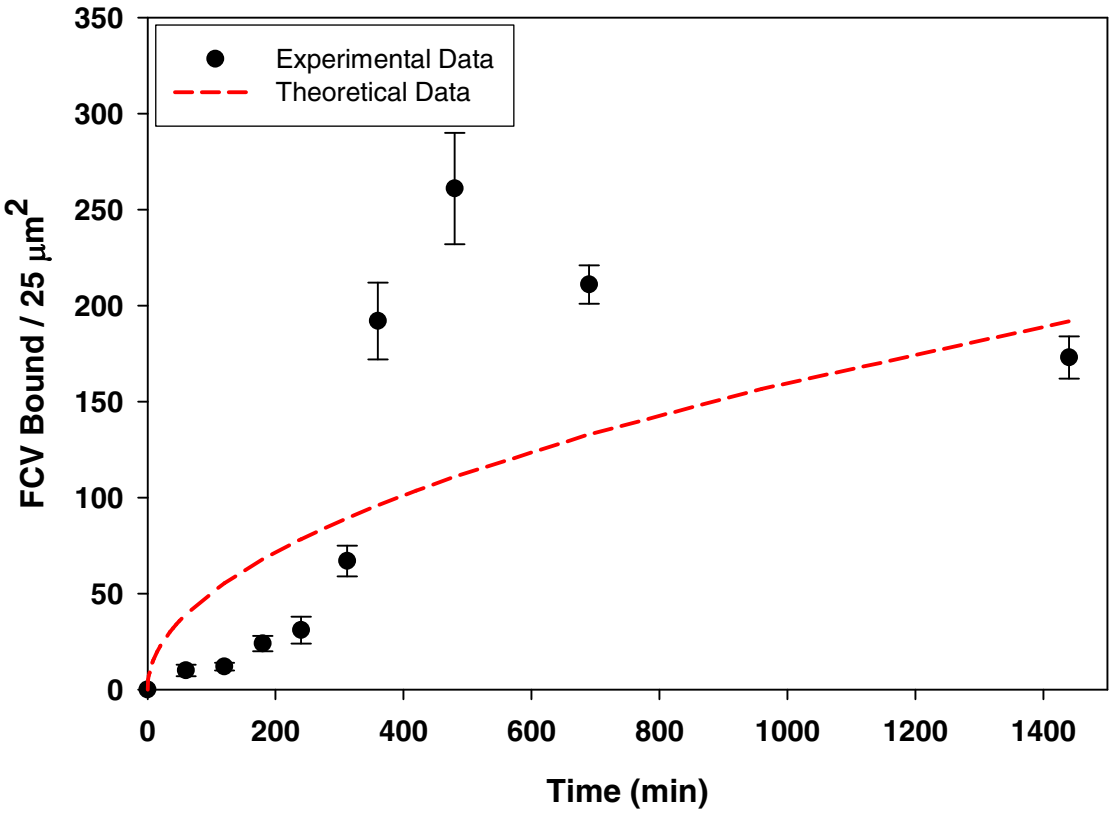

Figure 7. Accumulation as a function of incubation time at 25 ˚C for a FCV concentration of 1.0 x 10^{10} virus particles/mL. The experimental data were obtained by collecting AFM micrographs (5 x 5 μm) and averaging the number of enumerated FCV in five separate locations. The theoretical curve was determined according to Equation 2 by calculating Γ values at given times for a FCV concentration of 1.0 x 10^{10} virus particles/mL, and a diffusion coefficient of 1.4 x 10^{-7} cm^2/s (see Table 1).

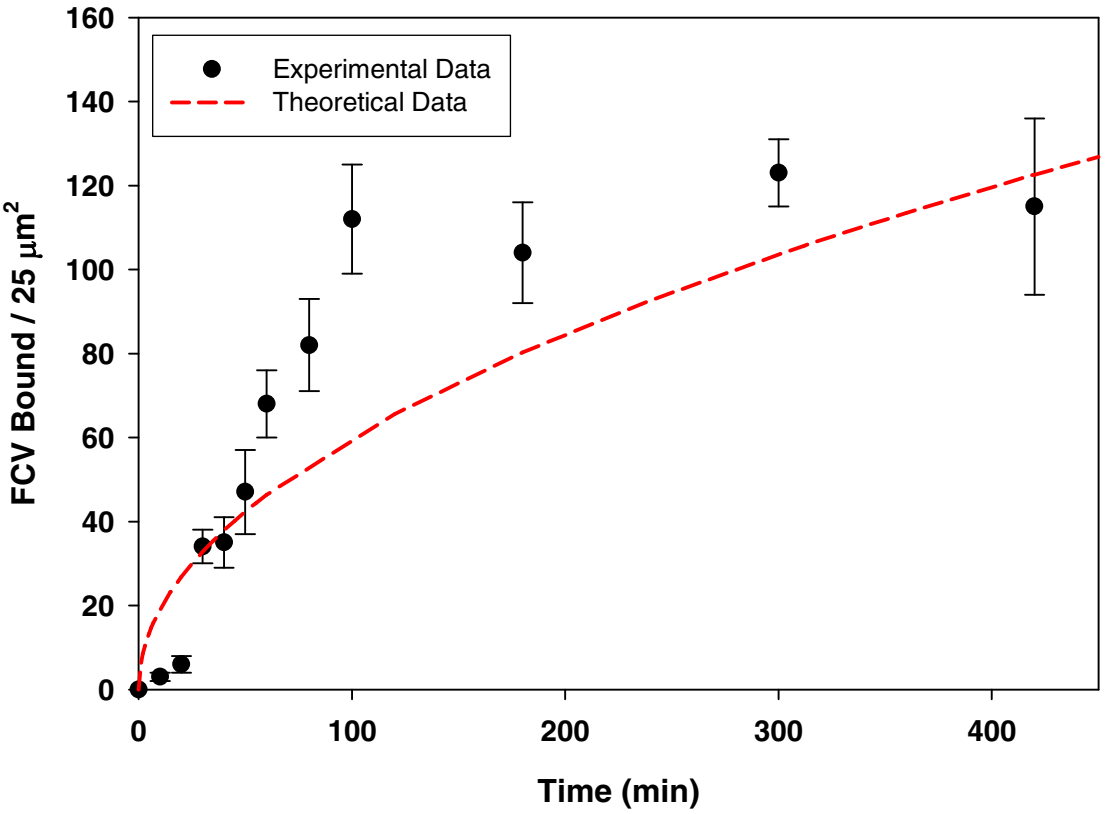

Figure 8. Accumulation as a function of incubation time at 39 ˚C for a FCV concentration of 1.0 x 10^{10} virus particles/mL. The experimental data were obtained by collecting AFM micrographs (5 x 5 μm) and averaging the number of enumerated FCV in five separate locations. The theoretical curve was determined according to Equation 2 by calculating Γ values at given times for a FCV concentration of 1.0 x 10^{10} virus particles/mL, and a diffusion coefficient of 2.0 x 10^{-7} cm^2/s (see Table 1).

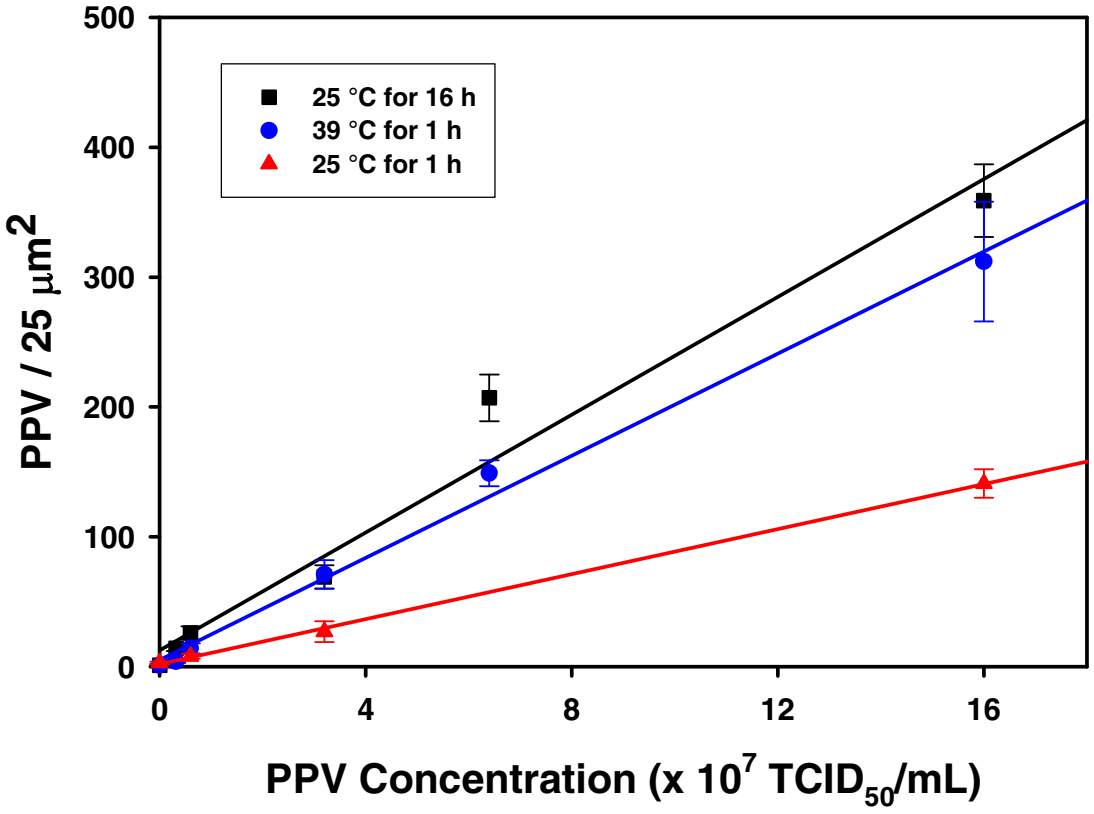

Figure 9. Dose response curves for PPV at 25 ˚C for 16 h and 1 h and 39 ˚C for 1 h. The data were obtained by collecting at least 5 AFM micrographs (5 x 5 µm) at each concentration and averaging the number of PPV bound in the imaged area.

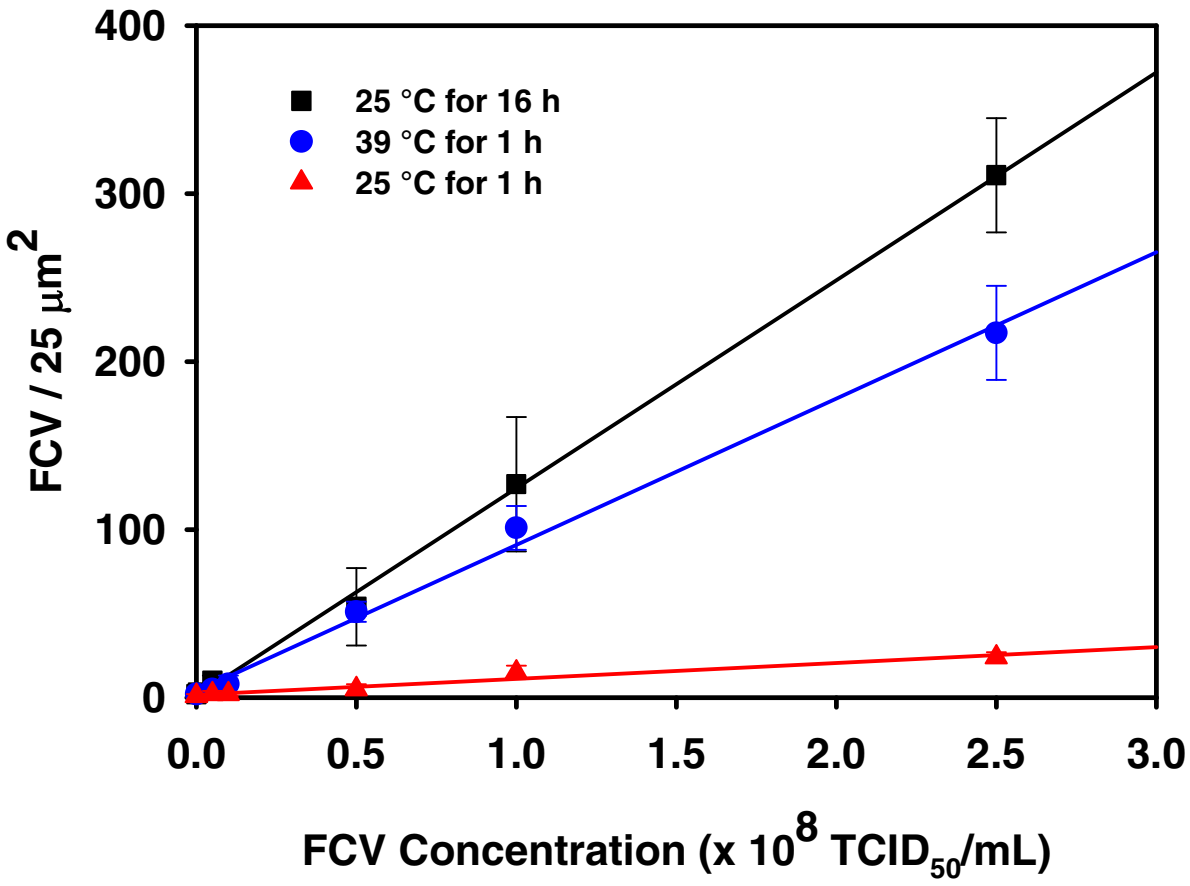

Figure 10. Dose response curves for FCV at 25 ˚C for 16 h and 1 h and 39 ˚C for 1 h. The data were obtained by collecting at least 5 AFM micrographs (5 x 5 μm) at each concentration and averaging the number of FCV bound in the imaged area.

CHAPTER 3: EFFECT OF CAPTURE SUBSTRATE AREA AND SAMPLE VOLUME ON DETECTION IN A HETEROGENEOUS IMMUNOASSAY: VIRUS READOUT WITH SURFACE-ENHANCED RAMAN SCATTERING

A manuscript in preparation for submission to *Analytical Chemistry*

Karen M. Kwarta*, Jeremy D. Driskell, Robert J. Lipert, and Marc D. Porter*

Institute for Combinatorial Discovery, Departments of Chemistry and Chemical and Biological Engineering, Ames Laboratory—U.S. DOE, Iowa State University, Ames, Iowa 50011-3020

Current Address: Center for Combinatorial Sciences, Biodesign Institute, Department of Chemistry and Biochemistry, Arizona State University, Tempe, AZ 85287

John D. Neill and Julia F. Ridpath

Virus and Prion Diseases of Livestock Unit, National Animal Disease Center, United States Department of Agriculture, Ames, Iowa 50010

ABSTRACT

Attomolar levels of detection were achieved for the analysis of porcine parvovirus (PPV) in a sandwich immunoassay format by exploiting the sensitivity of surface-enhanced Raman scattering (SERS) as a readout method and manipulating the area of the

capture substrate and sample volume. The low level of detection was achieved by using a two-fold approach. First, the area of the antibody-coated capture substrates was reduced from 7.0 x 10^{-2} to 4.0 x 10^{-4} μm^2. Second, the analyte volume was increased from 20.0 to 1000.0 μL. When coupled with surface-enhanced Raman scattering (SERS) and extrinsic Raman labels (ERLs), a level of detection of 4.5 x 10^5 PPV/mL (750 aM) was realized. Comparisons in limits of detection were made for larger sized (3-mm diameter) addresses using the two extreme volumes to understand the performance trade offs. These findings are also contrasted with those predicted from equilibrium considerations.

INTRODUCTION

Immunoassays are commonly used as diagnostic tests in human and veterinary medicine.[1] Current areas of focus have been on improving limits of detection, decreasing time requirements and simplifying the methodology in order to provide healthcare with tests to quickly and accurately provide diagnosis.[2, 3] Some pathogens (e.g. *E. coli* O157:H7, listeria, calicivirus, and avian influenza) can cause severe health problems like gastroenteritis at very low levels of exposure,[4-6] driving the need for ultra-sensitive detection techniques.

Methods for virus detection include electron microscopy,[7, 8] fluorescence-based labeling,[9, 10] polymerase chain reaction (PCR),[11-16] atomic force microscopy (AFM),[17-20] virus isolation,[21] and serologic testing.[22] However, these methods lack the sensitivity needed for detecting single viruses[6] (limits of detection ranging from 10^5 viruses/mL for fluorescence[9] to 10^8 viruses/mL for AFM detection[19]). To meet the demands of diagnosis for certain viruses and bacteria, lower levels of detection must be realized.

To reach ultra-low levels of detection, a high surface concentration of antigen bound to the sensor area is desirable, especially for readout methods that do not interrogate the entire sensor area. As an example, if the sensor area is 0.070 cm^2, the laser area is 4.5 x 10^{-6} cm^2, and the size of a virus is 25-nm in diameter (Scheme 1), only a small percent of the sensor area is interrogated by the laser. In order to achieve ultra-low limits of detection, then, the highest surface concentration of bound antigen for any given initial antigen concentration is desirable. Examination of the sensor area, sample volume, and equilibrium constant on the surface concentration of bound antigens, will provide insight into the conditions needed to achieve the highest surface concentrations of antigen, and therefore the lowest limits of detection. To achieve this condition, it is desirable to apply the principles of negligible depletion in order to retain the binding affinity of the capture antibody.[23] Depletion of the free concentration of analyte causes changes in the equilibrium, which in turn, affects the concentration of analyte that can be extracted.[24]

In this paper, we seek to understand the gains achieved by using small capture substrates and large sample volumes to detect low levels of porcine parvovirus (PPV). To study the effect of sample volume on the SERS signal for detection of PPV, three tests were performed. In the first two tests, large (0.071 cm^2) capture substrates were exposed to either small (20.0 μL) or large (1.0 mL) volumes of PPV and ERL solutions. For the third test, small capture substrates (4.0 x 10^{-4} cm^2) were treated with large volumes (1.0 mL) of PPV and ERL solutions. In each case, calibrations curves were constructed, and signal strengths and limits of detection were compared. The small gold substrates were fabricated on pyrex wafers and then modified with monoclonal antibodies specific for

porcine parvovirus (anti-PPV mAbs). Large gold substrates were also modified with anti-PPV mAbs, and the immunoassay procedure for both substrate sizes follows that previously optimized in our laboratory.[25] ERLs were constructed using 60-nm gold nanoparticles coated with an intrinsically strong Raman scatterer to provide the spectral signature, and anti-PPV mAbs to provide biorecognition. Since large biomolecules have small diffusion coefficients,[26] the viruses and ERLs were allowed to diffuse to the capture substrates for 24 h in an attempt to establish equilibrium.

SERS has been shown to be a sensitive readout method, and therefore provides a basis to push the envelope for ultra-low levels of detection. Current levels of detection for SERS readout methods are in the femtomolar regime, and for virus detection with SERS the current level of detection is 1 x 10^6 viruses/mL.[25] Previous studies in our laboratory have shown that as few as ~60 binding events can be detected using 30-nm gold nanoparticles with limits of detection of ~30 fM for prostate specific antigen in human serum.[27] We would like to exploit this sensitivity and reach far lower levels of detection by capitalizing on the high surface concentrations of antigen achieved with small capture substrates and large volumes.

THEORETICAL CONSIERATIONS

Equilibrium Model for Heterogeneous Immunoassays. We have modeled the equilibrium for a heterogeneous immunoassay as a function of the capture substrate surface area and the volume of the sample solution to determine the ideal conditions to reach low levels of detection. As a starting point, the equilibrium for a 1:1 binding stoichiometry can be expressed by[3]:

$$Ag_{soln} + Ab_{surf} \leftrightarrow AgAb_{surf} \qquad (1)$$

where Ag_{soln} is the antigen in solution, Ab_{surf} is the uncomplexed antibody immobilized on the surface, and $AgAb_{surf}$ is the antibody-antigen complex on the surface. The equilibrium constant, K (L/mol), for a heterogeneous assay is defined as:

$$K = \frac{\Gamma_{AgAb}}{[Ag]_{sol}\Gamma_{Ab}} \qquad (2)$$

where Γ_{AgAb} is the equilibrium surface concentration of bound antigen (mol/cm^2), $[Ag]_{sol}$ is the equilibrium solution concentration of antigen (mol/L), and Γ_{Ab} is the equilibrium surface concentration of uncomplexed antibody (mol/cm^2). Since the equilibrium in Equation 1 involves a liquid and solid phase, a full accounting of the system must include the area of the capture substrate, A, and the volume of the sample solution, V. The equilibrium concentration for the antigen in solution can then be written as:

$$[Ag]_{sol} = \frac{CV - \Gamma_{AgAb}A}{V} \qquad (3)$$

where C is the initial antigen solution concentration. By mass balance, we can determine Γ_{Ab} via Equation 4 :

$$\Gamma_{Ab} = \Gamma_{Ab,i} - \Gamma_{AgAb} \qquad (4)$$

where $\Gamma_{Ab,i}$ is surface concentration of the initial antibody immobilized on the capture substrate. By substituting Equations 3 and 4 into Equation 2 and rearranging, we obtain:

$$KA\Gamma_{AgAb}^2 + (-V - KCV - KA\Gamma_{Ab,i})\Gamma_{AgAb} + KCV\Gamma_{Ab,i} = 0 \qquad (5)$$

By using the quadratic equation, we can solve for Γ_{AgAb} as a function of several important experimental parameters (i.e., C, V, A, and K).

Table 1 summarizes the values of the key parameters that will be used to model the heterogeneous equilibrium. These values reflect, in part, the design of our experimental assay platform, including estimates of $\Gamma_{Ab,i}$ and possible values of K. Some of the values, however, were included in order to more fully delineate the intricacies of the equilibrium. The remainder of this section examines the impact of these parameters on the performance of an assay, focusing specifically on how to push the LOD to lower values.

As a starting point, the effect of K and C on Γ_{AgAb} was examined using our 3-mm diameter capture substrate (A = 0.070 cm^2) and a 1.0-mL sample. These results are presented in Figure 1. For all values of K, the dependence of Γ_{AgAb} on C has the sigmoid-like shape expected for a typical distribution plot,[3, 28] which arises from a shift in the heterogeneous equilibrium towards an increase in the absolute amount of antigen captured by the immobilized antibodies. A more detailed examination of these plots reveals three additional points. First, the profiles all reach the same upper value for Γ_{AgAb}. This result reflects the limitation imposed by the surface concentration of capture antibodies (6.7 x 10^{-13} mol/cm^2, see Table 1).[29]

Second, the profiles all move to larger values of C as K decreases. This trend highlights the impact of the affinity between the antigen and immobilized antibody on the LOD. If, for example, the readout technique can detect a Γ_{AgAb} of 6.7 x 10^{-14} mol/cm^2, the LOD at a K of 1.0 x 10^7 would be ~1 x 10^{-8} M. Furthermore, the plots show that a decade-increase in K lowers the LOD by a factor of ten.

Third, the above trend holds until moving up to a K value of 10^{10}. Above K values of 10^{10} the improvement in LOD with increases in K drops dramatically. From a

graphical perspective, this change corresponds to a marked deterioration in the shape of the plots in Figure 1 in that as *K* becomes larger, the profile becomes more truncated. The truncation in shapes arises from a perturbation in the initial concentration of the antigen solution, *C*, from the extraction of antigens by the capture substrate. As a consequence, the surface concentration of the antigen-antibody complex is not pushed to the level that would be achieved in the absence of any depletion of the initial antigen solution concentration, and the LOD is higher than would be the case in the absence of depletion.

The importance of depletion and its connection to sample volume are examined in more detail in Figures 2A-C. These plots summarize the effect of sample volume (20-1000 μL) and the equilibrium constant (10^9 – 10^{13}) on Γ_{AgAb}. In general, the profiles have a shape that becomes increasingly truncated as volume decreases and *K* increases. Both trends can be attributed to how the experimental conditions affect depletion. That is, larger volumes and smaller values of *K* will not be as sensitive to depletion as test conditions at smaller sample volumes and larger values of *K*. The plots in Figure 2 also illustrate how the sample volume affects the LOD. At each value of *K*, the LOD decreases as the sample volume increases. Moreover, the ideal case for detection at a given value of *K* occurs when depletion is negligible. This situation is demonstrated by the coalescence of the plots in Figure 2A. This coalescence corresponds to an assay that is independent of sample volume, i.e., an assay carried out in a negligible depletion mode.[23, 24, 30]

One approach to alleviate the dependence of volume on the number of antigens bound at equilibrium would be to use a capture substrate with a smaller area and a sample with a larger volume. At small capture substrate areas (4.0×10^{-4} cm^2) and large sample

volumes (1.0 mL), different values of K show the expected sigmoid shape (Figure 3), and truncation is not as pronounced as when large capture substrates are used. The profiles for the small capture substrates reach the same upper limit of Γ_{AgAb}, that is found for the large capture substrates, a consequence of both models being assigned the same value for $\Gamma_{Ab,i}$. For a sensor area of 4.0 x 10^{-4} cm^2, and a K value of 1.0 x 10^{11}, the surface concentration of antigen bound, Γ_{AgAb} is plotted in Figure 4 with respect to the initial antigen concentration, C. The curves deviate only slightly when small volumes are used, suggesting that small capture substrate areas provide a means to achieve high surface concentrations of antigen at low sample volumes by reducing the effect of depletion.

The importance of volume on the equilibrium of the system can be expressed by calculating the values required to prevent perturbation of the initial antigen concentration. For our purposes, we have defined the volume for minimal depletion as that which upholds the condition, $[Ag]_{soln} = 0.09C$. The results of this calculation for different K and C values are shown in Figure 5. Figure 5A and 5B show the volume necessary to prevent sample depletion for large and small capture substrates, respectively. Higher values of K require larger solution volumes to prevent depletion, an observation that is more pronounced for low initial antigen concentrations. To remain volume independent, and thus achieve the highest surface bound antigen concentrations (Figures 2 and 4), larger volumes are required for larger capture substrates as compared to smaller capture substrates. An additional consequence of this observation is that the reproducibility of the assay is more sensitive to variations in small volumes with larger capture substrates. The next several sections detail experiments designed to explore these predictions.

EXPERIMENTAL

Reagents. Anti-PPV mAbs were provided by National Animal Disease Center (NADC; Ames, IA) as a 1.0 mg/mL stock and were purified with a protein G column (Pro-Chem) to 99.9% purity. PPV stock solutions were also supplied by NADC in phosphate buffered saline (PBS) with a concentration of 3.2×10^9 $TCID_{50}$/mL. The conversion factor for PPV from $TCID_{50}$/mL to virus particles/mL is ~1400 and was derived from fitting experimental curves of PPV accumulation with respect to rotation rate.[31]

Gold nanoparticles (60 nm, 2.6×10^{10} particles/mL) were purchased from Ted Pella. Octadecanethiol (ODT), PBS packs (10 mM), sodium chloride, dithiobis(succinimidyl propionate) (DSP), and bovine serum albumin (BSA) were purchased from Sigma. Superblock and borate buffer packs (50 mM) were received from Pierce. 5,5'-dithiobis(succinimidyl-2-nitrobenzoate) (DSNB) was synthesized according to literature.[27]

ERL Preparation. ERLs integrate a strong Raman scatterer with an immunorecognition element such as an antibody. DSNB was designed as the Raman reporter molecule because of its inherently strong Raman scattering cross section due to the symmetric stretch of the nitro group tethered to an aromatic ring. In addition, DSNB spontaneously adsorbs to the gold nanoparticles through cleavage of the disulfide moiety and covalently attaches antibodies to the succinimidyl ester group by forming an amide bond with the amine groups found on antibodies.

To prepare 1.0 mL of ERLs, the pH of the 60-nm gold nanoparticle solution was adjusted to 8.5 by adding 40.0 μL of 50 mM borate buffer. The nanoparticles were then

coated with DSNB by adding 10 μL of 1 mM DSNB in acetonitrile and mixing for 8 h. For immunospecificity of the colloidal solution, 20 μg of anti-PPV mAb was added to the suspension for ~12 h. Finally, the colloidal suspension was stabilized and blocked by adding 10% BSA in 2 mM borate buffer (100.0 μL) for 6 h. For removal of residual proteins and DSNB, the nanoparticles were centrifuged at 2000 *g* for 10 min. The supernatant was decanted, and the particles were resuspended in 1.0 mL of 2 mM borate buffer containing 1% BSA. This rinsing cycle was repeated twice to thoroughly remove any excess reagents. In the final resuspension step, 100.0 μL of 10% NaCl was added to the 1.0 mL suspension to reach a final physiological salt concentration of ~150 mM. Aggregates were removed by passage of the solution through a 0.22-μm syringe filter (Costar).

Preparation of Small Area Capture Substrates. The small area (200 x 200 μm) substrates were prepared using conventional photolithographic and metal lift-off techniques. A 0.5-mm thick pyrex wafer (University Wafer) was first coated with positive photoresist (AZ4330, Clariant) at 2000 rpm for 30 s and then softbaked at 110 ˚C for 1 min. The resist-coated wafer was then exposed to UV light for 4 s through a photomask and post-exposure baked for 1 min at 110 ˚C. The wafer was subsequently immersed in developer (3:1 water:Shipley 351 developer) for 2 min. Next, the patterned wafer was coated with an 8-nm titanium adhesion layer (0.1 nm/s), followed by a 75-nm layer of gold (0.1 nm/s). Lift-off of the gold-coated photoresist was achieved by sonication in acetone (Fisher) and an ethanol post rinse. The substrates were finally dried

with a stream of high-purity nitrogen. The wafers were then cut into 1 x 1 cm sections by American Dicing.

To modify the sample squares with a linker molecule to covalently immobilize the capture antibody, the squares were first cleaned with a 40-W argon plasma for 1 min at 1 Torr and then immediately placed in a 0.1 mM ethanolic solution of DSP for ~5 h. The samples were then rinsed with ethanol and dried under high-purity nitrogen.

Preparation of Large Area Capture Substrates. Microscope slides (Fisher) cut to 1 x 1 cm were cleaned sequentially in an ultrasonic bath in diluted Contrad 70, deionized water, and ethanol for 30 min each. Then, the clean glass chips were placed in an Edwards 306A resistive evaporator. First a chromium adhesion layer (~10 nm) was resistively evaporated onto the glass chips followed by ~250 nm of gold (99.9% purity) at a rate of 0.1 nm/s. To create a capture substrate of the appropriate size, a piece of PDMS with a 3-mm diameter hole cut out of the center was soaked in an ethanolic ODT solution for ~1 min and placed on the clean gold substrates for ~30 s. The stamp was removed, and the substrates were rinsed with ethanol and placed in a 0.1 mM ethanolic solution of DSP for ~12 h. Finally, the substrates are rinsed with ethanol and dried with high purity nitrogen. The ODT adlayer creates a hydrophobic barrier that confines sample solutions to a 3-mm diameter circle. The DSP-derived adlayer covalently couples the mAbs to the gold substrate.

Immunoassay Protocol. Immunospecificity was achieved by pipetting an anti-PPV mAb solution (20.0 μL, 100 μg/mL in 50 mM borate buffer (pH 8.5)) over the 200 x 200 μm gold squares or in the 3-mm capture area for ~12 h in a humidity chamber. The samples were then rinsed by submerging them sequentially three times in fresh 10 mM

PBS (3 mL). The samples were then placed in 1.0 mL or 20.0 μL of SuperBlock blocking buffer for ~8 h and then rinsed with 10 mM PBS. PPV samples were diluted in 10 mM PBS, and the samples were immersed in 1.0 mL or 20.0 μL of each PPV concentration for ~24 h. The samples were rinsed three times with 2 mM borate buffer containing 150 mM NaCl and then exposed to 1.0 mL or 20.0 μL of prepared ERLs and incubated for ~12 h. After ERL binding, the substrates were rinsed with 2 mM borate buffer (150 mM NaCl) three times and then dried with a stream of high purity nitrogen. SERS spectra were then obtained for each substrate.

Instrumentation. A NanoRaman I fiber-optic-based Raman system (Concurrent Analytical) was used to collect the Raman spectra. The light source was a 30-mW, 632.8-nm He-Ne laser; the spectrograph was a *f*/2.0 Czerny-Turner imaging spectrometer (6-8 cm^{-1} resolution); and a Kodak 0401E CCD thermoelectrically cooled to 0 ˚C. The incident laser light (normal incidence) was focused to a 25-μm spot size on the 200 x 200 μm gold squares or in the 3-mm diameter sensor area. The objective has a numerical aperture of 0.68, and the power at the sample was ~3 mW. The same objective was used to collect the scattered radiation. Spectra were obtained with 1-s integration.

RESULTS AND DISCUSSION

Three tests were performed in order to assess the effect of the area of the capture substrate and volume of the sample on the concentration dependent signal strength and LODs. Two tests used our 3-mm diameter addresses and either 1.0-mL or 20.0-μL sample volumes. The third reduced the address size to 200 x 200 μm (4.0 x 10^{-4} cm^2) and

a 1.0-mL sample. For each experiment, SERS spectra were collected for various concentrations of PPV, with 24-h incubations employed in both the capture and ERL labeling steps. In all cases, the spectra show features that are consistent with the Raman reporter molecule, DSNB (e.g., the symmetric nitro stretch, $\nu_s(NO_2)$ at 1336 cm^{-1} and an aromatic ring mode at 1558 cm^{-1}), and have signal strengths proportional to PPV concentration. The intensity of $\nu_s(NO_2)$ was averaged from five different locations on each substrate in order to construct dose-response curves. The standard deviations in these plots are represented by the error bars.

Based upon the model, the expected surface concentrations of antigens at an initial antigen concentration of 1.0×10^{-17} M for the three tests performed are delineated in Table 2 for two values of *K*. As detailed in the table, small capture areas and large sample volumes are expected to yield the highest signals and the least sample depletion. The experimental results are presented below.

Test I. Large capture substrate area, small sample volumes. In this experiment, SERS spectra were collected for large area capture substrates (0.071 cm^2) using small volumes (20.0 μL) of virus and ERLs. Figure 6 presents spectra for concentrations up to 2.0×10^{10} PPV/mL. The dose-response curve from these spectra is found in Figure 7, which shows a leveling-off in signal about 9.0×10^9 PPV/mL. An analysis of these data yields a LOD of 2.1×10^7 PPV/mL. Interestingly, there is no detectable non specific binding of the ERLs in this set of experiments, an ideal, but only occasionally realized situation. Thus the blank signal is determined only by the noise in the measurement.

Test II. Large capture substrate area, large sample volume. This test used large substrates (0.071 cm^2 capture area) and large sample volumes (1.0 mL) of PPV and ERLs. The SERS spectra are shown in Figure 8 and the dose-response curve is given in Figure 9. There are two main observations to draw from this data. First, these samples all exhibit a detectable level of non-specific adsorption. However, we have not been able to determine why this proved problematic with these samples but not those in Test I. Second, the strength of the signal for these samples is larger than those prepared using the 20.0-μL sample volumes (Figure 6). For example, the response for a 1.0-mL sample at 4.5×10^8 PPV/mL, after accounting for the background signal, is more than five times stronger than that for the analogous 20.0-μL sample. We attribute this difference to how the sample volume alleviates depletion, and pushes a larger absolute number of antigens onto the capture substrate. Analysis of these data yields a LOD of 4.2×10^7 PPV/mL.

Test III. Small capture substrate area, large sample volume. Finally, 200 x 200 μm addresses, which are 1.4×10^{-3} times smaller in area than the 3-mm diameter addresses, were exposed to 1.0-mL of PPV and ERL solutions. The goal is to examine how much of an increase in PPV surface concentration will be realized by a reduction in the surface area of the capture substrate, which would be driven by a lower level of antigen depletion in the 1.0-mL sample. The SERS spectra and dose-response plot are presented in Figures 10 and 11, respectively. A comparison to the data in Figure 8 shows that the expectation of a larger signal is achieved. That is, the response for the exposure to 1.0-mL of 4.5×10^7 PPV/mL solution is 3086 cts/s (after accounting for the average blank signal) for the small address and only 2594 cts/s with the larger address. Moreover, if a linear dependence is assumed for the signals of Test I, the same sample

concentration, would yield only 103 cts/s at a 20.0-μL volume. In this case, the signal obtained from Test III is ~30 times greater than that projected for Test I. Taken together, the assay with the small sized capture addresses yields a LOD of 4.5 x 10^5 PPV/mL or 750 aM. Performance can also be cast within the context of $TCID_{50}$ units, which is a quantile measure of pathogenicity. By this measure, the LOD translates to 320 $TCID_{50}$/mL.

Further examination of the implications of the results in Figures 6-11 can be developed by establishing a correlation between the SERS response and number of bound virus particles. For this purpose, the dose-response curves in Figure 8 can be compared with that from a recent investigation that enumerated the capture of PPV (3-mm address, 20.0-μL sample) by atomic force microscopy (AFM).[32] Figure 12 summarizes both sets of data, noting that the AFM-based findings were extrapolated from 5 x 5 μm image sizes to the area interrogated by the 25-μm diameter laser spot size in the SERS experiments. Like the SERS data, the enumeration by AFM undergoes a linear increase at low PPV concentrations. Thus, the correlation between the two plots shows that the SERS signal for each captured virus is ~4 cts/s.

This correlation can then be used to delineate the number of viruses that give rise to the signal of the LOD for SERS measurements. Table 3 summarizes the analysis of the spectral data from all three tests, and includes estimates of the percentage of PPV depletion as a consequence of the capture step. The Table also projects the number of viruses in the laser focal area at levels approaching and below the LOD, and is given parenthetically. In each case, less than 100 viruses give rise to the signal at the LOD. The

Table also underscores the merits of minimizing sample depletion in reaching the LOD found for the small capture substrate/large volume (S/L) assay.

CONCLUSIONS

The lowest concentration of PPV studied in Test I (4.5×10^8 PPV/mL) gives a SERS signal of 1028 ± 91 cts/s. In comparison, the highest concentration of PPV studied in Test III (4.5×10^7 PPV/mL) gives a SERS signal of 3220 ± 286 cts/s, an improvement of 30 times. The limit of detection for large capture areas and small sample volumes is 100 times greater when small capture substrates and large volumes are employed. This improvement is attributed to the higher surface concentration of captured viruses achieved by conducting the analysis in a negligible depletion mode.

Non-specific binding plays a key role in the determination of limits of detection, often dictating the experimental limit of detection. As is seen in the findings herein, a lower level of detection is found in Test I as compared Test II largely because the non-specific binding is higher for Test II. The blank signal for the large substrate and small sample volumes is effectively immeasurable, that is, no non-specific binding could be detected. In comparison, the blank signal for Test II is 821 ± 142 cts/s and that for Test III is 134 ± 41 cts/s.

The use of small substrates exposed to large sample volumes allows for attomolar detection of viruses through increasing the surface bound concentration of viruses at low virus concentrations. However, a challenge remains in that the level of performance requires long incubation times. As has been recently shown, this difficulty can be overcome by substrate rotation[31] and elevations in temperature.[33] By combining substrate

rotation with small capture areas and large sample volumes to allow the highest surface bound concentration of antigen, and using the ultra-sensitive readout method of SERS, ultra-low levels of detection for pathogens can be achieved in relatively short times, providing an attractive method for diagnosis/identification in the event of an outbreak. These results emphasize that in order to realistically detect ultra-low levels of detection, large sample volumes and/or small capture substrates are clearly preferred embodiments.

ACKNOWLEDGEMENTS

This work was supported through a grant from USDA-NADC and by the Institute for Combinatorial Discovery of Iowa State University. K. M. Kwarta gratefully acknowledges the support of a Dow Chemical Fellowship. We would also like to acknowledge Ann Vorwald at the NADC for providing the PPV and anti-PPV. The Ames Laboratory is operated for the US Department of Energy through Iowa State University under contract W-7405-eng-82.

REFERENCES

(1) Sokoll, L. J.; Chan, D. W. *Anal. Chem.* **1999**, *71*, 356-62.

(2) Hage, D. S. *Anal. Chem.* **1999**, *71*, 294R-304R.

(3) Diamandis, E. P.; Christopoulos, T. K. *Immunoassay*; Academic Press: San Diego, 1996.

(4) Doyle, M. P. *Int. J. Food Microbiol.* **1991**, *12*, 289-301.

(5) Mead, P. S.; Slutsker, L.; Dietz, V.; McCaig, L. F.; Bresee, J. S.; Shapiro, C.; Griffen, P. M.; Tauxe, R. V. *Emerg. Infec. Diseases* **1999**, *5*, 607-24.

(6) Iqbal, S. S.; Mayo, M. W.; Bruno, J. G.; Bronk, B. V.; Batt, C. A.; Chambers, J. P. *Biosens. Bioelectron.* **2000**, *15*, 549-78.

(7) Kjeldsberg, E. *J. Virol. Meth.* **1986**, *14*, 321-33.

(8) Zheng, Y. Z.; Hyatt, A.; Wang, L. F.; Eaton, B. T.; Greenfield, P. F.; Reid, S. *J. Virol. Meth.* **1999**, *80*, 1-9.

(9) Donaldson, K. A.; Kramer, M. F.; Lim, D. V. *Biosens. Bioelectron.* **2004**, *20*, 322-7.

(10) Yoon, K.-J.; Iowa State Univeristy College of Veterinary Medicine: Ames, IA, 2004.

(11) Sykes, J. E.; Studdert, V. P.; Browning, G. F. *Arch. Virol.* **1998**, *143*, 1321-34.

(12) Sykes, J. E.; Allen, J. L.; Studdert, V. P.; Browning *Vet. Microbiol.* **2001**, *81*, 95-108.

(13) Helps, C.; Lait, P.; Tasker, S.; Harbour, D. *J. Virol. Meth.* **2002**, *106*, 241-4.

(14) Helps, C.; Harbour, D. *J. Virol. Meth.* **2003**, *109*, 261-3.

(15) Mackay, I. M.; EArden, K. E.; Nitsche, A. *Nucleic. Acid. Res.* **2002**, *30*, 1292-305.

(16) Ogilivie, M. *Rev. Med. Virol.* **2001**, *11*, 351-4.

(17) Kuznetsov, Y. G.; Malkin, A. J.; Lucas, R. W.; Plomp, M.; McPherson, A. *J. Gen. Virol.* **2001**, *82*, 2025-34.

(18) Kuznetsov, Y. G.; Low, A.; Fan, H.; McPherson, A. *Virol.* **2004**, *323*, 189-96.

(19) Nettikadan, S. R.; Johnson, J. C.; Mosher, C.; Henderson, E. *Biochem. Biophys. Res. Commun.* **2003**, *311*, 540-5.

(20) Nettikadan, S. R.; Johnson, J. C.; Vengasandra, S. G.; Muys, J.; Henderson, E. *Nanotech.* **2004**, *15*, 383-9.

(21) Payment, P.; Trudel, M. *Methods and Techniques in Virology*; Marcel Dekker: New York, 1993.

(22) Yoon, K.-J. *Department of Veterinary Diagnostic and Production Animal Medicine*; Iowa State University: Ames, IA, 2004.

(23) Heringa, M. B.; Hermens, J. L. M. *TrAC.* **2003**, *22*, 575-87.

(24) Dias, N. C.; Porter, M. D.; Fritz, J. S. *Anal. Chim. Acta* **2006**, *558*, 230-6.

(25) Driskell, J. D.; Kwarta, K. M.; Lipert, R. J.; Porter, M. D. *Anal. Chem.* **2005**, *77*, 6147-54.

(26) Sheehan, P. E.; Whitman, L. J. *Nano. Lett.* **2005**, *5*, 803-7.

(27) Grubisha, D. S.; Lipert, R. J.; Park, H.-Y.; Driskell, J. D.; Porter, M. D. *Anal. Chem.* **2003**, *75*, 5936-43.

(28) Harris, D. C., Ed. *Quantitative Chemical Analysis*, Fifth ed.; W. H. Freeman and Company: New York, New York, 1999.

(29) Dong, Y.; Shannon, C. *Anal. Chem.* **2000**, *72*, 2371-6.

(30) Nardi, L. *J. Chromatogr. A* **2003**, *985*, 85-91.

(31) Driskell, J. D.; Kwarta, K. M.; Lipert, R. J.; Vorwald, A.; Neill, J. D.; Ridpath, J. F.; Porter, M. D. *J. Virol. Meth.* **2006**, *138*, 160-9.

(32) Kwarta, K. M.; Driskell, J. D.; Porter, M. D.; Neill, J. D.; Ridpath, J. F. *Manuscript in Preparation* **2007**.

(33) Johnstone, R. W.; Andrew, S. M.; Hogarth, M. P.; Pietersz, G. A.; McKenzie, I. F. C. *Mol. Immunol.* **1990**, *27*, 327-33.

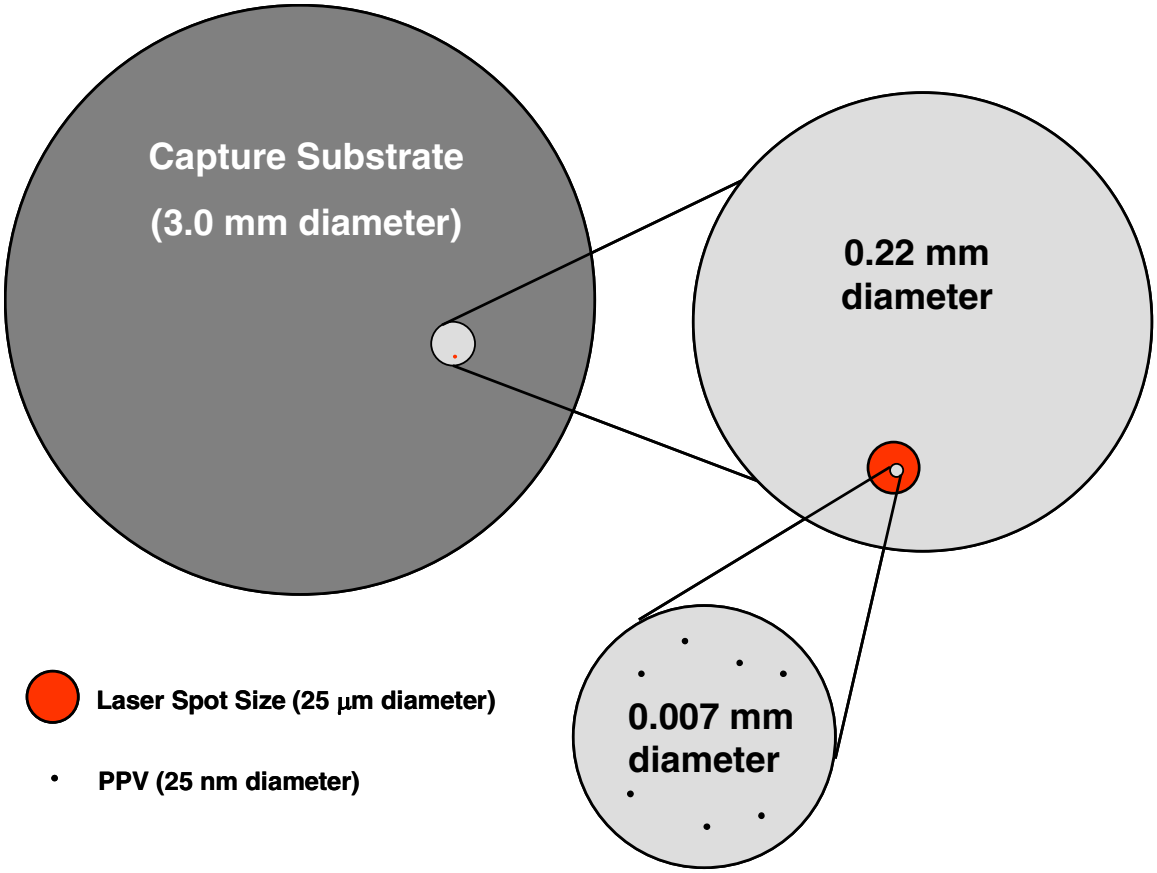

Scheme 1. Depiction (drawn to scale) of the size of the laser compared to a large capture substrate area (0.070cm^2).

Table 1. Model Parameters for Equilibrium Predictions.

Parameter	Range of Modeled Values
K (L/mol)[a]	$1.0 \times 10^{7} - 1.0 \times 10^{13}$
A (cm^2)[b]	7.0×10^{-2} and 4.0×10^{-4}
V (μL)[b]	20.0-1000.0
C (M)[c]	$1.0 \times 10^{-18} - 1.0 \times 10^{-6}$
$\Gamma_{Ab,i}$ (mol/cm^2)[d]	6.7×10^{-13}

a) Reference 3

b) We typically used 20 and 40-μL sample volumes and 3.0-mm diameter capture addresses in our assays, but expanded the volume to 1 mL and decreased the address to 200 x 200 μm as possible approaches to improve the LOD.

c) The lower limit represents values found in this work.

d) This value represents an estimate based on the closest-packing of the immobilized antibodies and a ~30% viability after immobilization. The latter accounts for the observed viability of immobilized antibodies, as detailed by Shannon and co-workers (reference 29).

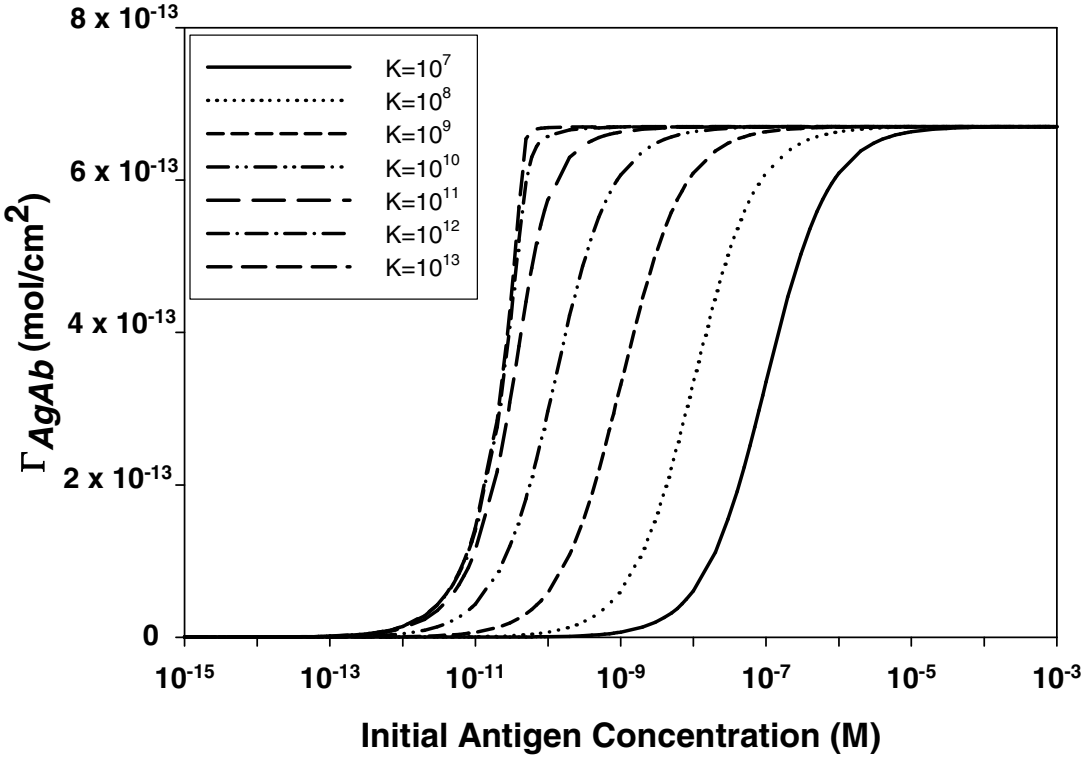

Figure 1. The effect of the equilibrium constant, *K*, and the initial concentration of antigen, *C*, on the surface concentration of antigens bound to the capture substrate, Γ_{AgAb}. Capture substrate area: 0.070 cm^2; sample volume: 1.0 mL.

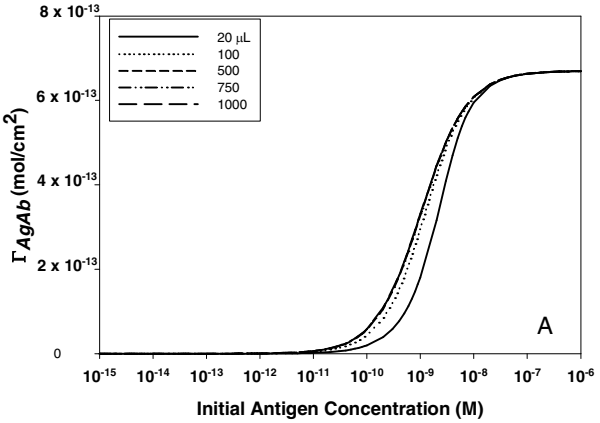

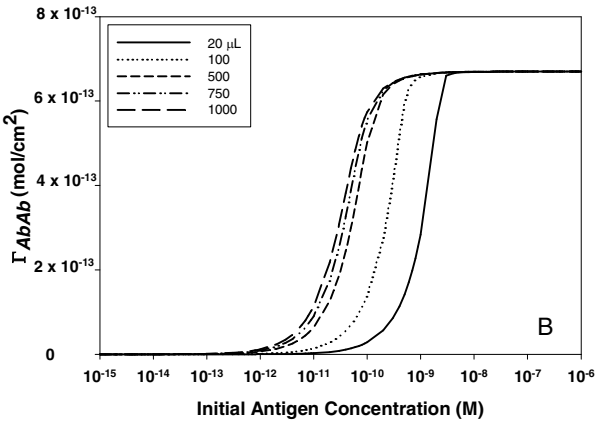

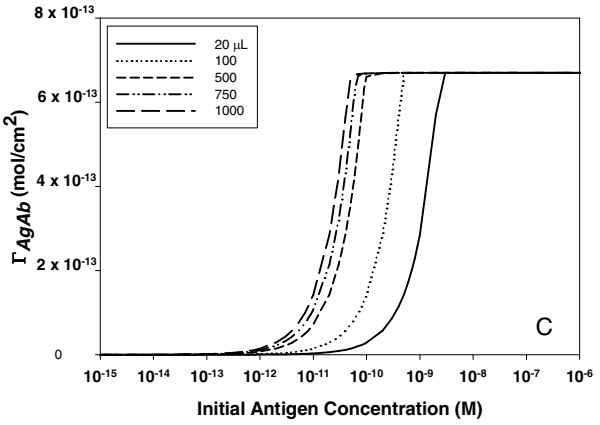

Figure 2. Effect of sample volume, *V*, on the surface concentration of captured antigen, Γ_{AgAb}, for a capture substrate area of 0.070 cm^2 and equilibrium constants, *K*, of (A) 1.0 x 10^9, (B) 1.0 x 10^{11}, and (C) 1.0 x 10^{13}.

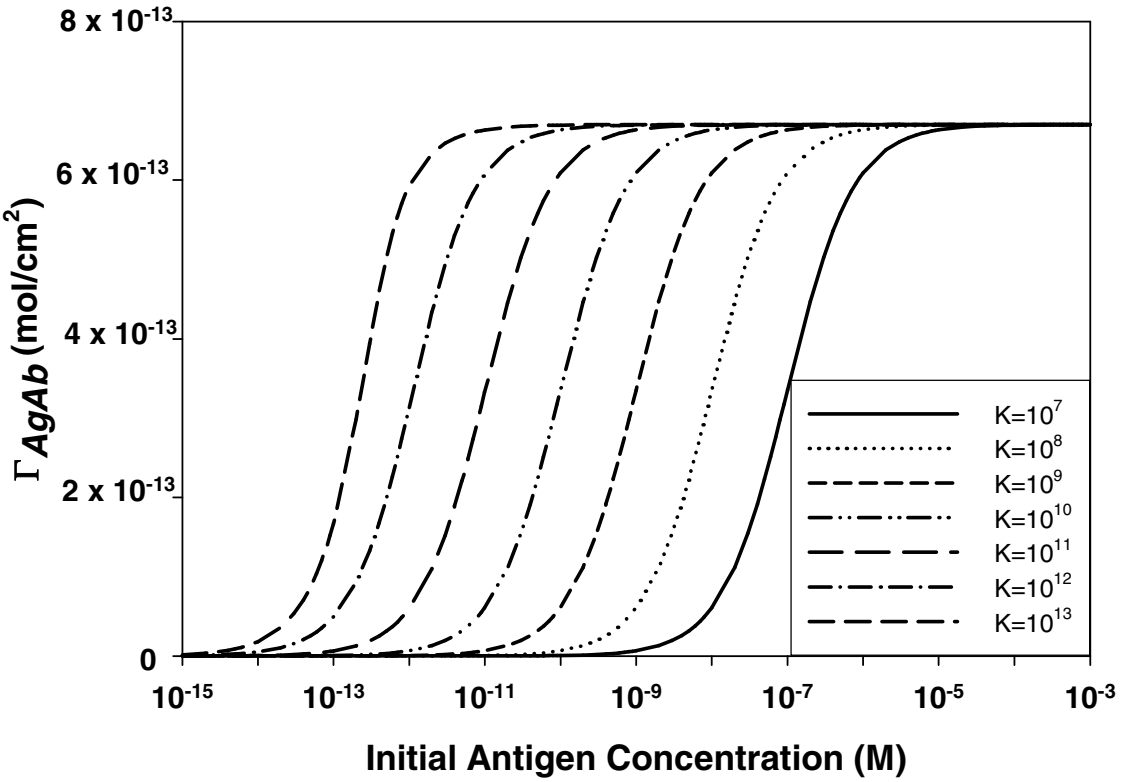

Figure 3. The effect of the equilibrium constants, *K*, and the initial concentration of antigen, *C*, on the surface concentration of antigens bound to the capture substrate, Γ_{AgAb}. Capture substrate area: 4.0 x 10^{-4} cm^2; sample volume: 1.0 mL.

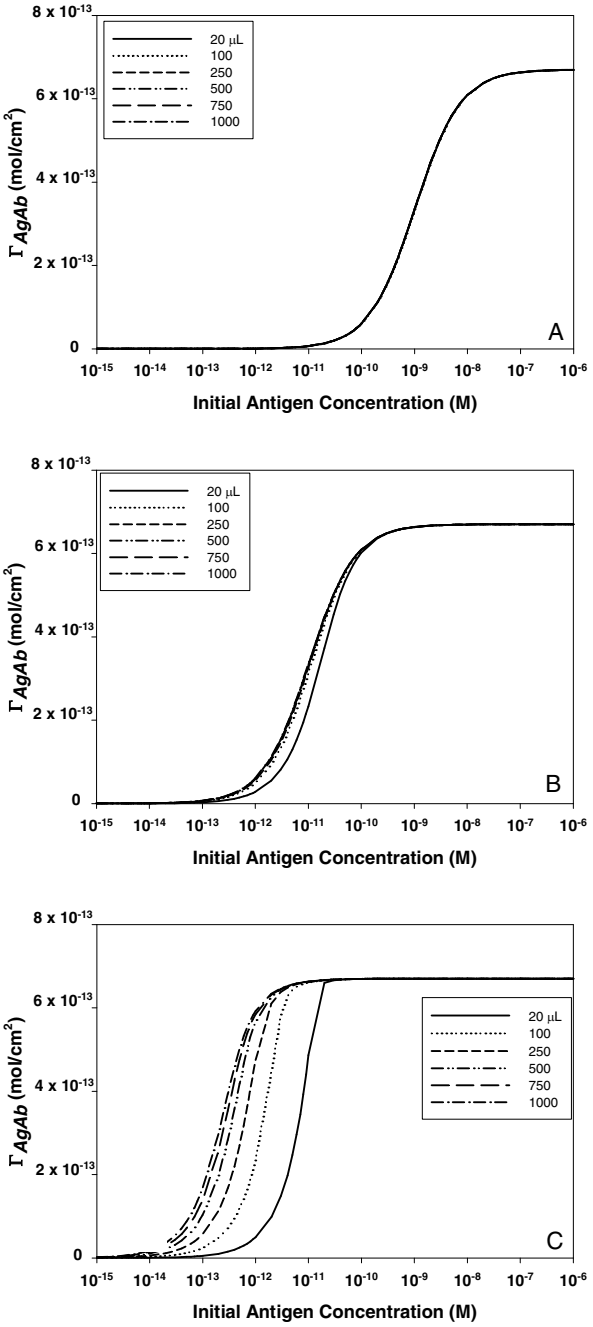

Figure 4. Effect of sample volume, *V*, on the surface concentration of captured antigen, Γ_{AgAb}, for a capture substrate area of 4.0 x 10^{-4} cm^2 and equilibrium constants, *K,* of (A) 1.0 x 10^9, (B) 1.0 x 10^{11}, and (C) 1.0 x 10^{13}.

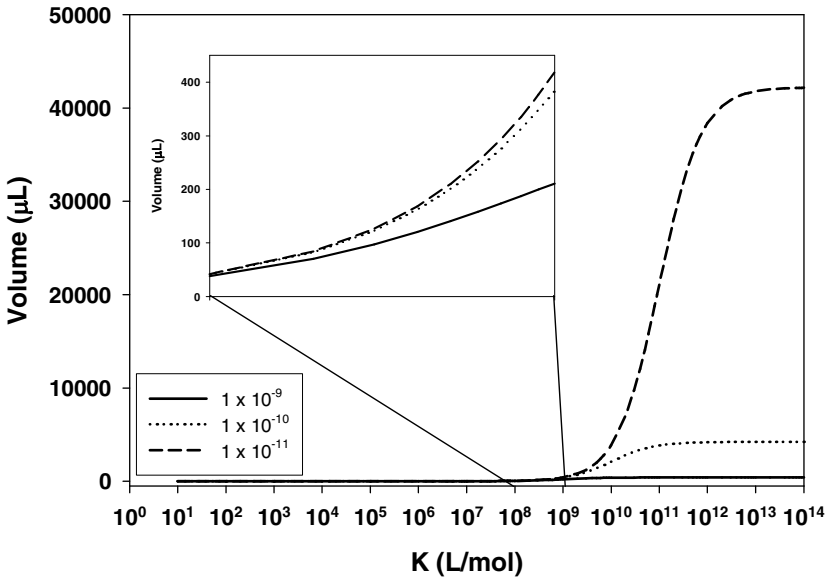

A

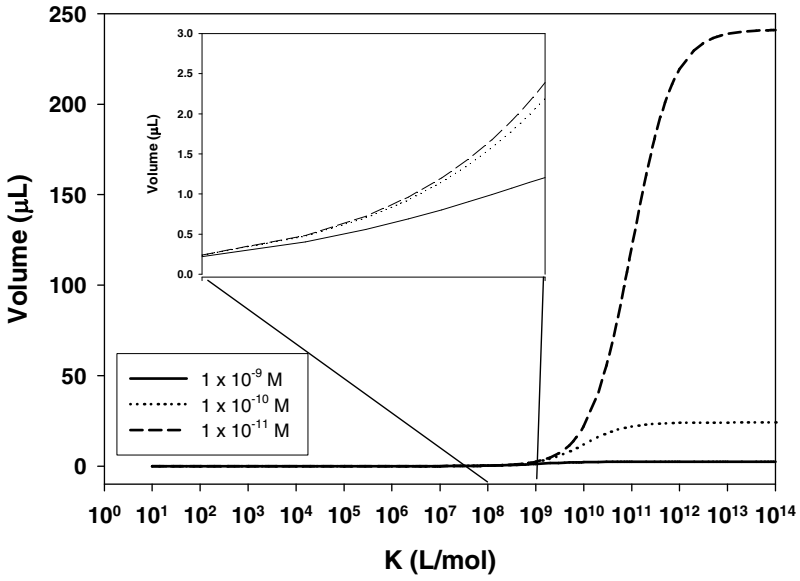

B

Figure 5. Volume, *V*, required to keep the equilibrium concentration of antigen in solution at 90% of the initial concentration of antigen for different equilibrium constants, *K,* and different initial concentrations, *C*, at capture substrate areas, *A*, of (A) 0.070 cm^2 and (B) 4.0 x 10^{-4} cm^2.

Table 2. Tabulated values given an initial antigen concentration, C, of 1.0×10^{-17} M.

K (L/mol)	Capture Area (cm^2)	Sample Volume (μL)	Total Antigens (particles)	Surface Conc. of Antigens (mol/cm^2)	Total Captured Antigens (particles)	Antigens in Laser Spot (particles)	% Depletion
10^{11}	0.070	20.0	120	2.8×10^{-21}	120	0.009	100
	0.070	1000.0	6020	1.2×10^{-19}	4962	0.35	82.4
	0.0004	1000.0	6020	6.5×10^{-19}	157	2.0	2.6
10^{13}	0.070	20.0	120	2.9×10^{-21}	120	0.009	100
	0.070	1000.0	6020	1.4×10^{-19}	6007	0.43	99.8
	0.0004	1000.0	6020	1.8×10^{-17}	4384	54.8	72.8

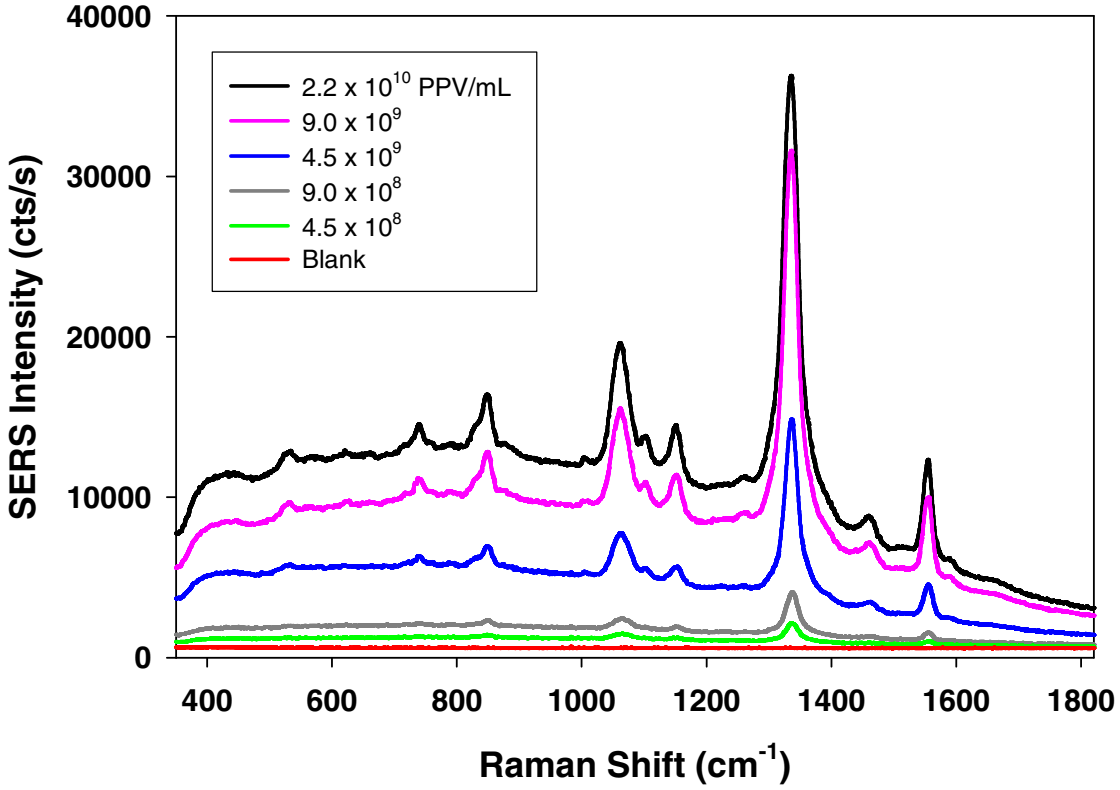

Figure 6. SERS spectra for a sandwich immunoassay using a 3-mm diameter capture substrate and 20.0-μL incubations in both the PPV capture step and the ERL labeling step.

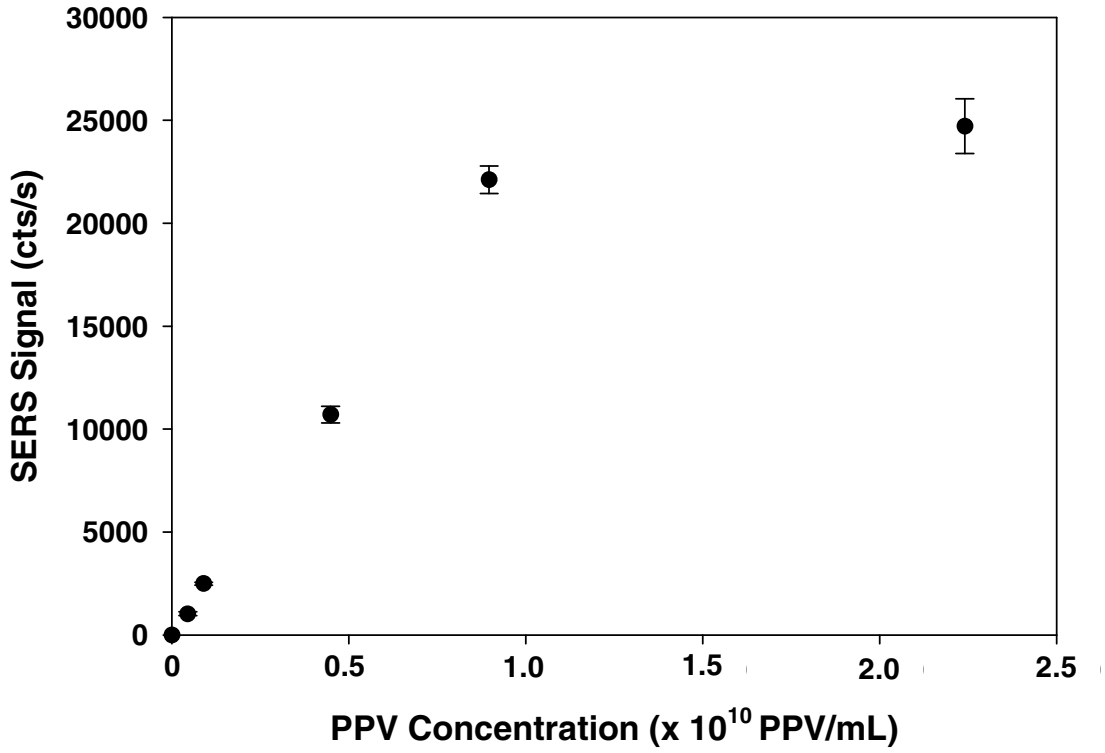

Figure 7. Dose-response plot using the intensity of the $\nu_s(NO_2)$ for a sandwich immunoassay using a 3-mm diameter capture substrate and 20.0-μL incubations in both the PPV capture step and the ERL labeling step.

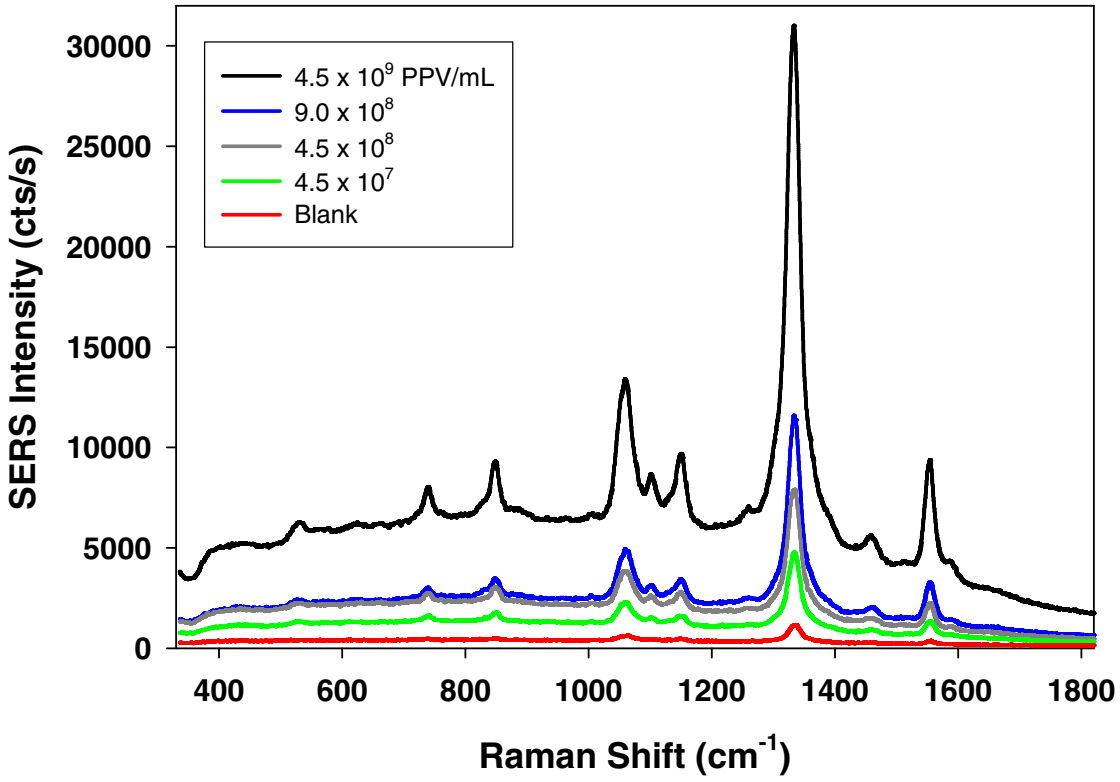

Figure 8. SERS spectra for a sandwich immunoassay using a 3-mm diameter capture substrate and 1.0-mL incubations in both the PPV capture step and the ERL labeling step.

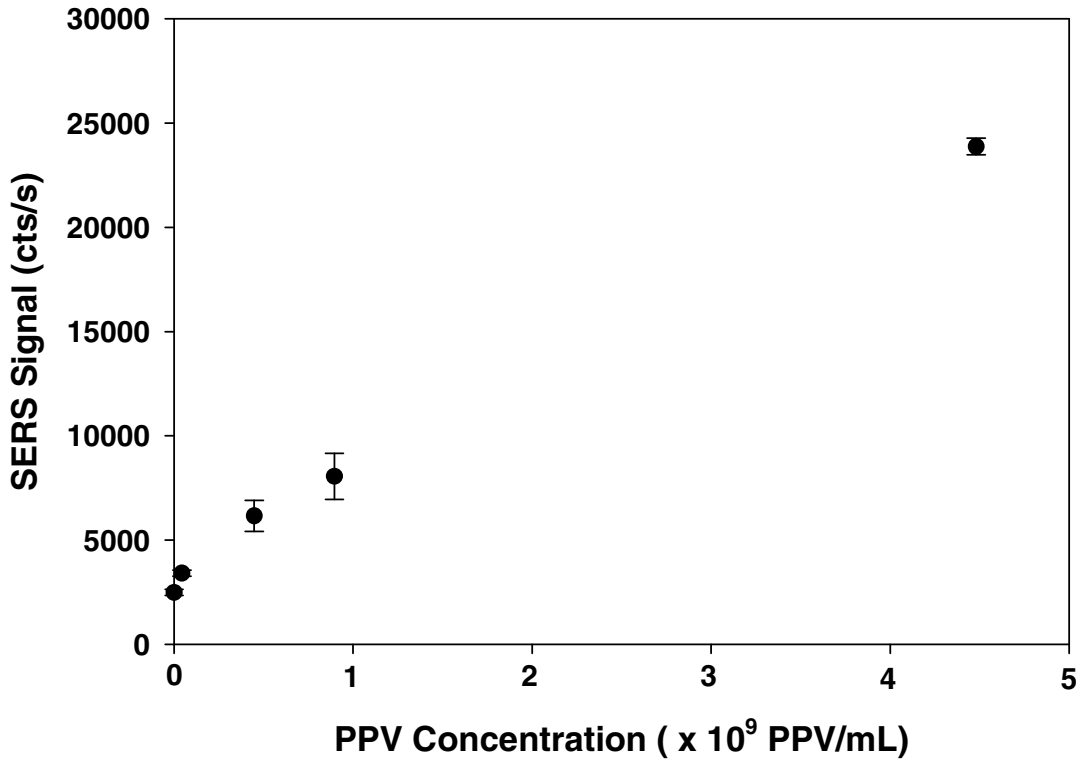

Figure 9. Dose-response plot using the intensity of the $\nu_s(NO_2)$ for a sandwich immunoassay using a 3-mm diameter capture substrate and 1.0-mL incubations for both the PPV capture step and the ERL labeling step.

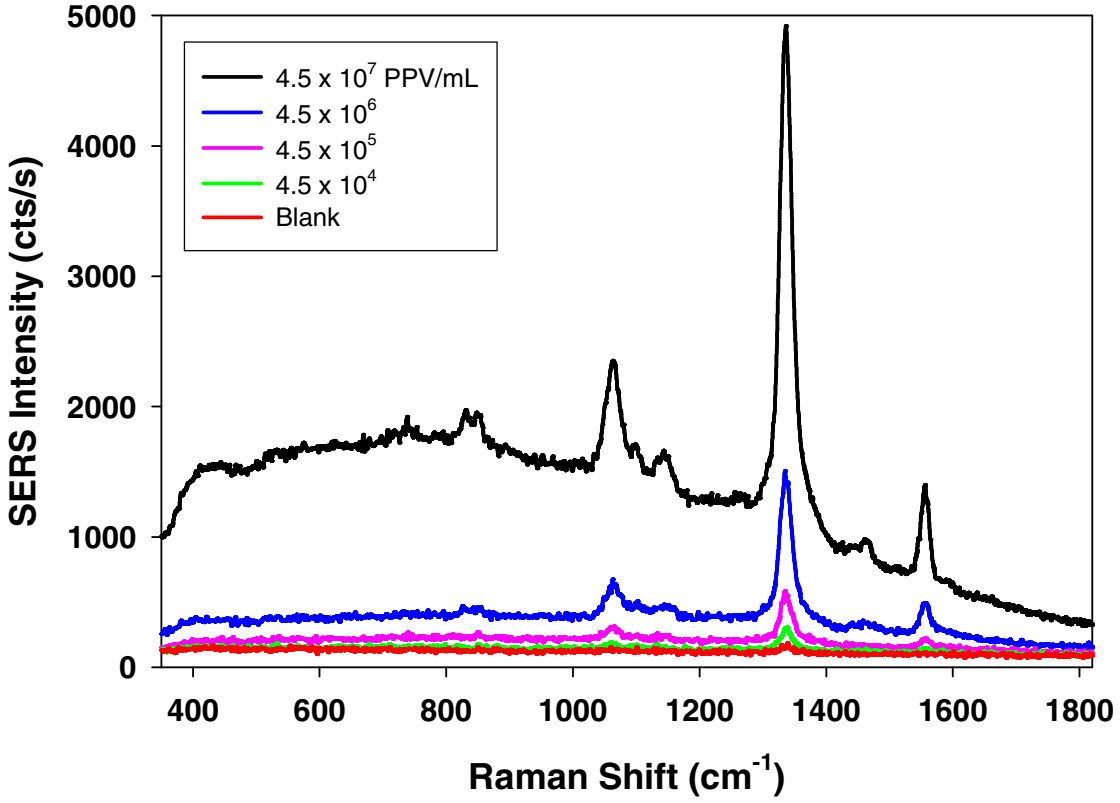

Figure 10. SERS spectra for a sandwich immunoassay using a 200 x 200 μm capture substrate and 1.0-mL incubations in both the PPV capture step and the ERL labeling step.

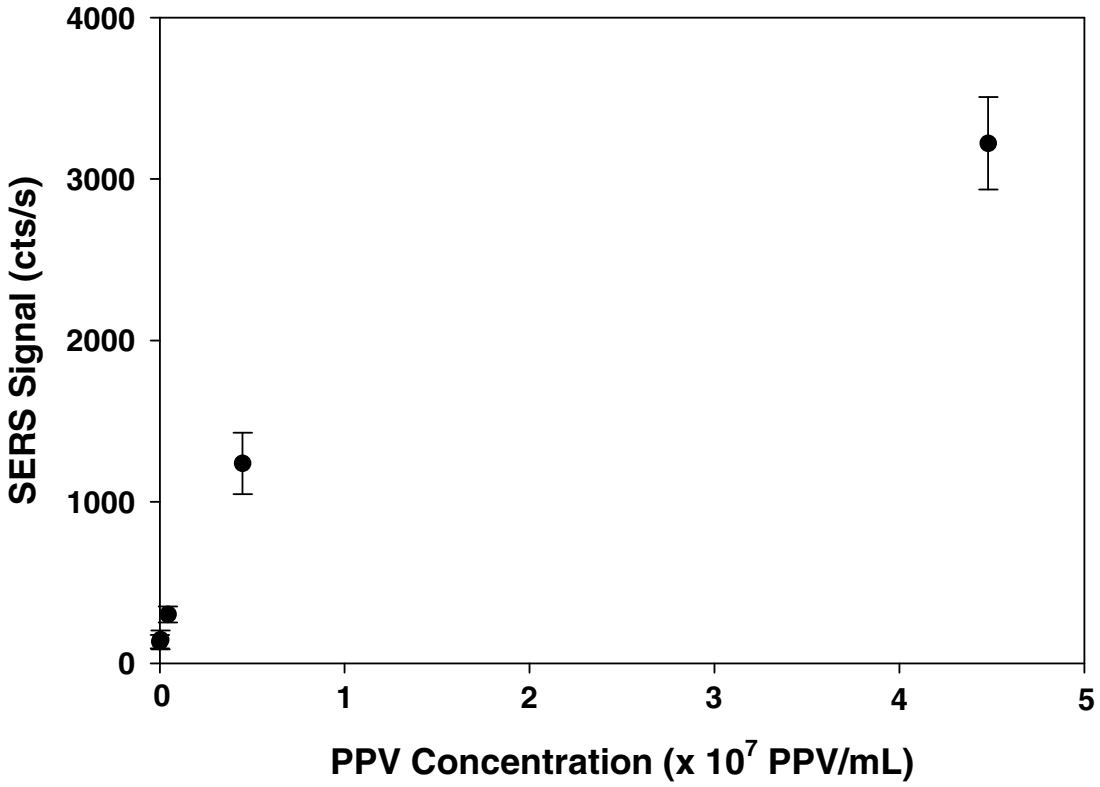

Figure 11. Dose-response plot using the intensity of the $\nu_s(NO_2)$ for a sandwich immunoassay using 200 x 200 μm capture substrate and 1.0-mL incubations in both the PPV capture step and ERL labeling step.

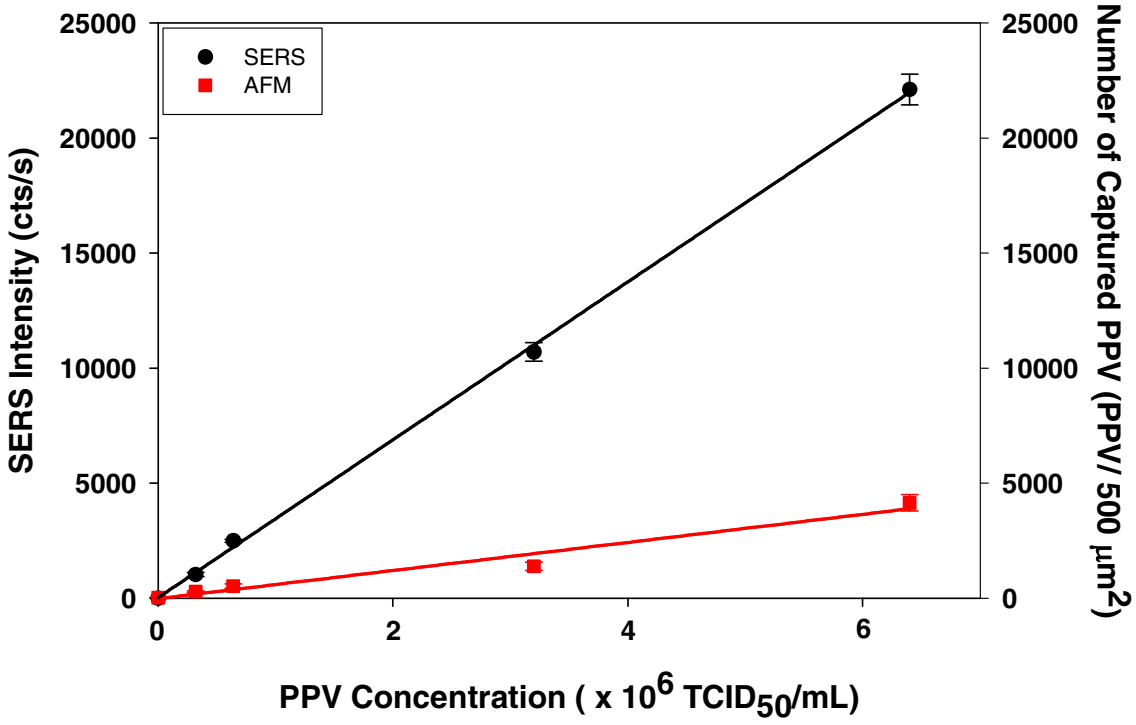

\

Figure 12. Dose-response curves for SERS-based (circles) and AFM-based (squares) detection of PPV on capture substrates with an area 0.070 cm^2, and a sample volume of 20 μL. The SERS calibration curve is constructed with the intensity of the nitro band at 1336 cm^{-1}, the data points representing the average signal from five different locations on the same sample. Each AFM data point is the average number of PPV bound from five images collected for each sample.

Table 3. Number of viruses interrogated by the laser and the % PPV left in solution as a function of concentration, capture substrate area, and sample volume. L/S: 0.070-cm^2 capture area, 20.0-µL sample volume, L/L: 0.070-cm^2 capture area, 1.0-mL sample volume; and S/L: 4.0 x 10^{-4} cm^2-capture area, 1.0-mL sample volume.

		# PPV in Laser			% PPV in solution		
PPV/mL	**$TCID_{50}$/mL**	**L/S**	**L/L**	**S/L**	**L/S**	**L/L**	**S/L**
2.2 x 10^{10}	16000000	6178			81		
9.0 x 10^{9}	6400000	5527			57		
4.5 x 10^{9}	3200000	2675	5969		58	98	
9.0 x 10^{8}	640000	622	2013		51	97	
4.5 x 10^{8}	320000	257	1539		60	95	
4.5 x 10^{7}	32000	(26)	854	805		73	99
4.5 x 10^{6}	3200	(3)	(85)	310			99
4.5 x 10^{5}	320	(0.3)	(9)	76			99
4.5 x 10^{4}	32	(0.03)	(0.9)	36			94

CHAPTER 4: SERS DETECTION OF THROMBIN: APTAMER- AND ANTIBODY-BASED ASSAYS

A manuscript in preparation for submission to *Analytical Chemistry*

Karen M. Kwarta* and Marc D. Porter*

Institute for Combinatorial Discovery, Departments of Chemistry and of Chemical and Biological Engineering, and Ames Laboratory—U.S. DOE, Iowa State University, Ames, Iowa 50011-3020

Current address: Center for Combinatorial Sciences, Biodesign Institute, Department of Chemistry and Biochemistry, Arizona State University, Tempe, AZ 85287

ABSTRACT

Aptamers are potential alternatives to antibodies as molecular recognition elements. We present herein a comparison of antibodies and aptamers as capture reagents in a surface-enhanced Raman scattering (SERS) based assay for thrombin by using thrombin binding aptamer (TBA) and sheep-anti-human thrombin antibody. The conditions employed for an aptamer-based assay, much like antibody assays, are central to performance and require extensive optimization. This work examined how TBA immobilization and binding buffer composition affected assay performance. The procedure for immobilization of TBA on a gold substrate was optimized by addition of a spacer reagent (6-mercapto-1-hexanol (MHx)), which reduced electrostatic interactions

between the DNA (aptamer) backbone and the gold substrate, and promoted TBA orientation along the surface normal to the substrate. The optimal concentrations of TBA and MHx were determined to be 10 μM each, with MHx being allowed to displace TBA for 1 h. Next, the binding buffer composition for extraction of thrombin was analyzed by addition of cations that are known to stabilize the TBA quadruplex structure required for thrombin binding. The addition of 1 mM $MgCl_2$ and 100 mM KCl to the 10 mM PBS binding buffer was found to impart little improvement on thrombin binding. Limits of detection using antibody and aptamer as capture reagents were 30 pM and 200 pM, respectively. Finally, as a test of the robustness, both capture substrates were dried and stored for 48 h without significant compromises to sensitivity.

INTRODUCTION

Aptamers were discovered independently in 1990 in the laboratories of Joyce,[1] Szostak,[2] and Gold[3] using an in vitro selection and amplification method termed SELEX (Systematic Evolution of Ligands by Exponential Enrichment). The invention of SELEX subsequently triggered the development of small oligonucleotides (40-100 bases) that bind non-nucleic acid targets with specificities and affinities that rival those of antibodies (Abs).[4] With SELEX, aptamers have been selected for a variety of targets, ranging in size from small organic molecules to proteins.[5-7] The ability to discriminate between enantiomers has also been reported.[8]

Aptamers offer several potentially distinct advantages over antibodies. Aptamers can be produced and purified synthetically,[9, 10] eliminating the use of animals. In addition, the types of targets that can be screened with aptamers is far greater than with

antibodies, and includes materials that are toxic or non immunogenic. Furthermore, screening begins with a larger pool of oligonucleotides (10^{13}-10^{18} sequences per experiment),[9] while antibodies are limited to the diversity of IgG and IgM molecules and can be challenged by batch to batch variations.[9, 11] Moreover, the chemical simplicity of aptamers facilitates long term storage without denaturation and degradation,[9] and use under physiological conditions is not required. Finally, aptamers can be engineered more easily than antibodies to incorporate site-specific labels that do not affect their affinity (affinities range from 1 pM – 1 μM).[10, 12] In contrast, antibodies are only stable in physiological environments and the addition of labels can affect their affinities.

Although aptamers have some distinct advantages over antibodies, there are also some drawbacks. They are susceptible to nuclease attack, especially RNA aptamers, which limits their lifetime. In addition, since binding depends on the aptamer adopting a specific three-dimensional conformation, optimization requires a case-by-case study. Some of the parameters that must be taken into consideration are use of stabilizing cations, buffer composition, immobilization procedure with heterogeneous assays, and temperature (i.e., must be below the melting temperature).[9]

Thrombin binding aptamer (TBA = 5'-GGTTGGTGTGGTTGG) was the first aptamer developed *in-vitro* for a non-nucleic acid binding protein, and has been extensively studied and characterized.[13-18] It has binding affinities ranging from 25-200 nM.[10, 13-18] TBA forms a unimolecular quadruplex structure consisting of a stack of two guanine quartets that is stabilized by cations such as K^+, Pb^+, Ba^{2+}, and Sr^{2+}.[15, 16] Thrombin is thought to bind adjacent to the two TT loops that connect the G-quartets.[10]

TBA has been employed in many bio-sensing applications, including an enzyme linked aptamer assay (ELAA)[9, 18] and a molecular beacon concept.[12, 19] Other promising methods for "aptasensor" development include the use of electrochemical,[20-22] impedimetric,[23] fluorescence,[10] optical,[24] and mass[25] based schemes. Detection limits of 1 nM were achieved using a mixed ELISA/ELAA sandwich format,[18] and evanescent-wave-induced fluorescence anisotropy.[10] We report herein on a sandwich aptamer assay for thrombin using surface enhanced Raman scattering (SERS) for readout. SERS is emerging as a highly versatile technique for the detection of biomolecules, including viruses and cancer markers (e.g., prostate specific antigen), and can reach femtomolar detection limits.[26, 27]

This paper examines the potential merits of combining SERS and aptamers as assay platforms. To this end, it compares and contrasts the use of TBA and thrombin antibodies to capture thrombin. Labeling of thrombin for SERS detection relied on the fabrication of extrinsic Raman labels (ERLs) that contain a Raman active molecule and an antibody specific for thrombin (Scheme 1). Our method begins with a capture surface constructed of TBA, modified with a six-carbon linking chain and a thiol group, immobilized on a gold surface. The architecture of the adlayer is then modified by immersion of the substrate in a dilute solution of 6-mercapto-1-hexanol (MHx), which coadsorbs on the gold surface and/or displaces TBA. This "capping" step is necessary in order to overcome the electrostatic interactions with gold that disrupt the TBA quadruplex structure. The capture surface is next exposed to thrombin. Finally, ERLs coated with sheep-anti-thrombin antibody solutions are used to selectively tag the captured thrombin. Conditions, including salt concentration and MHx concentration, for

the aptamer assay were optimized and limits of detection were calculated. The antibody-based assay follows a course similar to that for the aptamer-based assay, with antibodies covalently immobilized to the gold substrate used as the capture substrate.

EXPERIMENTAL

Reagents. TBA, supplied by Sigma Genosys, was modified on the 3' end with a six carbon linking chain and terminated on the distal end by a thiol (5'-GGTTGGTGTGGTTGG[6THS]) which directs the immobilization on the gold surface. Thrombin (37 kDa) from human serum (1000 National Institute of Health (NIH) units/mL, 0.10 mg/mL), phosphate buffer saline (PBS) packs (10 mM, pH 7.2), bovine serum albumin (BSA), octadecane thiol (ODT), dithio-bis succinimidyl proprionate (DSP), and MHx were acquired from Sigma Aldrich. Borate buffer packs (50 mM, pH 8.5) and SuperBlock were from Pierce, while KCl, $MgCl_2$, and NaCl were from Fisher. Sheep-anti-human thrombin antibody was purchased from US Biologicals. Gold nanoparticles (60 nm, 2.6 x 10^{10} particles/mL) were from Ted Pella and DSNB [5,5'-dithiobis(succinimidyl-2-nitrobenzoate] was synthesized according to a literature procedure.[26] Contrad 70 (Decon Labs), a mild detergent, was used to clean the glass substrates. Poly(dimethyl siloxane) (PDMS, Dow Corning) was utilized to prepare microcontact printing stamps.

ERL preparation. ERLs are designed to package immunospecificity and provide a strong Raman scattering signal. The use of the thrombin antibody imparts specificity, whilst DSNB coats the nanoparticles with a strong Raman scatterer. DSNB is a key ingredient in ERL development due to: 1) the inherently strong Raman scattering cross

section of its symmetric nitro stretch; 2) its ability to chemisorb to gold surfaces through sulfur-gold interactions; and 3) its facility to covalently immobilize amine containing compounds (i.e., the reaction of antibodies with the succinimidyl ester).

ERLs are constructed by combining 40.0 μL of 50 mM borate buffer and 1.0 mL of 60-nm gold nanoparticles in order to adjust the pH to 8.5, which deprotonates the amine groups of the antibodies that are added in subsequent steps. Next, 10.0 μL of 1.0 mM DSNB in acetonitrile are mixed into the suspension and allowed to react for ~12 h and thereby form a DSNB-derived monolayer on the particles. Sheep-anti-human thrombin (100 μL of a 0.20 mg/mL solution in 2 mM borate buffer) was then added to the suspension and reacted with the succinimidyl groups on DSNB for ~8 h to form an amide linkage. Next, BSA (100 μL of 10% in 2 mM borate buffer) acting as blocking/stabilizing agent was added to the mixture. After ~ 12 h the suspension was centrifuged at 2000 *g* for 10 min to remove excess reagents and was re-suspended in 1.0 mL of 2 mM borate buffer with 1% BSA. This cleanup procedure was repeated twice with a final, 500 μL suspension of 2 mM borate buffer, 1% BSA, and 150 mM NaCl; NaCl is used to mimic physiological conditions. Finally, the ERLs were passed through a 0.22-μm syringe filter (Costar) to remove any large aggregates. Subsequent tests showed that the antibody-modified particles remained stable as suspensions and active as labels for at least 5 months when stored at 4 ˚C.

Gold Chip Preparation. Glass microscope slides (Fisher) were cut into 1 x 1 cm squares and ultrasonically cleaned in 10% Contrad 70, deionized water, and ethanol for 30 min each. The squares were dried with nitrogen and placed in a resistive evaporator

(Edwards 306A) where 15 nm of chromium and then 250 nm of high purity (99.9%) gold were deposited at a rate of 0.1 nm/s and a pressure less than 7.5 x 10^{-7} Torr. After removal from the evaporator, the gold chips were exposed (~30 s) to an ODT-saturated PDMS stamp that had a 3-mm hole cut in its center. This inking procedure forms a hydrophobic ring that defines the sample area to localize reagents as well as to minimize sample and label consumption. The gold chips are then rinsed with ethanol and dried with a high-purity stream of nitrogen.

Antibody Assay Protocol. The antibody assay protocol follows the procedure optimized previously in our laboratory.[27] The gold substrates were immersed in a 0.1 mM ethanolic solution of DSP for ~8 h and then rinsed with ethanol and dried with high purity nitrogen. Next, sheep-anti-human thrombin antibody was covalently immobilized on the gold substrates by pipetting 20.0 μL of a 100 μg/mL solution onto the DSP-modified domain of the capture substrate; the reaction proceeded for ~8 h. The substrates were subsequently rinsed three times with 2 mL of 10 mM PBS. The next step placed 20.0 μL of SuperBlock blocking buffer onto the capture substrate for 12 h. The substrate was again rinsed three times with 2 mL of 10 mM PBS. Once the capture substrate was prepared in this manner, the thrombin (20.0 mL diluted in 10 mM PBS) was incubated for ~8 h. The substrates were then rinsed with 2 mM borate buffer, 150 mM NaCl. The labeling process (~12 h incubation) was performed by pipetting 20.0 μL of anti-human thrombin ERLs onto the capture substrate. Finally, the substrates were rinsed with 2 mM borate buffer, 150 mM NaCl, dried with high purity nitrogen, and the SERS spectra were collected.

Aptamer Assay Protocol. The unmodified center of the gold chips was exposed to 20.0 μL of TBA (10 μM in 10 mM PBS) for ~12 h. These substrates were rinsed with 2 mL of 10 mM PBS and exposed to MHx for 1 h to orient TBA. Different concentrations (100, 10, or 5 μM) of MHx were tested to find the optimal ratio of TBA to MHx. The substrates were then rinsed with 10 mM PBS. The binding buffer composition for extraction of thrombin was examined by diluting thrombin in 10 mM PBS containing either 1.0 mM $MgCl_2$ or 100 mM KCl. A sample volume of 20.0 μL was placed on the capture surface and the thrombin was allowed to bind for ~8 h. The substrates were then rinsed with 2 mM borate buffer (150 mM NaCl) and 20.0 μL of the ERLs were added and allowed to bind for ~2 h. The substrates underwent a final rinse in 2 mM borate buffer (150 mM NaCl), were dried with high purity nitrogen, and then interrogated by SERS.

Instrumentation. Raman spectra were collected with a NanoRaman I (Concurrent Analytical) fiber-optic Raman system. The excitation source is a 30-mW, 632.8 nm HeNe laser. The spectrograph consists of an f/2.0 Czerny-Turner imaging spectrometer (resolution of 6-8 cm^{-1}) and a thermoelectrically cooled CCD (Kodak 0401E). The probe objective focuses the laser to a 25-μm diameter spot on the substrate surface; it also collects the scattered Raman radiation. All spectra were obtained with a 1-s integration time.

RESULTS AND DISCUSSION

Antibody Assay. As a starting point and a means to assess and contrast the effectiveness of the antibody and aptamer assays, a sandwich immunoassay was performed with sheep-anti-human thrombin used as the recognition element in both the capture and labeling steps. These results are compared to those for an aptamer-based assay as a means to contrast performance. Operationally, thrombin samples were prepared by dilution in 10 mM PBS to varying concentrations and SERS spectra were obtained for capture substrates exposed to each sample (Figure 1). The signal intensity of these spectra, which contain features characteristic of the DSNB-based Raman reporter molecule that confirm the presence of the ERLs, and exhibit an increase with the increase in thrombin levels. The dominant feature in the spectra is the symmetric nitro stretch [$\nu_s(NO_2)$] at 1336 cm^{-1}, which was used for quantification of thrombin.

The average intensity of $\nu_s(NO_2)$ from measurements collected at five different locations on the sample was determined and plotted verses thrombin concentration (Figure 2) to construct a dose-response curve. The error bars represent the standard deviation in the signal. The horizontal line at 96 cts/s in Figure 2 represents the response after addition of a signal that is three times the standard deviation of the blank; this threshold is used to calculate the limit of detection (LOD). Based on these data, the antibody sandwich assay for thrombin yields a limit of detection of 30 pM (2×10^{-3} NIH units/mL), which is well below levels found in human plasma (5-500 NIH units/mL).[28]

Specificity of the capture substrate was examined by exposing the anti-thrombin substrate to 1000 ng/mL of rabbit IgG, followed by labeling with ERLs prepared with anti-rabbit IgG. This control study yielded SERS signals on par with the blank signal.

TBA Immobilization Optimization. TBA was modified on the 3' end with a six carbon linker chain terminated at the distal end by a thiol group, which functions to immobilize TBA to the gold substrate through a gold-thiolate linkage. Previous reports have found that detection limits are compromised when TBA is immobilized to the capture substrate via the 3'-end. This observation suggests that either 3' modification/immobilization interferes with folding of the aptamer, or that 5' modification/immobilization improves its ability to form the quadruplex structure.[18] Additionally, surface bound TBA exhibits higher binding when a carbon spacer chain is included, presumably due to the increased flexibility (reduced steric hindrance) of the quadruplex structure.[18] MHx is used as a co-absorber because its length matches that of the six carbon linker chain on the TBA, and therefore should not interfere with TBA folding or reactions with thrombin.[29] MHx, a displacing molecule, orients the thiol modified TBA along the surface normal to the substrate by reducing electrostatic interactions between the DNA backbone and the gold surface.[30] As a consequence, the appropriate ratio of TBA and MHx must be determined in order to orient TBA, while minimizing its displacement. Significant displacement of TBA would lower the amount of TBA on the capture substrate, reducing the level of thrombin extracted from solution.[31]

Monolayers of TBA were constructed by exposure of the gold substrate to 10 μM TBA for ~8 h. The TBA-adlayer was then partially displaced by three different concentrations of MHx (5, 10, 100 μM) for 1 hr to overcome the electrostatic interactions between the DNA and the gold surface. Thrombin was diluted to varying concentrations in 10 mM PBS and then exposed to the capture substrate. Finally, antibody-coated ERLs

were exposed to the captured thrombin and SERS spectra were obtained. The intensity of $\nu_s(NO_2)$ was used for quantification and the results are summarized in Figure 3.

A high concentration of MHx (100 μM) shows approximately the same, relatively large, SERS signal for all concentrations of thrombin, including the blank. We speculate that the highest concentration of MHx displaces a significant amount of TBA,[31] producing a capture surface predominately coated with MHx, which appears to non-specifically bind ERLs. Capture substrates prepared using the lowest concentration of MHx, on the other hand, exhibit a much lower level of ERL binding at all thrombin concentrations. We hypothesize in this case that only a small amount of the TBA has been oriented properly to successfully extract thrombin (i.e., most of the TBA is electrostatically attracted to the gold substrate through the DNA backbone and is primarily oriented parallel to the surface).[29, 31] Of these sets of tests, the optimal concentration of MHx was found to be 10 μM, which is presumably a compromise between reducing the non-specific interactions between ERLs and MHx, and more favorably orienting the TBA for improved thrombin and subsequently ERL binding.

Binding Buffer Optimization. The importance of buffer composition was examined by adding two different salts to the 10 mM PBS binding buffer, 100 mM KCl or 1 mM $MgCl_2$, and utilizing the optimized 10 μM MHx incubation. The cations of these salts have been shown at these concentrations to shift the equilibrium of TBA from a random conformation to the quadruplex conformation responsible for thrombin binding.[15, 16, 18, 19]

Dose-response curves for thrombin in different binding buffers are depicted in Figure 4, which shows that the SERS signals obtained for each binding buffer do not

differ much from one another. The assay employing 1 mM $MgCl_2$ as an additive to the binding buffer exhibited the highest non-specific binding (i.e., blank signal of 343 ± 215 cts/s), yielding a LOD of 560 pM. The lowest blank signal (316 ± 99 cts/s) was obtained using the 100 mM KCl binding buffer, but the responses were the least reproducible, producing a LOD of 840 pM. The 10 mM PBS binding buffer had the most reproducible responses and a low blank signal (453 ± 105 cts/s), yielding a limit of detection of 200 pM. Therefore, the addition of salt to the binding buffer did not improve the LOD, suggesting that the cations do not have a strong impact on the stability of TBA with this particular experimental design. We attribute this observation to two possible phenomena, which may act alone or in concert. First, a few reports have indicated that cations only facilitate quadruplex stability when near the TBA melting temperature (~46 ˚C). Our experiments are performed at room temperature. Second, the TBA quadruplex formation is induced by binding of thrombin, meaning the TBA folds upon association with thrombin and thrombin becomes an integral part of the nucleic acid structure.[13, 32] It was concluded from these results that 10 mM PBS was the optimal binding buffer.

TBA Assay. Using the optimized conditions (i.e., 10 μM MHx and 10 mM PBS binding buffer), an assay for thrombin was performed and compared to results from the antibody assay (Figure 5). Both data sets exhibit the expected trend in SERS signal with thrombin concentration. Interestingly, the SERS signal from the aptamer-based assay is greater at all thrombin concentrations than that for the antibody-based assay. However, the level of non-specific binding is more pronounced for the aptamer-based assay (blank signal of 453 ± 105 cts/s), yielding a LOD of 200 pM (0.02 NIH units/mL).

A control study for the aptamer-based assay exposed the TBA substrate to 1000 ng/mL of rabbit IgG, followed by labeling with ERLs prepared with anti-rabbit IgG. This test of specificity yielded SERS signals that did not exceed those of the blank signal.

Although the signal intensity from the aptamer-based assay is larger than that of the antibody-based assay, the LOD for the antibody-based assay was nearly seven times lower at 30 pM. This difference largely reflects the smaller blank signal (72 ± 8 cts/s) in the antibody-based assay.

Nonetheless, these results raise an important question: what is the orgin(s) of the longer signal strengths in the aptamer-based assay? Potential answers to this question can be developed by comparing the two sets of experiments. The higher SERS signals in the aptamer-based assay could be attributed to a combination of three factors: 1) a higher level of non-specific ERL binding due to ERL binding to the MHx spacer; 2) higher surface concentration of the aptamer on the capture substrate due to its smaller size and 3) larger SERS enhancements because of a smaller separation between ERLs and the gold substrate. Each of these possibilities are now examined in turn.

The first factor explaining the difference in signal intensities is that the aptamer capture substrate has a higher level of non-specific binding due to interactions between the MHx and ERLs. When, however, the blank response is subtracted from each trial, the SERS signals from the aptamer-based assay are in all cases still greater than those from the antibody assay. After background correction, the SERS signal is ~30% greater for the aptamer assay at high thrombin concentrations (> 100 ng/mL), but is only ~5% greater at low thrombin concentrations (<100 ng/mL). This observation suggests that other factors are contributing to the signal differences in the two types of assays.

A second explanation for the larger SERS signal for the aptamer assay rests with a difference in the possible packing density of the recognition element for the two types of capture substrates. That is, a TBA molecule is ~20 times smaller than an IgG antibody. Assuming a 10nm diameter[33] (area of 78 nm^2), the surface concentration of a closest-packed layer of antibodies is 2 x 10^{-12} mol/cm^2. In contrast, the area occupied by TBA is estimated based on the width of double stranded DNA (~2 nm) by the height of the TBA structure (~3 nm).[34] Using an area of 5 nm^2 for TBA, the surface concentration is 3 x 10^{-11} mol/cm^2. If the MHx displaces half of the TBA (1:1 mixture), the surface concentration of TBA would still be 10 times greater than that for the capture antibody.

Assuming all of the TBA and antibodies on the capture substrate are active, the higher density of TBA would push the binding equilibrium to the TBA-thrombin complex. At high concentrations of thrombin, then, more thrombin can be extracted, and higher SERS signals can be achieved with the aptamer-based assay. For low concentrations of thrombin, however, the differences in SERS signal might be less pronounced because all thrombin may be extracted in both cases. The higher surface concentration of TBA accounts for the higher SERS signals at high concentration, and since the SERS signal after background correction for low thrombin concentrations is still slightly larger for the aptamer capture, yet another factor must be considered.

The higher SERS signal for the aptamer assay may also be a consequence of a larger SERS enhancement factor. This situation arises because the ERLs are closer to the underlying gold substrate in the aptamer assay than in the antibody assay. A TBA adlayer is ~2.6 nm high, while the antibody layer is as much as ~10 nm tall.[33] It has been demonstrated that the separation between an ERL and the underlying gold substrate has a

profound effect on SERS enhancement.[35-37] This dependence develops from the sensitivity of the coupling between the surface plasmons of the gold cores of the ERLs and the underlying gold of the capture substrate. [34] ERLs were found for our experimental design, which utilizes a HeNe laser at 633 nm, to have a five-fold larger signal when positioned closer to the underlying gold substrate (~1.2 nm vs ~2.3 nm).[35] The ERLs bound by aptamers should be closer than those at the capture antibody substrate, resulting in larger signals at all thrombin concentrations.

We speculate that the high signals of the aptamer-based assay exhibited at higher concentrations of thrombin are due to a combination of all three factors. That is, more non-specific binding of the ERLs, more specific binding of thrombin due to the increased surface concentration of TBA, and greater SERS enhancements because the ERLs are closer to underlying substrate.

Low concentrations of thrombin, on the other hand, may only be experiencing enhanced signals from two of the contributions: non-specific binding of ERLs, and gap distance. The increased signal because of a higher surface concentration of TBA may not have a significant impact at low thrombin concentrations, since in both the TBA-based assay and the antibody-based assay all of the thrombin may be extracted. The small signal increase of the TBA-based assay over the antibody-based assay (after background correction) at low concentrations of thrombin, then, may be due solely to enhancements from the smaller gap distance between the ERLs and the underlying substrate.

Finally, the blank (non-specific binding of ERLs) may be strongly influenced by the ERLs being closer to the underlying substrate. If the same numbers of ERLs are non-specifically bound in the aptamer- and antibody-based assays, the blank signal for the

aptamer-based assay will be larger because those ERLs are closer to the gold substrate. The higher background signal manifests itself into lower limits of detection for the aptamer-based assay. As is the case with many sandwich immunoassays, the limit of detection is controlled by non-specific binding.

Robustness of Capture Substrates. The antibody and aptamer capture substrates were dried after preparation to test the robustness of both platforms. Substrates were prepared following the optimized protocols, and then dried under a stream of high purity nitrogen, and stored in a dessicator for 48 h. Results from tests of both the as-prepared and the stored substrates compared to those prepared and used immediately are shown in Figure 6. Both types of capture substrates show higher signals when dried and stored, including higher blank signals.

The dried TBA substrates give a LOD of 2 nM compared to 0.2 nM for substrates used immediately, a tenfold difference. The dried antibody substrate has a LOD of 500 pM, while those used without delay has a LOD of 32 pM. Drying the substrate has a slightly larger impact on the antibody assay, with a 15-fold difference. This observation is likely a result of the antibodies becoming irreversibly denatured when dried. Aptamers, on the other hand, can reversibly undergo a change in structure. Nonetheless, experiments to address the stability of these systems to facilitate long term storage are being designed.

CONCLUSIONS

An aptamer based sandwich assay for thrombin detection using SERS as a readout technique was developed and optimized. First, the immobilization procedure of the TBA

to the gold substrate was optimized; the best conditions were found to be 10 μM TBA incubation overnight followed by 10 μM MHx displacement for 1 h. Binding buffer compositions were also studied and the optimal buffer was determined to be 10 mM PBS. The limit of detection using antibodies is 30 pM (2 x 10^{-3} NIH units/mL) while the limit of detection using aptamers is 200 pM (0.02 NIH units/mL). Both of theses limits of detection are competitive with other methods for thrombin detection (112 pM for aptamer beacons,[19] 1 nM for ELAA,[18] and 3.5 nM with electrochemistry[20]) and are well within the concentration range found in human plasma (5-500 NIH units/mL).

This paper shows the potential of aptamers as replacements for antibodies in a SERS detection platform. The aptamer-based assay gives rise to higher analytical signals at all thrombin concentrations (after background correction). These larger signals, if non-specific binding can be reduced, offer a unique way of improving the limits of detection that can be achieved using SERS as a readout technique. Methods to combat non-specific binding are currently being investigated in our laboratory in order to fully exploit the ultra-sensitive readout capabilities of SERS. SERS signals could be further increased by preparing ERLs using aptamers as biorecognition moieties instead of antibodies, which would place the ERLs even closer to the underlying substrate. Experiments to this end are planned. Combining the sensitivity of SERS with the selectivity of aptamers presents an opportunity to create analytical assays to detect low levels of pathogens or toxins.

ACKNOWLEDGEMENTS

This work was supported through a grant from USDA-NADC and by the Institute for Combinatorial Discovery of Iowa State University. K. M. Kwarta gratefully

acknowledges the support of a Dow Chemical Fellowship. The Ames Laboratory is operated for the US Department of Energy through Iowa State University under contract W-7405-eng-82.

REFERENCES

(1) Robertson, D. L.; Joyce, G. F. *Nature* **1990**, *344*, 467-8.

(2) Ellington, A. D.; Szostak, J. W. *Nature* **1990**, *346*, 818-22.

(3) Tuerk, C.; Gold, L. *Science* **1990**, *249*, 505-10.

(4) Jayasena, S. D. *Clin. Chem.* **1999**, *45*, 1628-50.

(5) Gold, L. *Nucleic Acids Symp. Ser.* **1995**, *33*, 20-2.

(6) Osborne, S. E.; MAtsumura, I.; Ellington, A. D. *Curr. Opin. Chem. Biol.* **1997**, *1*, 5-9.

(7) Famulok, M.; Mayer, G. *Curr. Top. Microbiol. Immunol.* **1999**, *243*, 123-36.

(8) Geiger, A.; Burgstaller, P.; von der Eltz, H.; Roeder, A.; Famulok, M. *Nucleic Acid. Res.* **1996**, *24*, 1029-36.

(9) Baldrich, E.; Acero, J. L.; Reekmans, G.; Laureyn, W.; O'Sullivan, C. K. *Anal. Chem.* **2005**, *77*, 4774-84.

(10) Potyrailo, R. A.; Conrad, R. C.; Ellington, A. D.; Hieftje, G. M. *Anal. Chem.* **1998**, *70*, 3419-25.

(11) Diamandis, E. P.; Christopoulos, T. K. *Immunoassay*; Academic Press: San Diego, 1996.

(12) Hamaguchi, N.; Ellington, A.; Stanton, M. *Anal. Biochem.* **2001**, *294*, 126-31.

(13) Baldrich, E.; O'Sullivan, C. K. *Anal. Biochem.* **2005**, *341*, 194-7.

(14) Bock, L. C.; Griffin, L. C.; Latham, J. A.; Vermaas, E. H.; Toole, J. J. *Nature* **1992**, *355*, 564-6.

(15) Smirnov, I.; Shafer, R. H. *Biochemistry* **2000**, *39*, 1462-8.

(16) Fialova, M.; Kypr, J.; Vorlickova, M. *Biochem. Biophys. Res. Comm.* **2006**, *344*, 50-4.

(17) Basnar, B.; Elnathan, R.; Willner, I. *Anal. Chem.* **2006**, *78*, 3638-42.

(18) Baldrich, E.; A., R.; O'Sullivan, C. K. *Anal. Chem.* **2004**, *76*, 7053-63.

(19) Li, J. J.; Fang, X.; Tan, W. *Biochem. Biophys. Res. Comm.* **2002**, *292*, 31-40.

(20) Mir, M.; Vreeke, M.; Katakis, I. *Electrochem. Comm.* **2006**, *8*, 505-11.

(21) Bang, G. S.; Cho, S.; Kim, B.-G. *Biosens. Bioelectron.* **2005**, *21*, 863-70.

(22) Hansen, J. A.; Wang, J.; Kawde, A.-N.; Xiang, Y.; Gothelf, K. V.; Collins, G. *J. Am. Chem. Soc.* **2006**, *128*, 2228-9.

(23) Radi, A.-E.; Sanchez, J. L. A.; Baldrich, E.; O'Sullivan, C. K. *Anal. Chem.* **2005**, *77*, 6320-3.

(24) Pavlov, V.; Xiao, Y.; Shlyahovsky, B.; Willner, I. *J. Am. Chem. Soc. Comm.* **2004**, *126*, 11768-9.

(25) Hianik, T.; Ostantna, V.; Zajacova, Z.; Stoikova, E.; Evtugyn, G. *Bioorg. Med. Chem. Lett.* **2005**, *15*, 291-5.

(26) Grubisha, D. S.; Lipert, R. J.; Park, H.-Y.; Driskell, J.; Porter, M. D. *Anal. Chem.* **2003**, *75*, 5936-43.

(27) Driskell, J. D.; Kwarta, K. M.; Lipert, R. J.; Porter, M. D. *Anal. Chem.* **2005**, *77*, 6147-54.

(28) Lee, M.; Walt, D. R. *Anal. Biochem.* **2000**, *282*, 142-6.

(29) Herne, T. M.; Tarlov, M. J. *J. Am. Chem. Soc.* **1997**, *119*, 8916-20.

(30) Levicky, R.; Herne, T. M.; Tarlov, M. J.; Satija, S. K. *J. Am. Chem. Soc.* **1998**, *120*, 9787-92.

(31) O'Brien, J. C.; Stickney, J. T.; Porter, M. D. *Langmuir* **2000**, *16*, 9559-67.

(32) Hermann, T.; Patel, D. J. *Science* **2000**, *287*, 820-5.

(33) Silverton, E. W.; Navia, M. A.; Davies, D. R. *Proc. Natl. Acad. Sci.* **1977**, *74*, 5140-4.

(34) Berg, J. M.; Tymoczko, J. L.; Stryer, L., Eds. *Biochemistry*, Fifth Edition ed.; W. H. Freeman and Company: New York, New York, 2002.

(35) Driskell, J. D.; Lipert, R. J.; Porter, M. D. *J. Phys. Chem. B* **2006**, *110*, 17444-51.

(36) Liver, N.; Nitzan, A.; Gersten, J. I. *Chem. Phys. Lett.* **1984**, *111*, 449-54.

(37) Zhang, P.; Haslett, T. L.; Douketis, C.; Moskovits, M. *Phys. Rev. B J1 - PRB* **1998**, *57*, 15513-8.

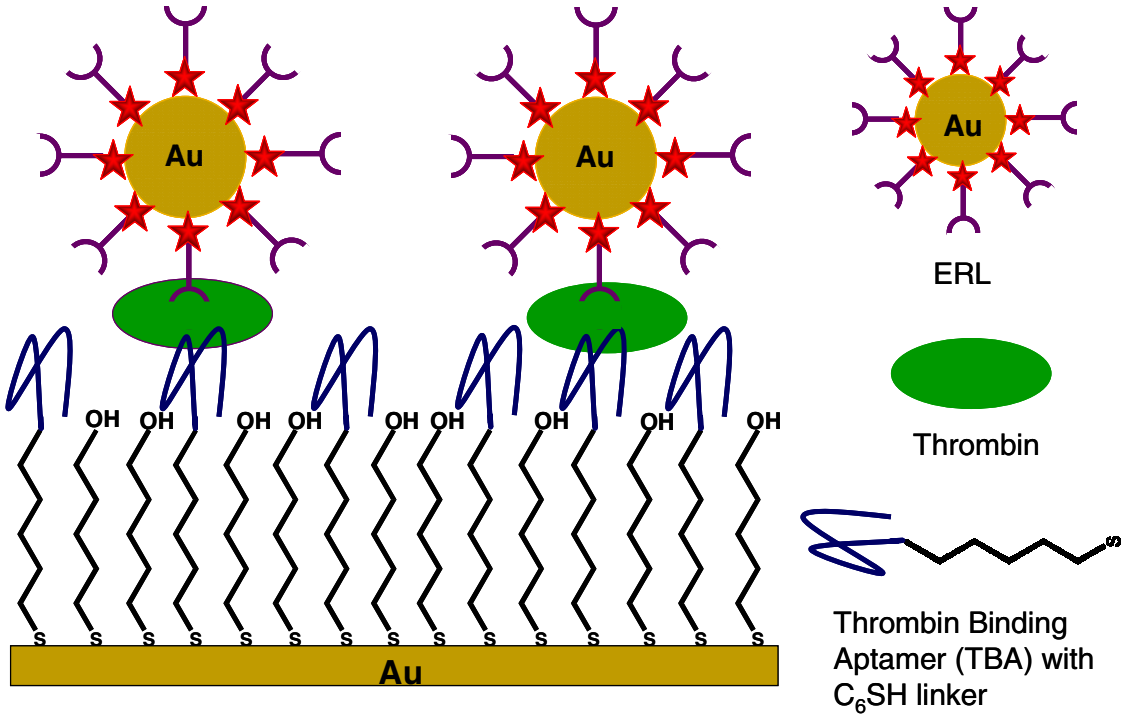

Scheme 1. Schematic representation of the aptamer assay platform. TBA is immobilized on a gold substrate, followed by displacement of non-specifically bound TBA with MHx. Thrombin is then extracted from solution and labeled with ERLs specific for thrombin.

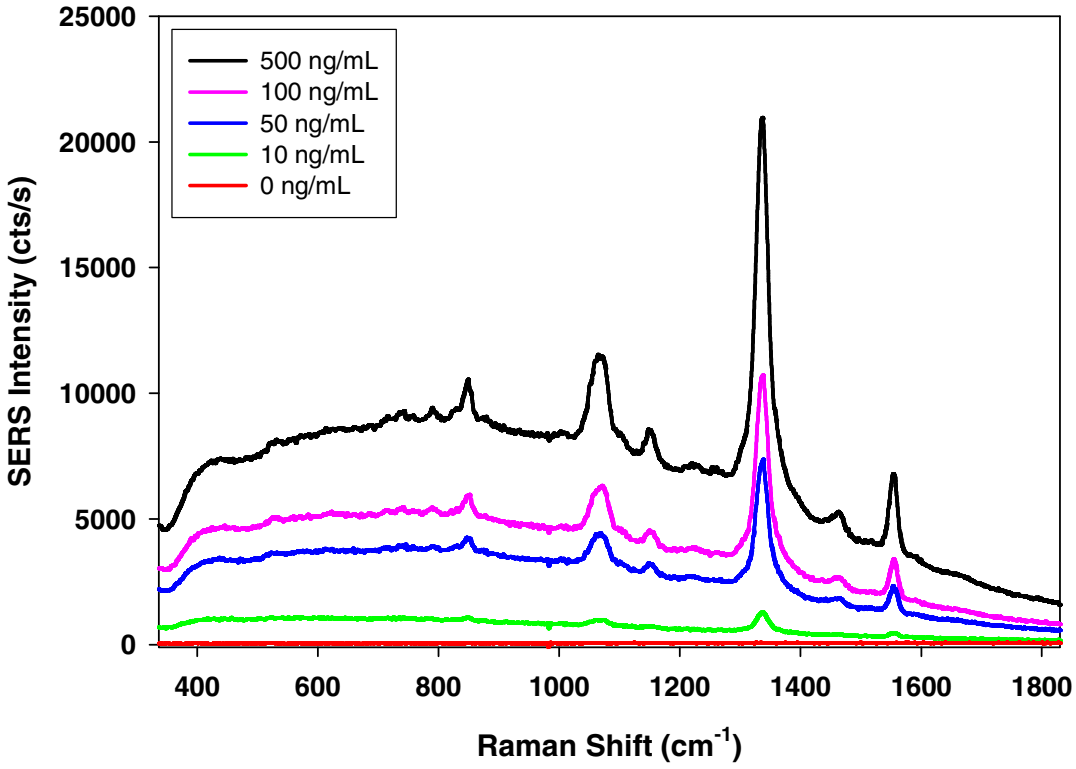

Figure 1. SERS spectra (1-s integration) for different concentrations of thrombin, diluted in 10 mM PBS, in the antibody sandwich immunoassay.

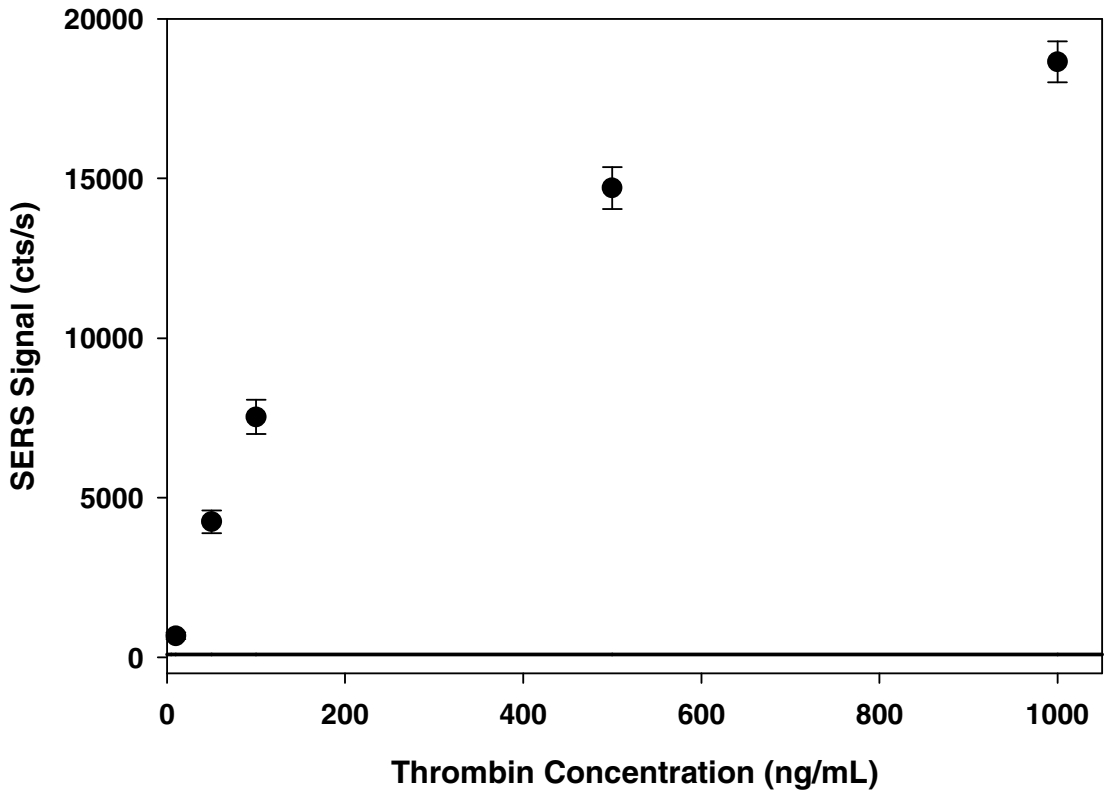

Figure 2. Dose-response curve for detection of thrombin in an antibody sandwich assay. The solid line represents the blank signal plus three times its standard deviation.

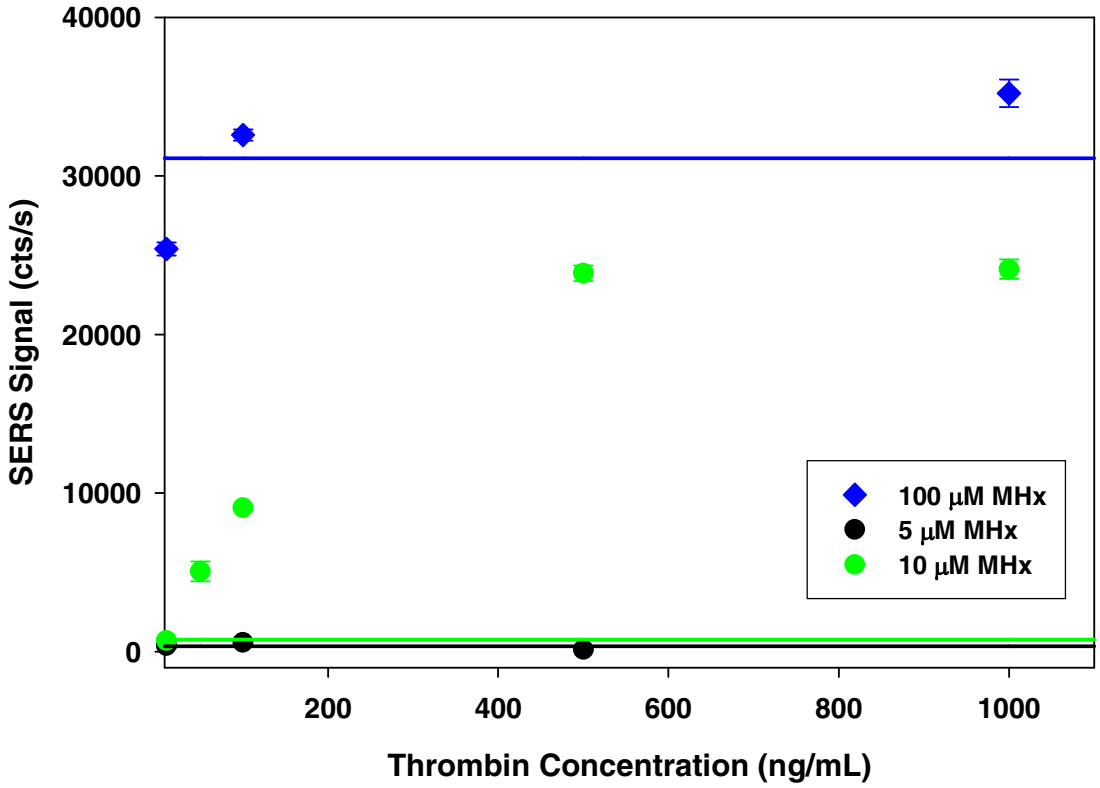

Figure 3. Dose-response curve for detection of thrombin in the aptamer/antibody sandwich immunoassay at different MHx concentrations. The solid lines represent the blank signal plus three times its standard deviation for each MHx concentration.

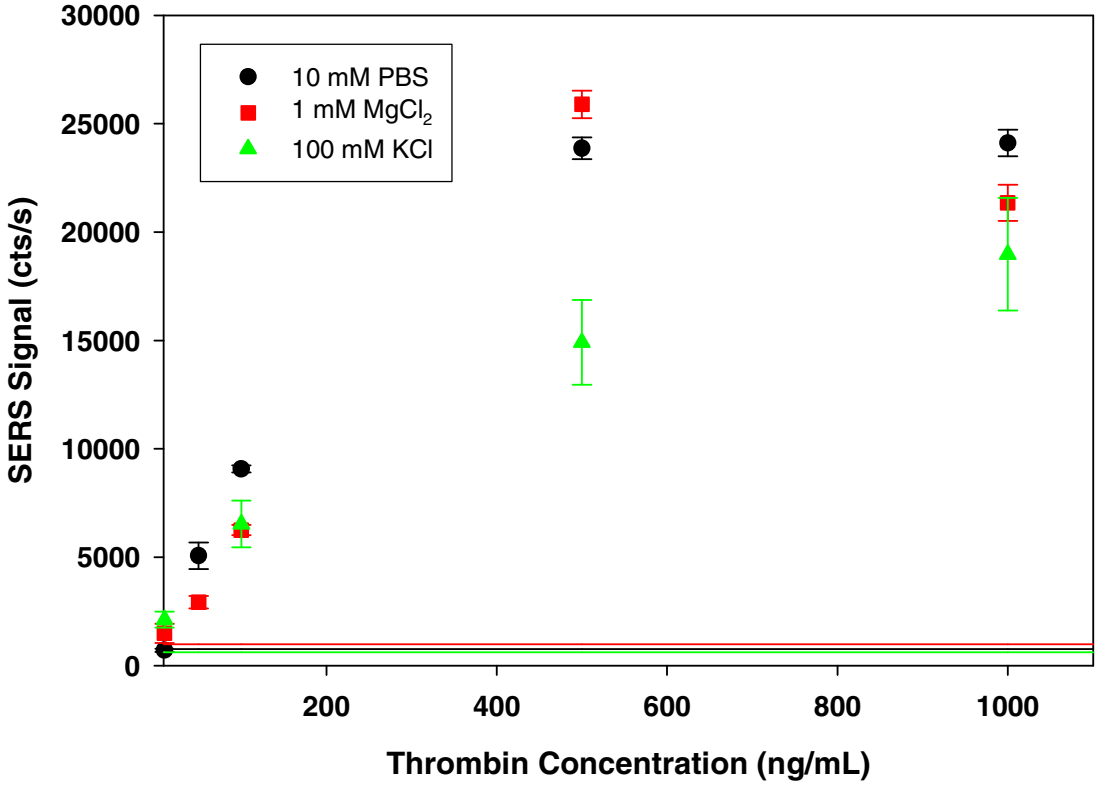

Figure 4. Dose-response curve for detection of thrombin in the aptamer/antibody sandwich immunoassay with different binding buffers. The solid lines represent the blank signal plus three times its standard deviation for each binding buffer.

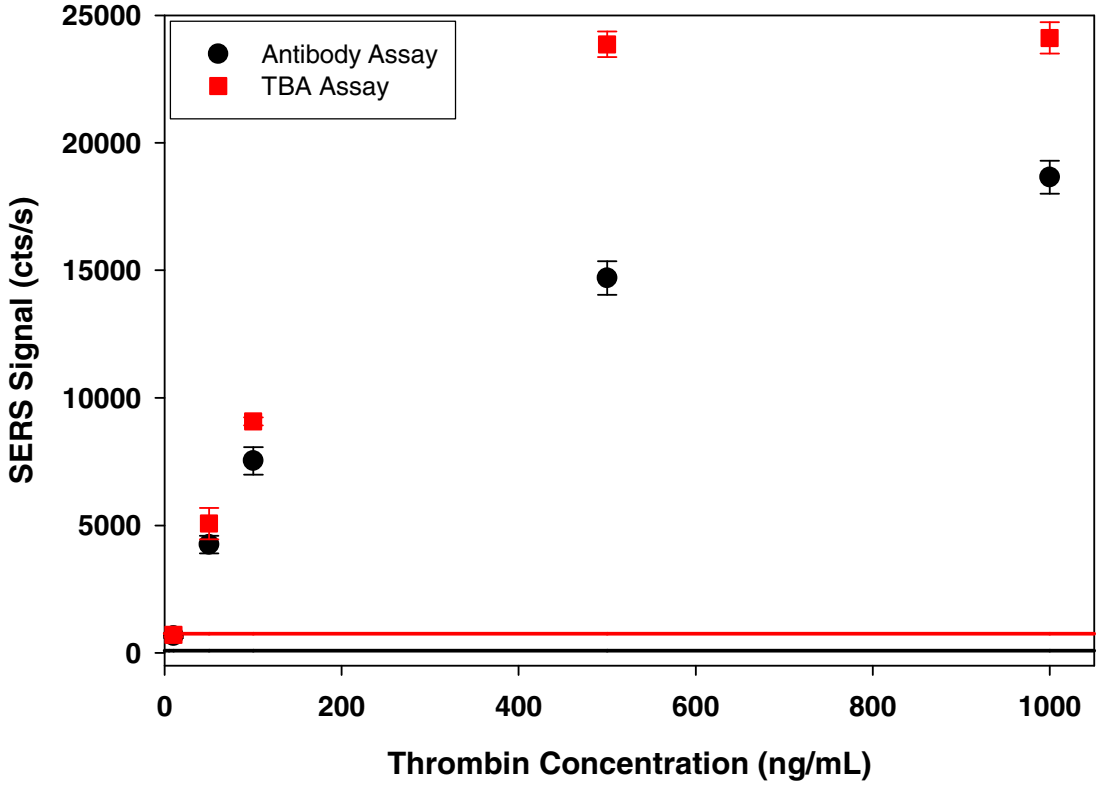

Figure 5. Comparison of optimized assays for thrombin using a TBA or antibody capture substrate. The solid lines represent the blank signal plus three times its standard deviation.

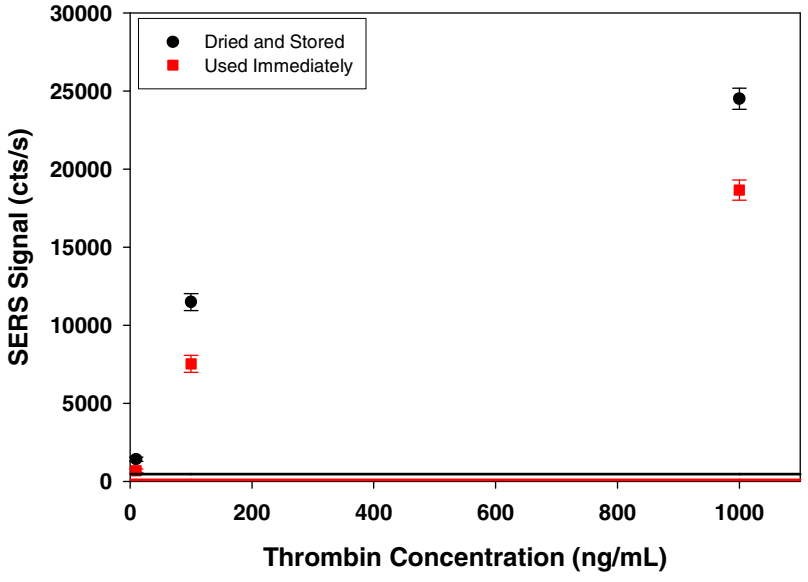

A

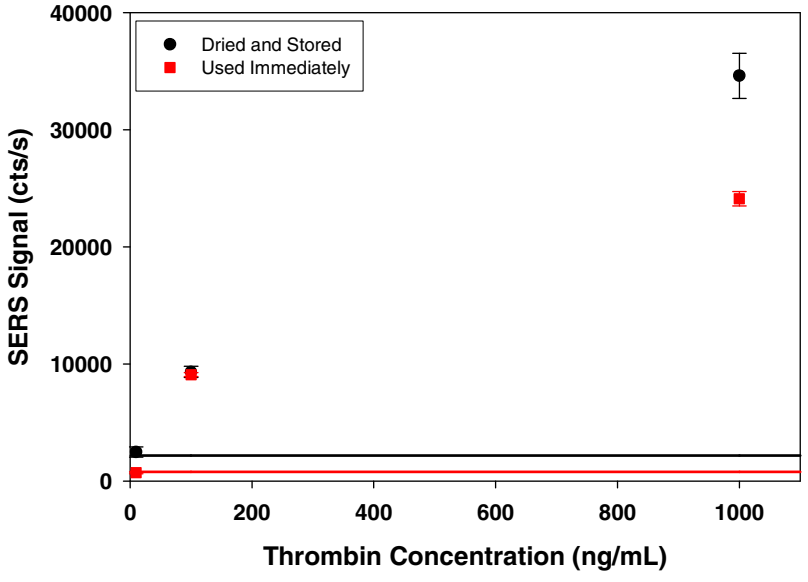

B

Figure 6. Dose-response curves for the detection of thrombin using A) antibody substrates and B) aptamer substrates that were prepared and used immediately or dried and stored for 48 h. Each solid line represents the blank signal plus three times its standard deviation.

GENERAL CONCLUSIONS

Research Overview

The main goal of this dissertation was to investigate several parameters that dictate immunoassay performance. Chapter 1 began by investigating the assay conditions required for detection of porcine parvovirus (PPV) and feline calicivirus (FCV) using atomic force microscopy (AFM) as a readout method. Several antibodies for each virus were screened to establish their effectiveness in a heterogeneous assay. The specificity of the assay was examined, along with a method of converting the units of $TCID_{50}$/mL to number of virus particles/mL for FCV. A preliminary investigation of sample volume considerations suggested that the use of large sample volumes would provide a simple means for improving limits of detection. This concept was explored further in Chapter 3. Limits of detection using the optimized conditions were 3.2×10^6 $TCID_{50}$/mL for FCV, and 6.4×10^4 $TCID_{50}$/mL for PPV. The immunoassay procedures optimized in Chapter 1 were utilized in Chapters 2 and 3.

In an effort to extend the work of Chapter 1, Chapter 2 described a method of improving mass transport of PPV and FCV to the capture substrate through the use of elevated temperatures. Elevated temperatures can have many effects on the system including: 1) an increase in the diffusion coefficient, 2) a change in the association and dissociation rate constants between the reactants, and 3) an increase in analyte mass transport due to thermally induced convection. The accumulation rates of PPV and FCV were examined, both experimentally (by AFM) and theoretically, at different temperatures. The accumulation of PPV followed the trend based upon the model, while

curves for FCV deviated significantly from the predicted curve, presumably due to the complex sample solution of the FCV. From this investigation, it was determined that incubation times could be reduced from ~16 h to ~1 h with limits of detection being reduced by less than a factor of 2. The findings of Chapter 2 emphasize the mass transport limitations of many biosensing applications due to the small diffusion coefficients of many biological elements.

Chapter 3 explored the manipulation of capture substrate area and sample volume on the equilibrium concentration of bound PPV to understand the factors that contribute to limits of detection. Surface-enhanced Raman scattering (SERS) was utilized as the readout technique for this study due to its high sensitivity. The goal of this work was to understand the achievable limits of detection for SERS readout. Theoretical considerations revealed that in order to attain the highest surface concentration of antigen at equilibrium, the volume of the antigen solution must be large enough to prevent depletion. The experimental results show that the improvements in limits of detection can be achieved by using small capture substrates and large volumes. A limit of detection of 750 aM was accomplished in this manner for PPV detection with SERS readout.

Finally, the use of aptamers as recognition elements for detection of thrombin was investigated in Chapter 4. Aptamers have been shown to rival antibodies in their sensitivity and specificity, and the merits of their use for SERS readout were investigated. The conditions required for aptamer performance in a SERS-based detection platform were optimized. Immobilization procedures and binding buffer composition were examined and the results of the aptamer-based assay were compared and contrasted to those from an antibody-based assay. Limits of detection for the aptamer-based and

antibody-based platforms were 200 pM and 30 pM, respectively. Higher SERS signals were obtained at all thrombin concentrations, including the blank, in the aptamer-based platform. Since non-specific binding dictates the limit of detection, the antibody-based assay yielded a better limit of detection.

Prospectus

The findings of this dissertation provide useful insights into the phenomena that govern immunoassay performance. Chapter 1 detailed the effect of immobilization on antibody activity for mAbs for PPV and FCV. Aptamers offer advantages over antibodies in that they are less prone to denaturation, but the optimal experimental conditions must be determined for each aptamer-based assay. The higher SERS signals observed in the aptamer-based assay over the antibody-based assay for thrombin detection may provide some insight into the mechanisms that govern SERS enhancements. The aptamer-based assay places the ERLs closer to the underlying substrate, which may provide a means of signal enhancement. A more detailed exploration into this observation would prove useful for understanding the effect of gap distance between ERLs and the underlying gold substrate on the SERS signal. The use of aptamers for both capture of the target and labeling of the target (i.e., preparation of ERLs with aptamers as the biorecognition moiety) would place the ERLs much closer to the underlying substrate than the analogous antibody-based assay. Fixing of the antibody-based assay and the use of photo-aptamers would allow rigorous rinsing of both substrates, and the number of ERLs bound for each platform could be determined by AFM. The SERS signal for each ERL could then be estimated to determine if larger SERS signals are obtained with a smaller gap distance.

The results provided in Chapters 2 and 3 provide insights into the optimal conditions for achieving the lowest levels of detection with immunoassay platforms. First, long times are required to reach equilibrium for systems employing analytes with large diffusion coefficients. The best limits of detection are achieved when equilibrium has been established, as this condition yields the highest surface bound concentration of analyte. Additionally, the equilibrium constant dictates the amount of analyte solution required to prevent depletion, an ideal condition for achieving low limits of detection.

Even if the optimal conditions are employed to reach ultra-low levels of detection, for most immunoassay platforms, the limit of detection is dictated by the amount of non-specific binding. To capitalize on the sensitivity of SERS and AFM as readout methods for immunoassays, non-specific binding must be reduced or eliminated. Insights into the mechanisms that control non-specific binding would prove useful to improving limits of detection for all sandwich-type immunoassays. If non-specific binding could be eliminated, then ultra-low levels of detection could be reached by increasing the mass transport and working in negligible depletion mode, which would allow the highest surface bound concentration of analyte. Coupling these performance attributes with the sensitivity of SERS and AFM, zeptomolar levels of detection could be within reach.